2017

A Comprehensive Evaluation of Hybrid Wetting Configurations on Dropwise Condensation

Karim Khazal Egab
University of South Carolina

A Comprehensive Evaluation of Hybrid Wetting Configurations on Dropwise Condensation

By

Karim Khazal Egab

Bachelor of Engineering
University of Basrah, 2007

Master of Engineering
University of Basrah, 2010

Submitted in Partial Fulfillment of the Requirements

For the Degree of Doctor of Philosophy in

Mechanical Engineering

College of Engineering and Computing

University of South Carolina

2017

Accepted by:

Chen Li, Major Professor

Jamil Khan, Major Professor

Tanvir Farouk, Committee Member

Guiren Wang, Committee Member

Jasim Imran, Committee Member

Cherly L. Addy, Vice Provost and Dean of the Graduate School

DEDICATION

To my parents

May God has mercy on them

ACKNOWLEDGMENTS

I would like to express my sincere gratitude to my advisors Dr. Chen Li and Dr. Jamil A. Khan for giving me the opportunity to work on this subject and finding new ideas to support my project. I am grateful for their guidance, support, knowledge, great experience, and advice that led me to succeed.

I would also like to extend my sincere gratitude to all my committee members Dr. Tanvir Farouk, Dr. Guiren Wang and Dr. Jasim Imran. I am thankful to University of Basrah for supporting me and giving me the opportunity to study for Bachelor and Master degrees. Special thanks to my supervisor during Master period study Dr. Ameen A. Nassar for his support and encouragement.

I gratefully acknowledge the financial support provided in part by NSF (NSF CMMI-1266043). Special Thanks to Dr. Benli Peng, Dr. Wenming Li and Mr. Saad Oudah for their cooperation, and advice during my studies. I would like to thank my group members at the Micro/Nanoscale Transport Lab for supporting me all the time in my research study and offering me advice. Thanks to all my friends for their help and advice.

Thanks to my father and mother may God has mercy on them for supporting me in my initial study and encouraging me during the difficult times. Thanks to my family for their love and support during my life.

ABSTRACT

The heat transfer during condensation on a surface depends on the pattern design of the surface, which can highly influence hydrophobic/hydrophilic wettability. In this study hybrid pattern designs were studied. The relationship between the droplet dynamic and the hybrid pattern design can alter the drainage rates, droplet departure frequencies, and the condensation heat transfer rates. Therefore, two series of hybrid patterned surfaces have been designed, developed, and tested during condensation of water vapor on horizontal copper tubes, and compared to complete dropwise and complete filmwise condensation samples. This is to investigate the design that provides the maximum improvement in the droplet mobility and consequently the condensation heat transfer performance. In the first series, hydrophobic circular patterns on hydrophilic background were studied, the optimum pattern sizes/ratios were found for different subcooling temperatures. However, the corresponding maximum heat transfer rates were lower than a surface with a complete dropwise condensation. In the second series, hydrophilic circular patterns on hydrophobic background were employed and strategically examined as a function of the patterns diameter and gap. The corresponding optimum diameter that provides the peak heat transfer coefficient for this series which is 12% higher than that of the complete dropwise surface was found to be 1.5 mm when the gap is 0.5 mm. In addition, findings indicate that increasing the gaps between adjacent patterns reduces the number of bridging droplets, thereby increasing the condensation rate. The optimized dimensions of 1.5 mm were found for both pattern, and gap size, which enhanced the heat

transfer rate compared with the corresponding complete dropwise surface. Ultimately, changing the gap plays a more important role than changing the size of the pattern in governing the droplets departure frequency and thus the condensation heat transfer performance.

Moreover, droplet dynamics and departure characteristics during condensation on horizontal copper tubes with circular patterns have been investigated based on different patterns' sizes and the gaps between them. Initially, series hydrophobic circular patterns on hydrophilic copper tubes are tested at various subcooling temperatures and departure frequency optimum pattern sizes are found. However, it is determined that the corresponding departure frequencies are lower than complete dropwise surface. Second, series of hydrophilic circular patterns on hydrophobic copper tubes have been systematically studied based on the patterns' size and the gaps between them and corresponding optimum designs have been found. Results indicate that the influence of the gap between the patterns on the droplet dynamic and departure frequency is significant. The results show that when the gaps between the patterns decrease, droplets from neighboring patterns are more likely to merge, resulting in lower droplet departure frequencies, velocities, and mobility. On the other hand, increasing the gaps between the patterns promotes renewal of droplets on the condensing surfaces. The droplet departure frequency on the hybrid surface with a gap of 1.5 mm is 1.37 times higher than that of 0.5 mm gap. Moreover, the renewal droplet frequencies from the patterns are strongly affected by the gap sizes. The optimum design of the hydrophobic/hydrophilic patterns to enhance droplet dynamics is studied.

In addition, with regard of condensation on hybrid surfaces, the geometry of the patterns has a significant influence on droplets departure frequency and heat transfer performance. Therefore, different patterns geometries (circle, ellipse, and diamond) have been developed on horizontal copper tubes at atmospheric pressure. All the patterns have the same size, and the same identical gap between the adjacent patterns. Results show that the diamond hybrid surface has the best performance compared with elliptic, circular hybrid surfaces at the same pattern area with same neighbor gap distance between two patterns and complete dropwise condensation. However, the circle and ellipse hybrid surfaces outperform lower performance compared to complete dropwise surface. The gap between the patterns has a significant influence on droplets dynamic and heat transfer performance for all hybrid surfaces. The heat transfer rate increases with increasing the gap between the patterns on all hybrid surfaces. The heat transfer rate for the diamond hybrid surface is 40% higher than complete dropwise condensation surface when the gap is 1mm. However, the heat transfer rate for circle and ellipse hybrid surface increases with increasing the gap, but it does not advance the complete dropwise performance. This study clearly demonstrated that an optimal geometry and gap scale patterned surfaces exist regarding maximum condensation heat transfer rate and droplet departure frequency.

TABLE OF CONTENTS

LIST OF TABLES

LIST OF FIGURES

LIST OF SYMBOLS

A	The surface area of the tube (m^2)
C	The constant of Eq. 5
cp	Specific heat capacity (J/kg K)
D	Diameter (m)
g	Gravitational acceleration (m/s^2)
h	Heat transfer coefficient (W/m^2 K)
h_{fg}	Latent heat of evaporation (J/kg)
k	Thermal conductivity (W/m K)
L	Tube length (m)
m	Mass flow rate (kg/s)
Nu	Nusselt number
Pr	Prandtl number
Q	Heat transfer rate (W)
q"	Condensation heat flux (W/m^2)
R	Resistance (K/W)
Re	Reynold number
T	Temperature (K)
U	Overall heat transfer coefficient (W/m^2 K)

Greek Symbols

Δ	Difference
ρ	Density (kg/m^3)

μ	Dynamic viscosity (Pa s)

Subscripts

c	Coolant
c.conv	Coolant's convection inside the tube
c.w	Coolant at wall temperature
i	Inner
i.cs	The inner cross section of the tube
in.c	The inlet of the coolant
l	Liquid
LMTD	log mean temperature difference
o	Outer
out.c	The outlet of the coolant
sat	Saturation temperature
tot	Total
v	Vapor
FWC	Filmwise condensation
DWC	Driopwsie condensation
w	Wall
RAF	Renewal area frequency
γ	sandblasted regions
β	hydrophobic regions

CHAPTER 1

INTRODUCTION

1.1 Background

Condensation is a phase change transition process that takes place spontaneously in nature and industrial applications which are related to the heat and mass transfer technology as well as other areas of phase change processes. Unlimited developed techniques are in progress to improve condensation efficiency because of its wide practical significance in the removal of a large amount of heat flux in industrial applications such as power plants, water harvesting, thermal management, air conditioning and numerous electronic devices. Condensation occurs when steam at saturation temperature contacts with a solid surface whose temperature is lower than the saturation temperature. The difference in enthalpy from saturated steam to saturated liquid equals to the heat rejected by steam at constant temperature and pressure. Enhancement of the heat transfer rate during the condensation becomes a crucial issue because of its importance in determining energy generation and utilization efficiency as well as water harvest. Therefore, extensive efforts have been focused on promoting condensation heat transfer efficiency. The performance of condensation heat transfer can be improved by quickly removing the condensate's steam during the phase transition process. In general, the nature of condensation comes in two types, filmwise and dropwise, depending on the interaction between the condensate steam and the condensing surface, and on the wettability of the solid surface. Filmwise condensation occurs when

steam condenses as a film on the surface while dropwise condensation takes place when the steam condenses in the form of droplets on the surface. The rate of heat transfer during the two types of condensation is quite different for the same temperature difference. The heat transfer rate for dropwise condensation is desirable because it has a higher heat transfer rate than filmwise condensation. The thermal fluid resistance in filmwise condensation is higher than the thermal resistance in dropwise condensation because the high thermal resistance produces a thick liquid film which reduces the amount of condensing steam. Researchers have achieved a condensation heat transfer rate 5-20 times of filmwise condensation under the same conditions [1-6]. Moreover, the parameters and conditions that promote dropwise condensation were clarified in a research study. Therefore, it is better to introduce dropwise condensation in industrial and engineering applications.

1.2 Condensate contact angle

The main parameter which finds out the condensation state is the contact angle between the liquid droplets and solid surface. The large contact angles more than 90^{o} can be obtained on hydrophobic surfaces that cause the droplets to speed up on the surface.

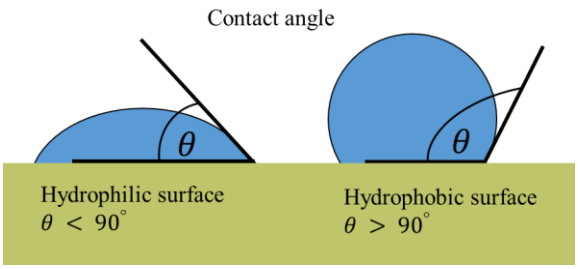

Figure1.1: The schematic contact angle on hydrophobic and hydrophilic surfaces.

However, a lower contact angle can be found on hydrophilic surfaces which cause the droplets to spread on the surface where the contact angle is less than 90°. Figure1.1 shows the schematic image of contact angle on hydrophobic and hydrophilic surfaces. The contact angle values between the d roplets and solid surface depend mainly on the surface structure, interaction between the condensing steam and solid surface, and surface wettability. A few theories have explained the mechanism of interaction between the droplets and condensing surfaces. The wettability of surface plays a major role in understanding condensation phenomena and droplets dynamic. The modes of interactions as shown in Figure 1.2 classified into three types of contact angle depending on the surface wettability: Young mode, Wenzel mode, and Cassie mode [7]. The contact angle on an ideal smooth surface is known as Young contact angle. The Young contact angle equation demonstrates the balance at the three-phase contact of solid, liquid and vapor [8]. The balancing forces can be presented by below equation for the line of contact of the liquid, solid and vapor phases.

$$\gamma_{lv} \cos \theta_y = \gamma_{sv} - \gamma_{sl} \qquad (1\text{-}1)$$

Where, γ_{lv} is the liquid-vapor interfacial energy, γ_{sv} is the solid-vapor interfacial energy and γ_{sl} is the solid-liquid interfacial energy. The Young equation assumes that the surface is ideally smooth, homogenous. However, the non- ideal surfaces have different contact angle calculations depending on the roughness of the surfaces. The contact angle on real surfaces is given by the Wenzel mode and Cassie-Baxter mode [8]. In Wenzel mode, the droplets penetrate the roughness of the surface and have less mobility as shown in Figure 1.2. The contact angle can be expressed by the following [8]:

$$cos\,\theta_W = r\ cos\,\theta_y \qquad (1\text{-}2)$$

where, r is the roughness ratio (the ratio between the real and the projected surface area), r= 1 for a smooth surface and r > 1 for a rough surface, θ_y is the Young contact angle and θ_W is the Wenzel contact angle.

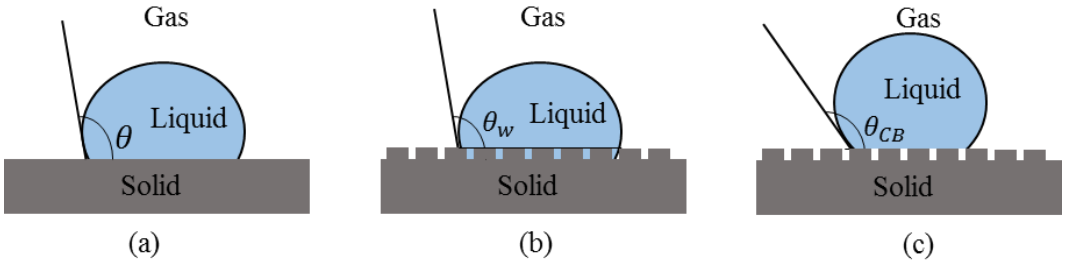

Figure 1.2: The modes of interactions between the solid surface and droplets (a) Young state (b) Wenzel state (c) Cassie-Baxter state.

In case where the liquid does not penetrate the roughness, the Wenzel mode does not apply, and Cassie-Baxter mode is used instead [8-10]. The droplets in Cassie mode have higher mobility compared to Wenzel mode because of the lower contact angle hysterias. The Cassie-Baxter contact angle can be expressed [8]:

$$cos\,\theta_{CB} = f\,cos\,\theta_y + (f - 1) \qquad (1\text{-}3)$$

Where, θ_{CB} is the contact angle in Cassie mode, θ_y is the Young contact angle and f is the fraction of solid/liquid interface where the droplet is in contact with the surface. The mode of condensation that results in high mobility of droplets and significant condensation heat transfer performance is dropwise [11]. Therefore, techniques to promote dropwise condensation by enhancing droplets mobility are in progress and focus of research.

1.3 Filmwise condensation

Filmwise condensation takes place when the steam condenses on the condensing surface in the form of a film, and the liquid film wets the surface. The wetting surface is called hydrophilic because it has high surface energy compared to water surface energy (high wettability). Generally, in filmwise condensation, the condensing surface is covered by the liquid film as shown Figure: 1.3. Figure: 1.3 shows filmwise condensation on horizontal copper tube when the subcooling temperature difference (ΔT) is 16 ℃. The liquid film reduces the amount of steam to condense at low temperature because it provides a thermal resistance or barrier to steam to be condensed. As the film's thickness increases, the thermal resistance increases and causes a significant decrease in condensation efficiency and heat transfer rates. Filmwise condensation can be promoted by increasing the surface area of the condensing surface using efficient heat transfer additives [12].

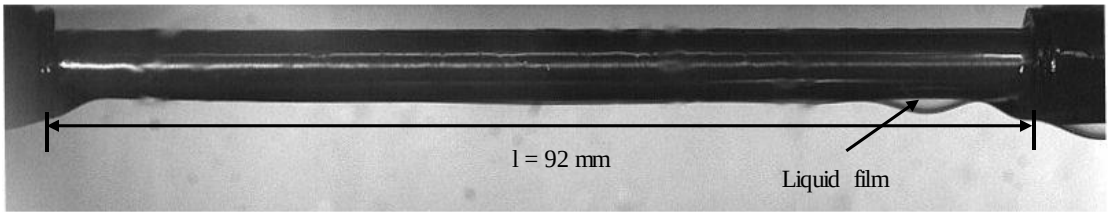

Figure: 1.3 Filmwise condensation phenomena on horizontal copper tube.

The additional surface area provides more convection heat transfer, decrease in hydrodynamic stability of the liquid-steam interface, and makes a disturbance in the condensing fluid film. Moreover, increasing the roughness of the condensing surface using porous media increases the heat transfer rate for filmwise condensation as well since the surface area will increase.

1.4 Dropwise condensation

Dropwise condensation takes place when the steam condenses as droplets on the condensing surface, and the droplets condensate do not wet the surface. The non-wetting surface is called hydrophobic because it has lower surface energy compared to water surface energy (low wettability). In dropwise condensation, droplets are only responsible for transferring heat from condensing surfaces. Figure 1.4 shows dropwise condensation on horizontal copper tube when the subcooling temperature difference (ΔT) is 8 ℃. During dropwise condensation, the droplets nucleate, grow, and coalesce with neighbor droplets until they become large enough to roll off the surface. Dropwise condensation becomes a great interest in condensation technology because it provides a high heat transfer rate compared to filmwise condensation. The condensation heat transfer is not uniform on the surface because the droplets have different sizes. However, it is difficult to maintain dropwise condensation for a long time because the droplets wash off the condensation surface and transfer to liquid film. Therefore, manufacturing a condensing surface for durable condensation is still in development and practice.

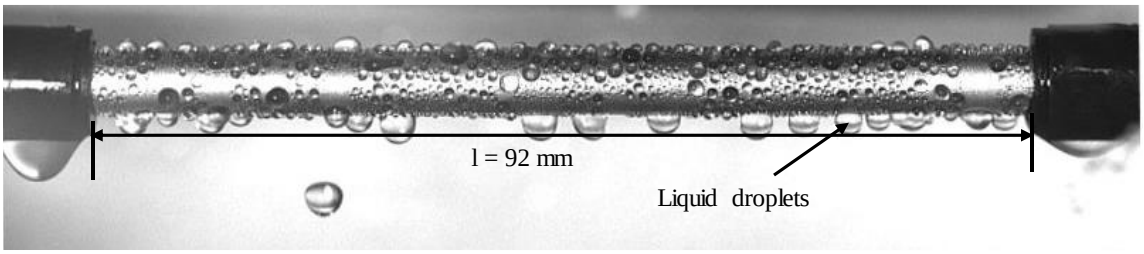

Figure 1.4: Dropwise condensation phenomenon on horizontal copper tube.

To obtain the expression for the total heat transfer through all droplets, one must integrate the total number of droplets and the whole size distribution of the droplets. The minimum and maximum diameters and the radius at which droplets coalesce and are

swept from condensing surfaces should be known. The droplet's size distribution for minimum and maximum droplets should also be calculated where the heat flux through a single droplet can be determined by calculating thermal resistances of a single droplet. The total heat flux can be calculated from the heat transfer and the droplet size distribution by including time droplet growth from the minimum droplet radius r_{min} to the maximum droplet radius r_{max}. Therefore, lots of methods have been applied to achieve dropwise condensation by increasing the droplets' removal from the condensing surfaces, increasing drainage droplets rate and fabricating the super-hydrophobic/hydrophobic coating. Extensive efforts have been made to obtain a durable dropwise condensation and to enhance the heat transfer rate. The study focused on improving dropwise condensation using hydrophobic coating, changing surface roughness, surface geometry and working fluid. However, most of these methods do not produce long lasting dropwise condensation.

1.5 Research objectives

The current dissertation is focused on investigating the heat transfer of dropwise condensation enhancement on horizontal copper tubes using hybrid surfaces. The study includes mainly three parts, the influence of patterns size on droplet dynamic and heat transfer performance, the effect of the gap between the patterns, and the influence of patterns geometry on droplets dynamic and condensation heat transfer rate. Since there is little existing scientific literature involving condensation on hybrid surfaces, this work is trying to gain some understanding of the physical phenomena of droplets involved during the condensation. The purpose of the study is to investigate the influence of patterns wettability on dropwise condensation heat transfer and droplet dynamics. Hydrophobic

patterns have been created on hydrophilic copper tubes. The effect of patterns size is explained where the optimum patterns size id found. Next, hydrophilic patterns have been developed on hydrophobic copper tubes. The influence of the size of the pattern on condensation heat transfer and droplet dynamics is studied. The objective and specific task of the research is divided into following sections:

(1) Evaluate the condensation on hybrid surfaces which have hydrophobic patterns.
(2) Investigate the effect of pattern's size on condensation heat transfer
(3) Study the effect of pattern's size on condensation phenomena, droplet dynamics, droplet departure frequency, and droplet departure diameter.
(4) Analyze the condensation on hybrid surfaces which have hydrophilic patterns.
(5) Clarify the effect of pattern's size and the gaps between the patterns on heat transfer performance during condensation.
(6) Study the influence of pattern's size, and the gap distances between the patterns on condensation phenomena, droplets dynamics, departure frequency, and droplet departure diameter.
(7) Investigate the effect of the geometry of patterns on condensation heat transfer and phenomena of condensation.
(8) Study the effect of the gaps between various patterns geometry on condensation performance, droplet dynamics, departure frequency, and heat transfer.

CHAPTER 2

LITERATURE REVIEW

A variety of experimental and theoretical analysis has been focused on the enhancement of heat transfer during condensation because of its need in the industrial projects which are applicable in our life. Dropwise condensation becomes a new face of technology because it reduces the size and the cost of the condenser for the same output in filmwise condensation and it increases the heat rate transfer compared to filmwise condensation. Researchers have achieved numerous methods to enhance dropwise condensation by changing the properties of the condensing surfaces and the working fluid. Moreover, changing the physical, chemical, thermal and geometrical properties of the condensing surfaces can improve the performance of dropwise condensation. In addition, the high-magnification imaging technique is popular for both material characterization and thermal condensation capturing [13-16]. The visual observation provides additional understanding for condensation phenomena and droplet dynamics.

2.1 Droplet dynamic analysis during dropwise condensation.

The behavior of droplet dynamics and droplet departure frequency can strongly influence dropwise condensation efficiency. It has been proved that the heat transfer for dropwise condensation could be promoted if the droplets migrate with high velocity and depart from the surface with high frequency. As more droplets migrate, new droplets nucleate, move, and roll-off from surfaces during condensation. In general, plenty of parameters can change the surface characteristics and enhance the droplet dynamics and droplet's departure such as using superhydrophobic surfaces, hydrophobic surfaces,

micro-nanostructures surfaces, gradient surfaces, hybrid surfaces and modifying surface geometry i.e. can improve the droplet dynamics. Numerous efforts have been achieved to study the increase in droplet mobility and departure frequency during dropwise condensation [17, 18]. The limitation of the mechanism of droplets growth during dropwise condensation at low pressure and ultra-lower pressure has been clarified [19]. The effect of steam pressure on the droplets size distribution, droplets departure frequency, and heat transfer rate was investigated at a pressure range from atmospheric to 1.5 KPa. The condensing droplets became large at low pressure and then the surface coverage ratio increased. The droplet departure size and density increased with decreasing steam pressure. Thermal resistance increased due to the increase in the droplet departure size and surface covered ratio. Figure 2.1 shows the droplets coverage ratio and the thermal resistance at various steam pressure levels. The steam pressure significantly improves the heat transfer rate because of decrease the volume of droplets and increase the droplet departure from the surface.

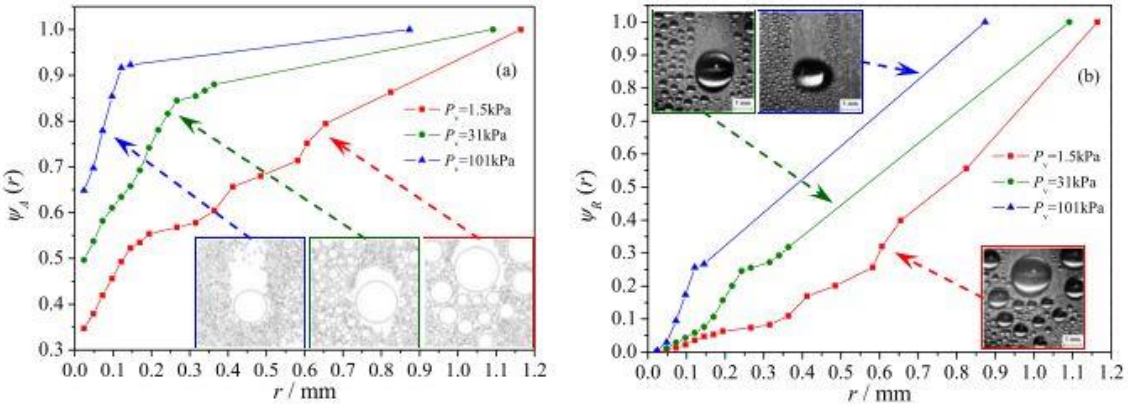

Figure 2.1: Droplet covered ratio at different steam pressure levels. (a) Droplets coverage ratio (b) The resistance [19].

Droplet departure frequency and droplets dynamic characteristics during dropwise condensation at atmospheric and low steam pressure (1.5 kPa) have been discussed [20]. Condensate droplets are large and roll off slowly from the surface at low pressure, but they are not at atmospheric pressure. The droplet viscosity increases five times at a pressure of 1.5 kPa while it decreases as conditions approach atmospheric pressure at the same surface subcooling temperature. Because of the higher droplet viscosity at low pressure, more viscous dissipation leads to the decreased droplet kinetic energy for the same falling distance. However, the falling droplet gives more oscillation and higher falling speed at the atmospheric condition as shown in Figure 2.2. Steam pressure significantly influenced the surface coverage distribution by droplets and affected the thermal resistance. A larger surface coverage was recorded at low pressure than at atmospheric steam pressure.

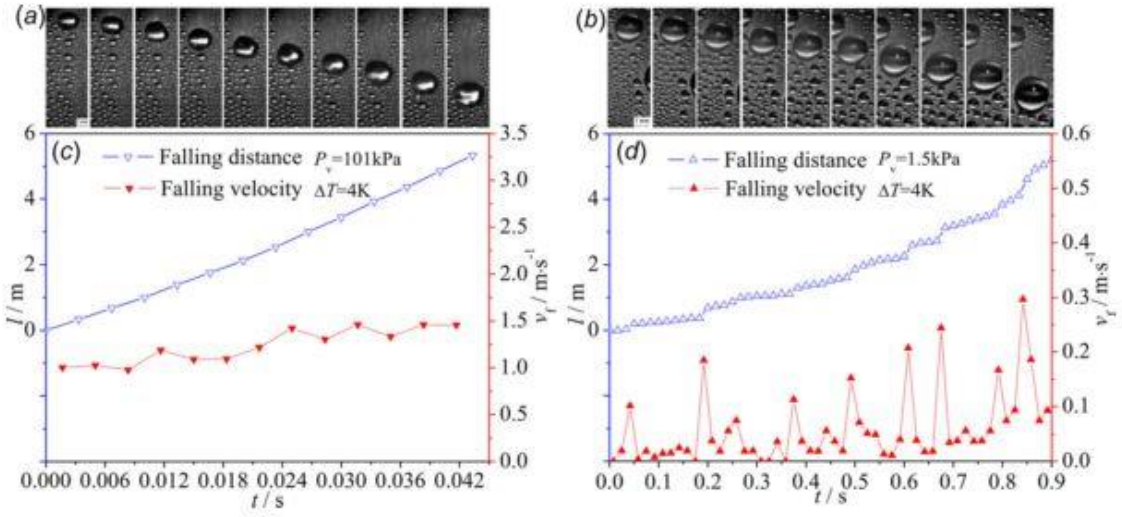

Figure 2.2: The falling droplets at a distance for different pressure [20].

Droplet dynamics on ultra-hydrophobic surfaces containing hydrophobic silicon pillars were studied during dropwise condensation environment [21]. The droplets which are located at the top of the pillars were pinned and migrated by the pillars to coalesce with the condensing water among the pillars. The transition from the Cassie-Baxter wetting mode to Wenzel wetting mode leads to increase hysteresis contact angle and decreases droplet mobility as shown in Figure 2.3. When the condensation process advances, the water among the pillars becomes unstable and moves up to coalesce with water condensed on the pillars. The coalescence covers the pillars on the condensing surface and prevents droplets from rolling off from the surface.

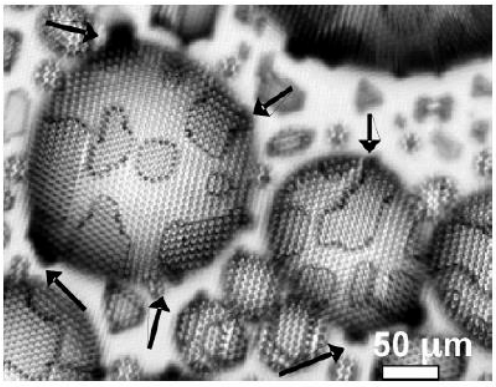

Figure 2.3: Large condensed of water droplets on the surface of hydrophobic silicon pillars [21].

Condensation behavior on microstructure hydrophobic surfaces and wetting transition from the Wenzel state to the Cassie state have been explained [22]. The droplets that are in Cassie state can be recognized by their spherical shape and their position on the top of the microstructure. The droplets that are in Wenzel state are located between the microstructures of the surface. The transition happened as shown in Figure 2.4 where the droplets which are in contact with the solid surface are in the dynamic process, and they have overcome the energy barrier that is isolating Wenzel state from

Cassie state as shown in Figure 2.4. The water repellency improved and the droplet velocity on the surfaces enhanced.

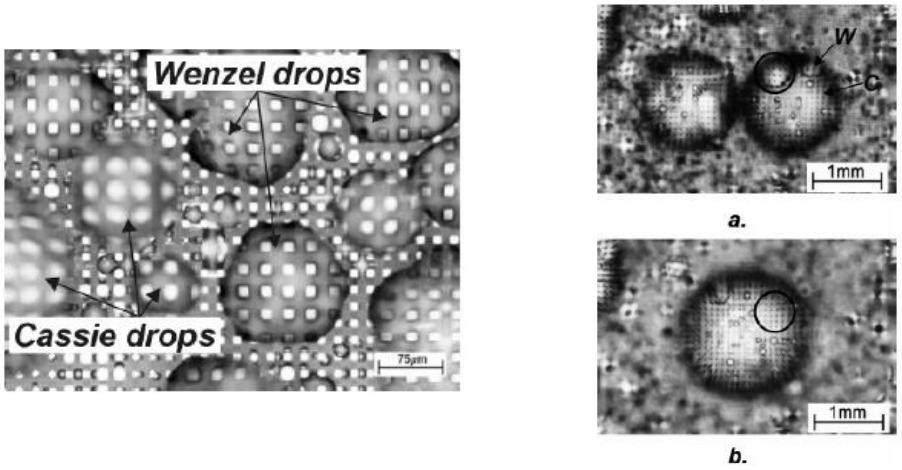

Figure 2.4: The transition from Wenzel state to Cassie state [22].

Condensate droplets can sweep spontaneously away on superhydrophobic surfaces but not on other superhydrophobic surfaces [23, 24]. Four superhydrophobic surfaces with different nanostructures have been examined to optimize the mobility of droplets during condensation in the ambient environment. Only a surface with a small enough Wenzel roughness (sisal-like nanoribbon structure) can allow the movement of condensate droplets to easily transform into Cassie state as shown in Figure 2.5. The droplet mobility depends mainly on the relative humidity in the condensation environment and the surface tension forces between the solid surface and condensate droplets in some superhydrophobic surfaces. Therefore, increase the of surface tension for other superhydrophobic surfaces as (defoliation like nanosheet structure) leads to a significant decrease in droplets mobility.

a

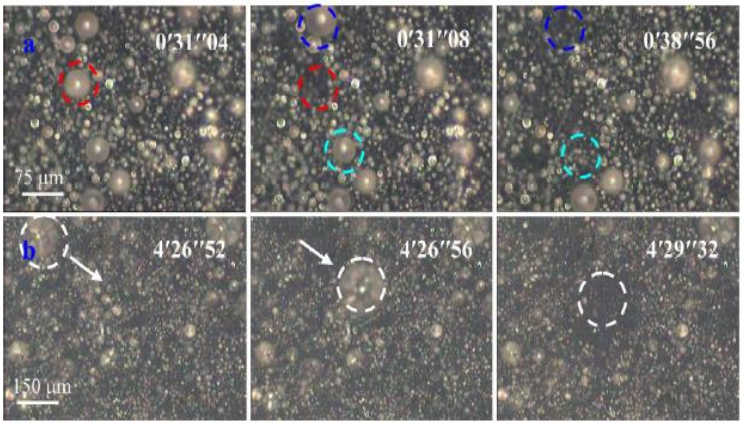

b

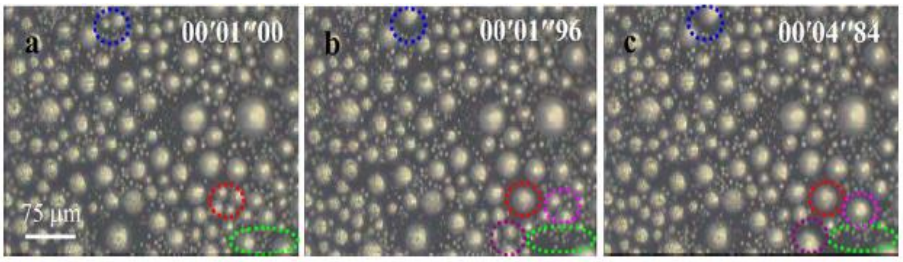

Figure 2.5: (a) The droplet motion on the superhydrophobic surface as sisal-like nanoribbon structure where the spontaneous droplet frequency is 72 droplets/s. (b) The droplet motion on the superhydrophobic surface with defoliation like nanosheet structure where the spontaneous droplet frequency is 7 droplets/s [24].

The migration of water droplets on hydrophobic-hydrophilic gradient surfaces which are fabricated using photo-degradation was analyzed [25]. The hydrophobic-hydrophilic ratios changed on the surface by changing the width of the regions and the capillary force for each region. The water droplets move from hydrophobic regions to more hydrophilic regions and spread rapidly on the surface. The movement of droplets was caused mainly by the capillary force with a high velocity which depends on the degree of gradation. Figure 2.6 shows the movement of water droplets on the gradient surface. A higher gradient degree performs a high droplets velocity and a rapid movement of droplets on the solid surface.

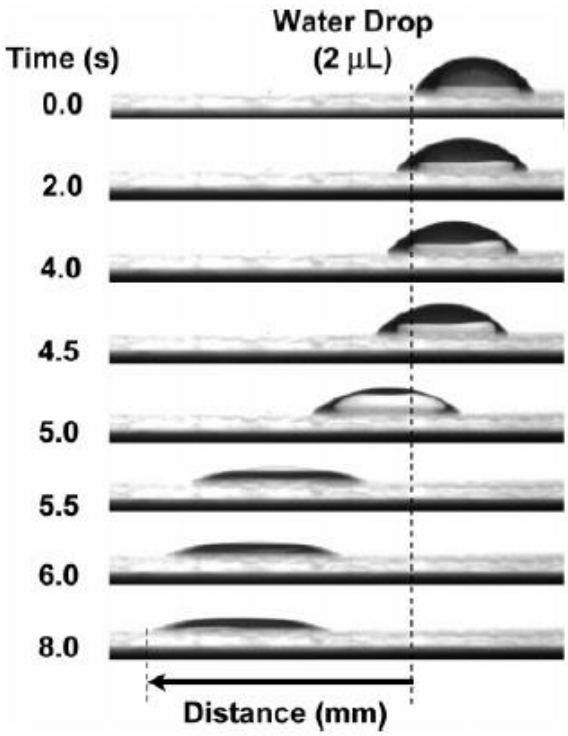

Figure 2.6: Droplets movement on gradient surfaces [25].

2.2 Enhancements of condensation heat transfer

2.2.1 Condensation heat transfer promotion by modifying surface geometry

The geometry of the condensing surfaces has an important effect on condensation heat transfer and droplets dynamics. Increasing the condensing's surface area increases increase the conventional heat transfer area and provide a large and significant room for steam to be condensed. The geometry should be designed in a way that the droplets move quickly with high mobility. However, some modified geometries that developed on condensing surfaces reduce the heat transfer performance and droplet dynamics because they cause flooding of the droplets on the condensing surfaces which increase droplet size and thermal resistance. The dropwise condensation is still existing during the condensation process, but the droplet is bigger compared to the smooth surfaces. The heat transfer of dropwise condensation is influenced by the behavior of rolling off

droplets from the surface. Study of a round shaped grooves fabricated on a copper plate to enhance dropwise condensation performance was investigated [26]. The chemical treatment of oleic acid was used as a coating to obtain dropwise condensation under atmospheric pressure. The plate was set to two positions vertical and horizontal as shown in Figure 2.7. The falling droplets were swept more frequently from the condensing surface when the plate set on vertical direction compared to the horizontal position. The depth of grooves was changed until the optimum depth was found. The maximum depth was (2-3) mm that enhance heat transfer performance and velocity of falling droplets as shown in Figure 2.8. However, the horizontal grooves work as a resistance against down flow of droplets movement as shown in Figure 2.7. The heat transfer rate reduced since the condensing droplets stuck on the grooves and increased the thermal resistance.

Figure 2.7: Condensation on vertical grooves and smooth surfaces [26].

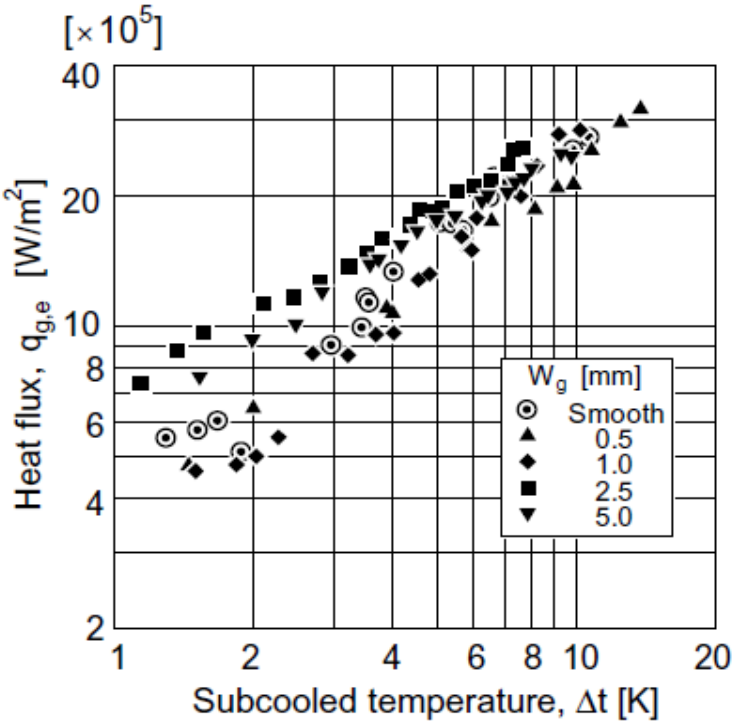

Figure 2.8: Comparison of Heat Transfer rate for condensation on horizontal, vertical grooves and smooth surfaces [26].

Condensation heat transfer on horizontal plain and finned that have different surface wettability was experimentally investigated [27]. The tubes were modified chemically to achieve hydrophilic, hydrophobic and superhydrophobic characteristics. The experimental conditions for condensation were taken place under pure vapor and with a significant amount of non-condensable gas. The condensation phenomena are shown in Figure 2.9, and the condensation modes were filmwise for finned tubes while the condensation was dropwise on hydrophobic and super hydrophobic plain tubes. The heat transfer rate for superhydrophobic plain surface presents a lower heat transfer performance at pure steam on finned tubes. The increase in the pining size for nanostructure at the contact area between the droplets and the surface reduce the droplet departure frequency, increase the droplet's size, and increase the thermal resistance.

Figure 2.10 clarifies the condensation heat transfer performance on finned and plain tubes. However, the heat transfer rate for the super-hydrophobic finned and super-hydrophobic hybrid finned tubes is the highest with a large amount of non-condensable gas.

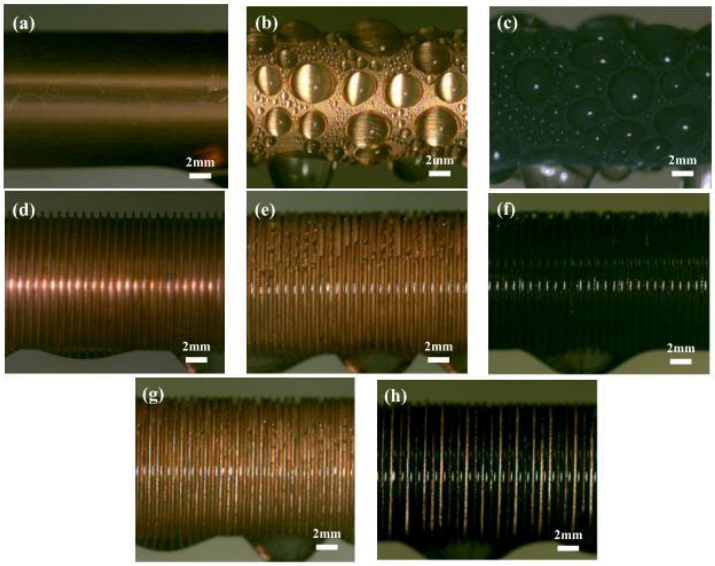

Figure 2.9: Condensation on different tubes with different wettability [27].

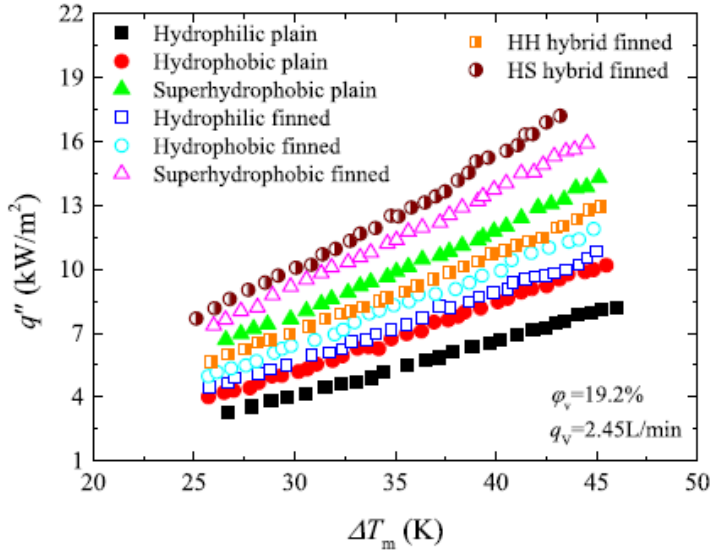

Figure 2.10: Condensation heat transfer performance on various tubes [27].

Convection heat transfer rate and condensation rate were enhanced on a polymer plate heat exchanger by adapting its geometry using polymer inserts [28]. Heat transfer coefficient increases by 90% compared to the heat transfer for a plate without inserts. The drainage rate was improved due to the proper choice of inserts density. The influence of insert density on convection heat transfer rate is shown in Figure 2.11. The increase in the heat transfer rate was due to increase the convection heat transfer surface area and existence the disturbances that cause the droplets to roll off down from the surface.

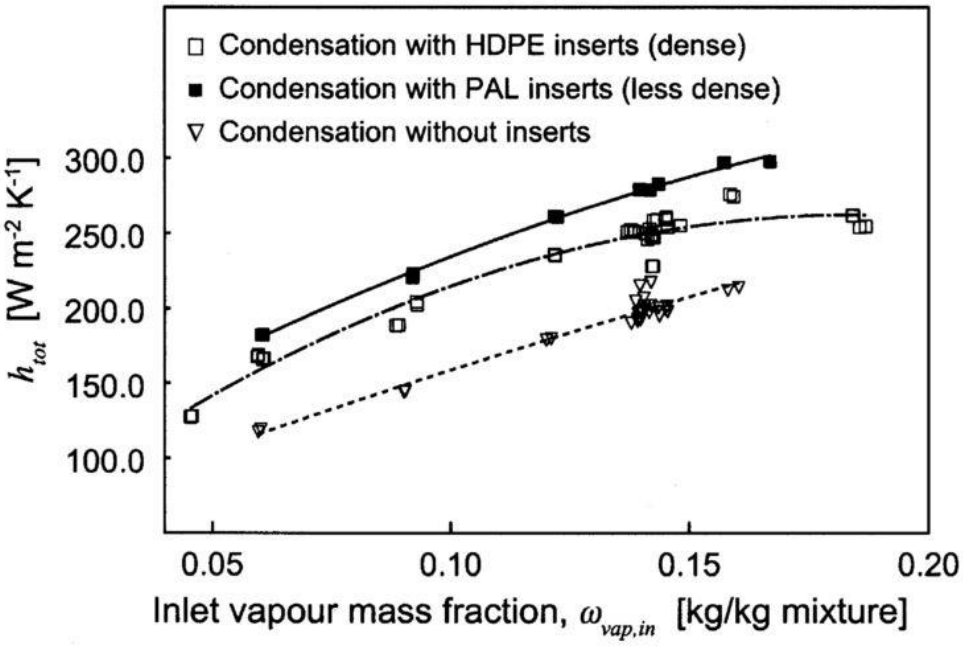

Figure 2.11: The effect of insert density on heat transfer enhancement [28].

An analytical study and predictions of condensation heat transfer and the thermal performance were investigated for the copper plate which has pin fins under free convection heat transfer [29]. The heat transfer rate increases with increasing the thermal conductivity of the fins at constant fins volume. The maximum heat transfer rate for

condensation enhanced with increasing the size of the fins. Figure 2.12 shows the effect of the fins volume in condensation heat transfer rate.

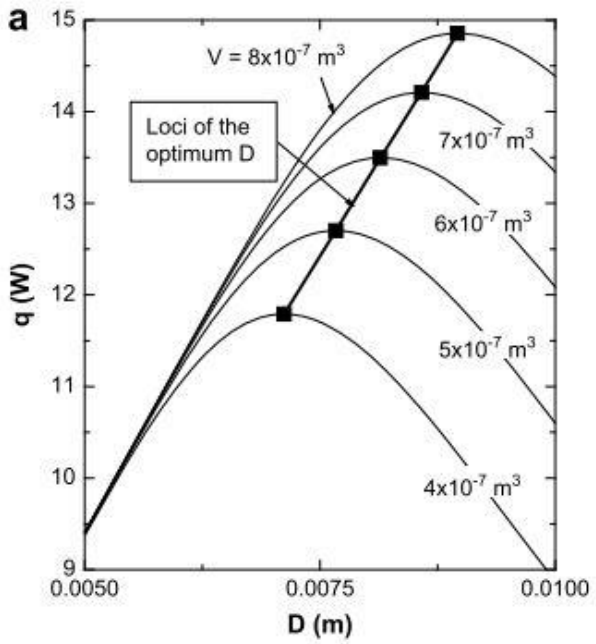

Figure 2.12: The influence of fins volume on condensation heat transfer [29].

An approximate analytical study about the performance of condensation on surfaces which have pin fins and subjected to forced convection was obtained [30]. The condensation rate of steam on the fins surface increases with increasing the Reynolds number due to evolving of the more latent heat of condensation. The effect of fins material on condensation heat transfer and the influence of fins volume were studied. The optimum design for fins volume that improves their efficiency and enhances condensation heat transfer was found in this study.

An extensive analytical solution for the enhancement of filmwise condensation on horizontal wire-wrapped tube has been investigated [31]. Three types of steam were used R113, ethylene glycol and pure steam to optimize the expression for different steam

conditions. The enhancement ratio of condensation heat transfer expression for wrapped tube was found regard to the plain tube. The improvement rate depends on tube and wire diameter, the pitch of the winding, the surface tension and density of condensate steam.

A numerical study of condensation heat transfer on horizontal copper tubes and copper tubes which are wrapped using steel wires [32] at atmospheric pressure and various types of steam. The steel wires have various diameters and different pitches as well to find the maximum dimensions and design that optimize the heat transfer rate. The condensation was completely filmwise for all experiments. Figure 2.13 shows the condensation enhancement ratio for wrapper wire tube for various types of steam and constant wire diameter regards to the plain copper tube. The enhancement ratio was 3 for R113 and 2 for ethylene glycol and steam.

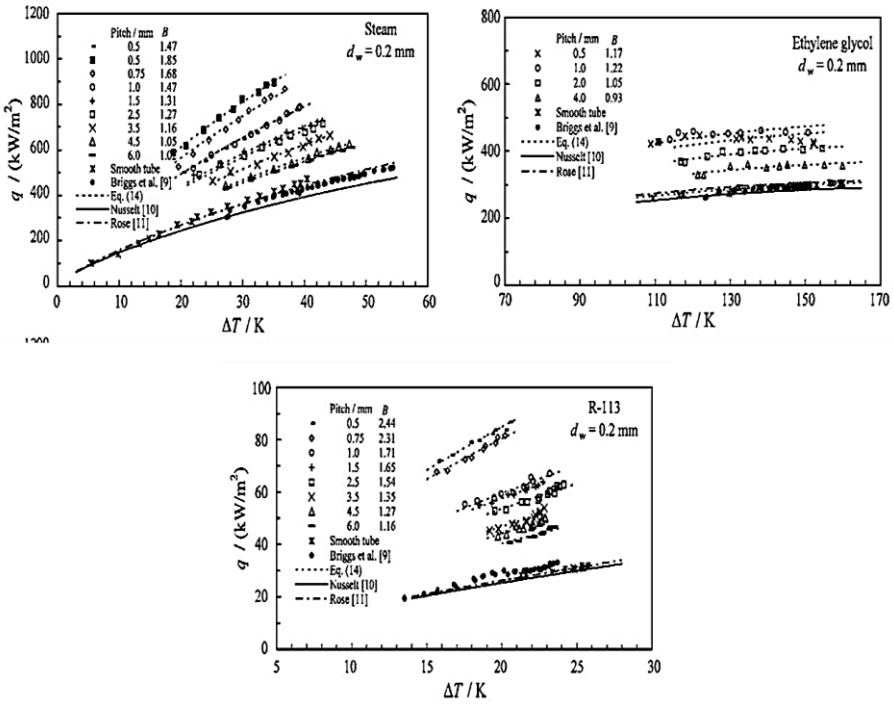

Figure 2.13: The enhancement ratio for wire wrapped tubes for different types of steam while the diameter of the wire maintained constant [32].

Condensation heat transfer on horizontal copper tubes which are wrapped with square copper and brass wires were studied experimentally [33] for free convection of steam. The effect of wire's dimensions, material, and the pitches was investigated. Figure 2.14 shows the design of wrapped wire on copper tubes for different pitches dimensions. The heat transfer rate of copper tube with copper square wires is higher than copper tube with brass square wire as shown in Figure 2.15 because the thermal conductivity of copper wires is higher than brass wires. The influence of the wires pitch on condensation performance was investigated. The effect of the pitches on the heat transfer rate for a copper tube with wrapped copper and brass square wires is shown in Figure 2.15 when the diameter of the wires is 0.8 mm. The highest heat transfer was obtained when the pitch is 4mm while the heat transfer decrease with further increase of pitch's dimensions because of flooding which causes less active of tube's surface area for condensation. In addition, the enhancement of heat transfer rate for 0.8mm copper square wire is lower than 0.8mm copper wire. However, the improvement of heat transfer rate for the 1mm copper square wire is higher than 1 mm copper wire diameter. The highest enhancement ratio is 1.53 when the wire diameter is 0.8 mm, and the pitch is 4mm regards to the plain copper tube.

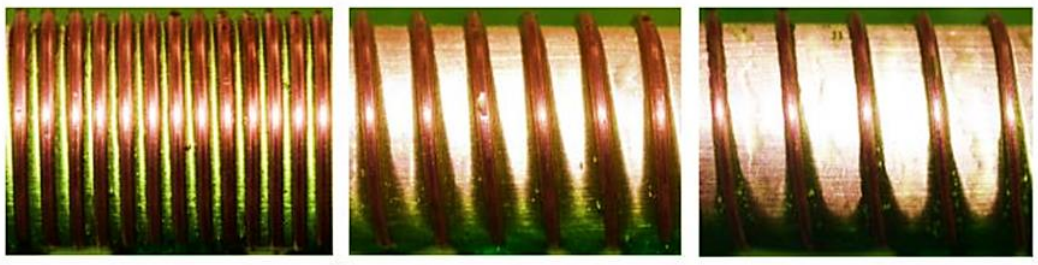

Figure 2.14: The horizontal copper tube with wrapped wires have various pitch dimensions [33].

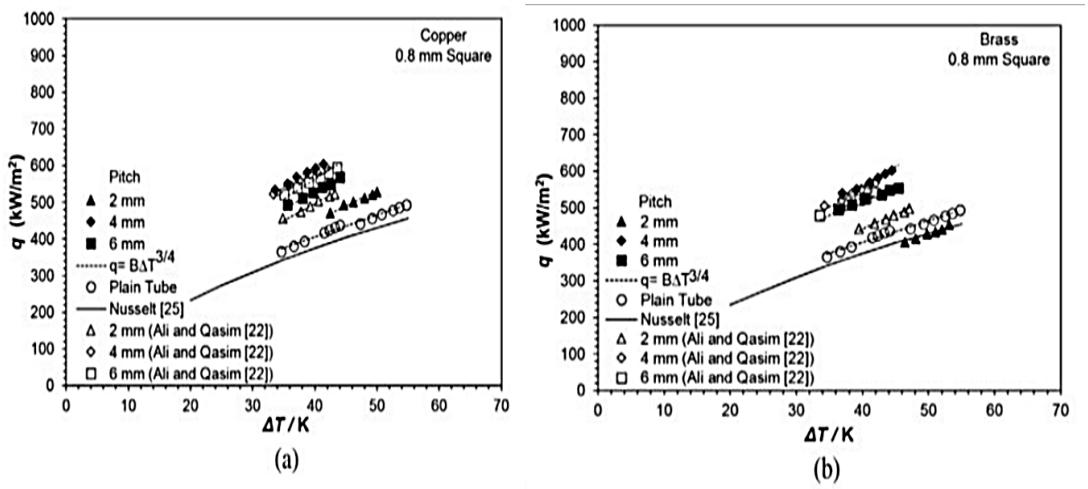

Figure 2.15: Heat transfer rate for wrapped copper tubes with different wire materials at constant wire diameter [33].

2.2.2 Binary vapor mixture effect on dropwise condensation performance

When a binary steam mixture condenses on the solid surface, different modes of condensation is observed and the condensation called Marangoni condensation or pseudo-dropwise condensation. The enhancement of condensation heat transfer using binary fluid depends on the concentration of the mixture and the surface tensions forces differences between the surfaces and condensed steam.

The influence of ethanol steam mixture on condensation heat transfer on copper block was studied [34]. The effect of two concentration range of ethanol is 1%, and 6% were discussed respectively on heat transfer rates. The velocities of binary fluid were 0.4 m/s and 1.5 m/s steam during condensation. The effect of ethanol concentration on the condensation phenomena and performance was obvious where the optimum concentration was found in this study. The increase in the heat transfer rate comes from increasing in surface tension gradient differences between the surfaces and condensed steam. The condensation heat transfer rate for mixture steam was 2-8 times higher than condensation for pure steam.

The influence of temperature gradient on Marangoni condensation heat transfer of water-ethanol mixture on copper plate was discussed experimentally [35]. A diverse range of ethanol concentrations was used under various steam pressure and velocities. The difference in the temperature gradient causes a difference in the film thickness and then significantly affects the thermal resistance during condensation. The highest performance of condensation heat transfer rate was obtained at low ethanol concentrations. The heat transfer rate for Marangoni condensation was lower than condensation heat transfer for pure steam when the concentration of ethanol is 50%. The improvement in the heat transfer rate was due to the surface tension difference that induced by the temperature difference on the surface. Moreover, the steam pressure and steam velocity have a significant influence on condensation heat transfer at different ethanol concentrations. Figure 2.16 shows the effect of steam pressure and steam velocity on condensation heat transfer rate at various ethanol concentrations.

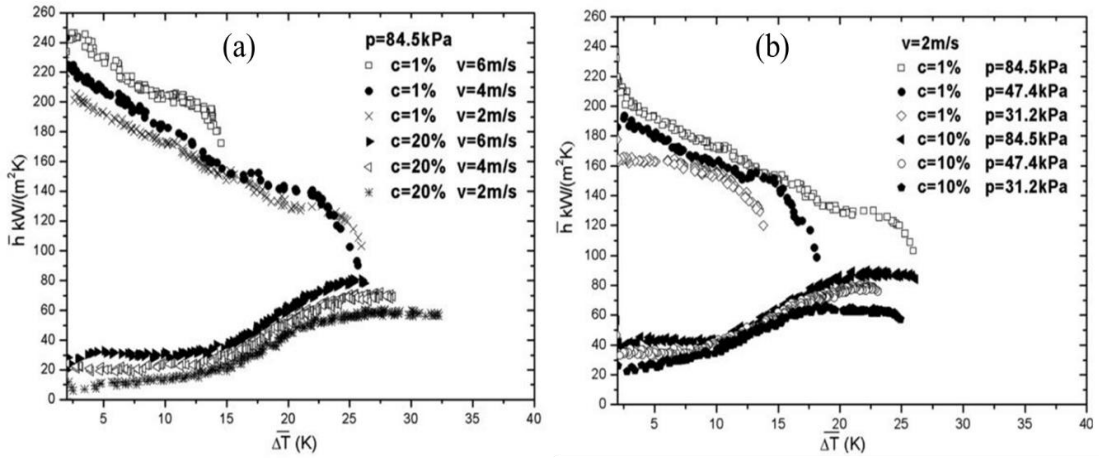

Figure 2.16: The influence of steam pressure and steam velocity at different ethanol concentration (a) The effect of pressure (b) The effect of steam velocity [35].

Condensation of binary steam on horizontal copper tubes at atmospheric pressure has been clarified [36]. The behavior of condensation enhancement on copper tubes was similar as for copper plates, but the difference in detail is found due to the geometry effect on condensation flow and fluid properties. The effect of ethanol concentration was investigated where the heat transfer rate increases with increasing the range of ethanol concentrations. The heat transfer rate is improved when the concentration of ethanol 1% compared to 0.05% concentration. Figure 2.17 shows the heat transfer rate enhancement for different ethanol concentrations. The improvement in the heat transfer came from the effect of different of surface tension forces between the condensing steam and the surface.

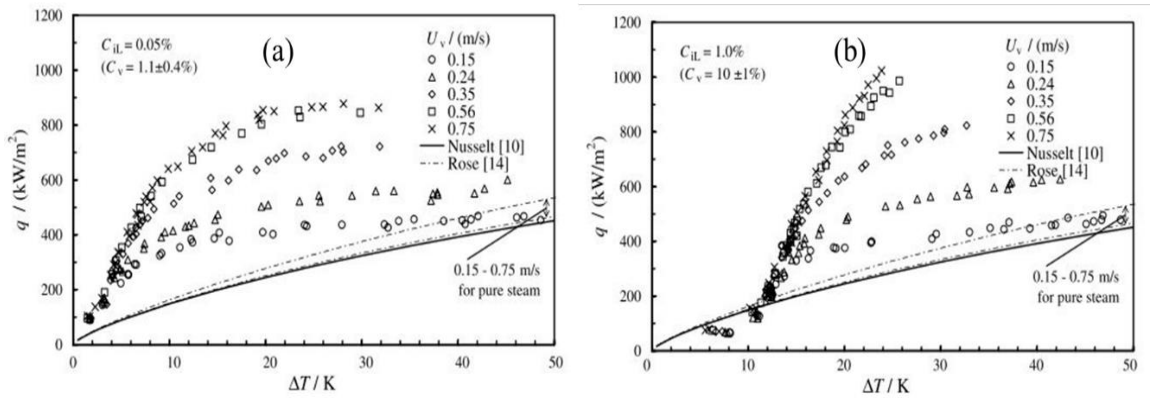

Figure 2.17: The heat transfer rate enhancement for various ethanol concentrations. (a) 0.05 % ethanol concentration (b) 1% ethanol concentration [36].

Condensate of a mixture of water-ethanol vapor on the vertical flat plate can enhance condensation heat transfer compared to the condensate of pure steam [37]. The condensation phenomenon was completely filmwise for pure steam as shown in Figure 2.18 at various temperature differences. However, dropwise condensation can be achieved when the mixture of water-ethanol as a vapor was used. The droplets distribution and their volume depend mainly on the concentration of ethanol. The condensation translated to be filmwise when the ethanol concentration further increases. The heat transfer rate was enhanced 50% compared to pure stem when 20% ethanol concentration is applied. In addition, the effect of steam pressure and steam velocity was investigated. Figure 2.19 shows the effect of steam velocity and pressure on condensation heat transfer at various ethanol concentrations. The condensation heat transfer increases with increasing the steam velocity due to the reduction in the diffusion resistance for steam and reducing the thermal resistances. The pressure has a significant influence on the performance of condensation heat transfer for mixture steam. The heat transfer rate improved with increasing the steam pressure because the droplets falling speed was fast and the condensation rate became strongly high at high steam pressure.

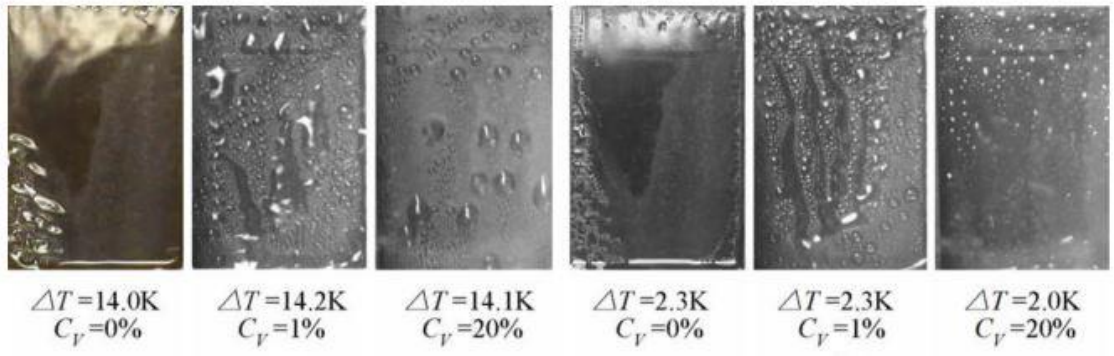

Figure 2.18: The condensation phenomena for pure steam and different concentrations of a mixture of steam at same temperature differences [37].

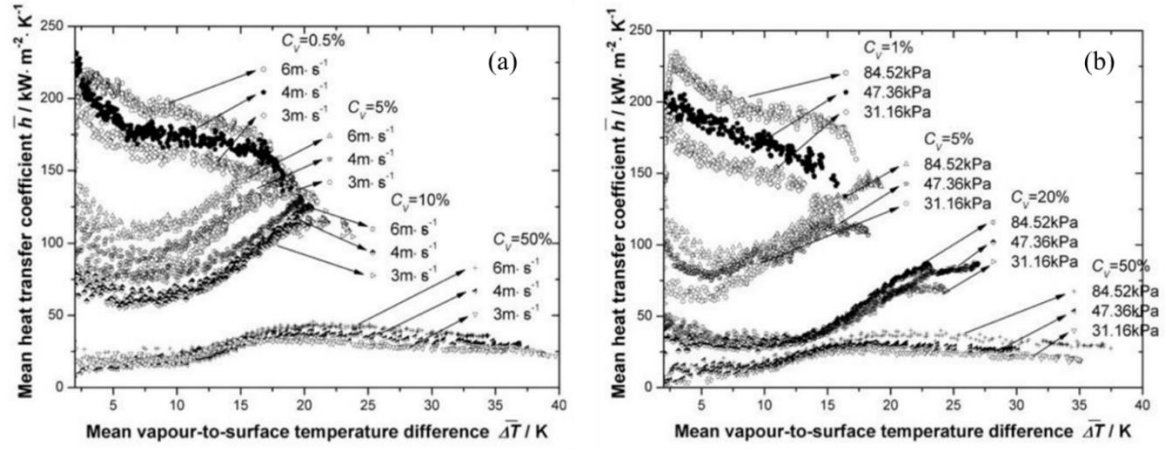

Figure 2.19: The effect of steam velocity and pressure on condensation heat transfer at various ethanol concentration. (a) Effect of steam velocity (b) Effect of steam pressure [37].

Dropwise condensation can be enriched by changing the condensing's steam properties using mixture working fluid [38] at atmospheric pressure. The condensation mode was filmwise, and then the condensation mode was varied with a variation of mixture composition of steam. Complete dropwise condensation was obtained at 0.17 volume fraction of ethanol. The transition of condensation modes from filmwise condensation to dropwise condensation is caused by the surface energy differences which was due to changing ethanol volume fraction. The effect of surface energy on

condensation phenomena and performance with the steam-ethanol mixture is monitored as shown in Figure 2.20. The increasing of surface energy difference speeds the transition from filmwise to dropwise condensation modes and improves the heat transfer rate.

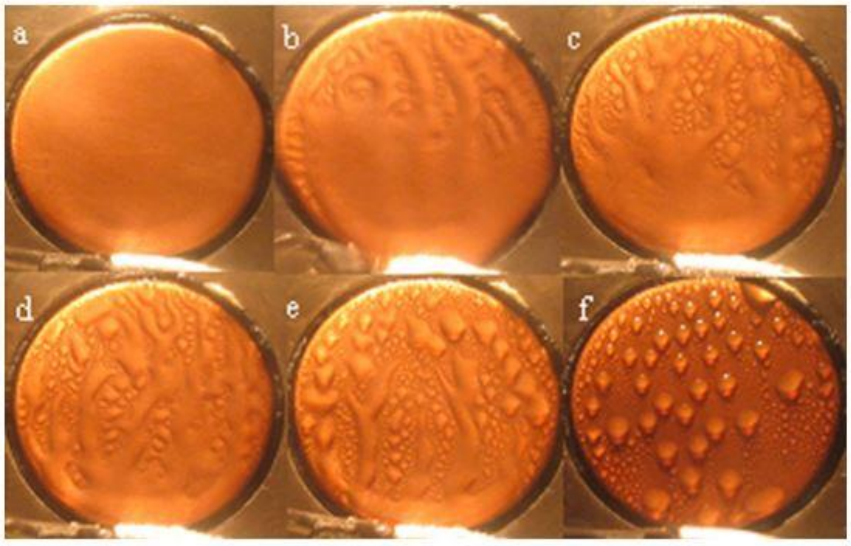

Figure 2.20: The effect of surface energy on condensation performance for the steam-ethanol mixture (a) Filmwise condensation (b-e) Transition state from filmwise to dropwise (f) Dropwise condensation[38].

2.2.3 Dropwise condensation on modified surfaces using ion-implanted method

Dropwise condensation heat transfer can be achieved and enhanced on different types of surfaces using plasma ion-implanted method. Ion-implanted method decreases the surface energy of the condensing surfaces, reduce the wettability and improve the condensation heat transfer rate. Numerous research boosted heat transfer rate performance of dropwise condensation by reducing the surface energy for condensing surface by using ion-plating and ion-beam mixing [39, 40] on different materials and alloys. The effect of a number of ion-dose and implantation energy on condensation efficiency, the surface energy, roughness, and oxidation were investigated.

Dropwise condensation of saturated steam on vertical aluminum surface using ion beam implantation method was studied [41]. The influence of steam pressure on condensation heat transfer was clarified while the number of ion dose and the implantation energy were maintained the same. The condensation was not completely dropwise from the visualization study as shown in Figure 2.21. The heat transfer rate increases with increasing the steam pressure due to the reducing the thermal resistance that prevents more steam to condense. Figure 2.22 shows the performance of condensation on unimplanted and implanted aluminum surfaces. The enhancement factor of condensation heat transfer was two compared to complete filmwise condensation.

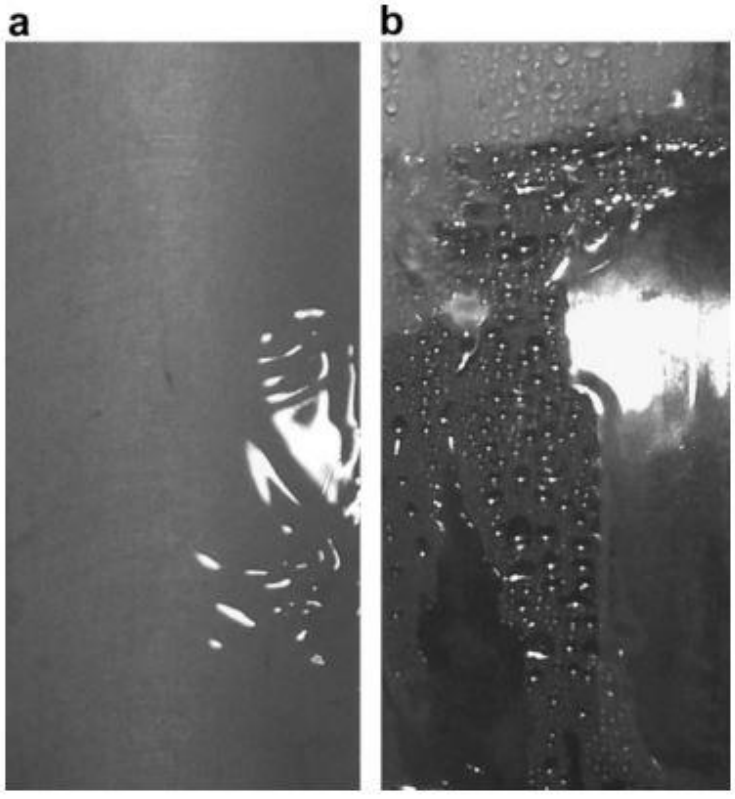

Figure 2.21: The condensation observation on the aluminum surface (a) Filmwise on the unmodified surface (b) Dropwise and filmwise on implanted surface [41].

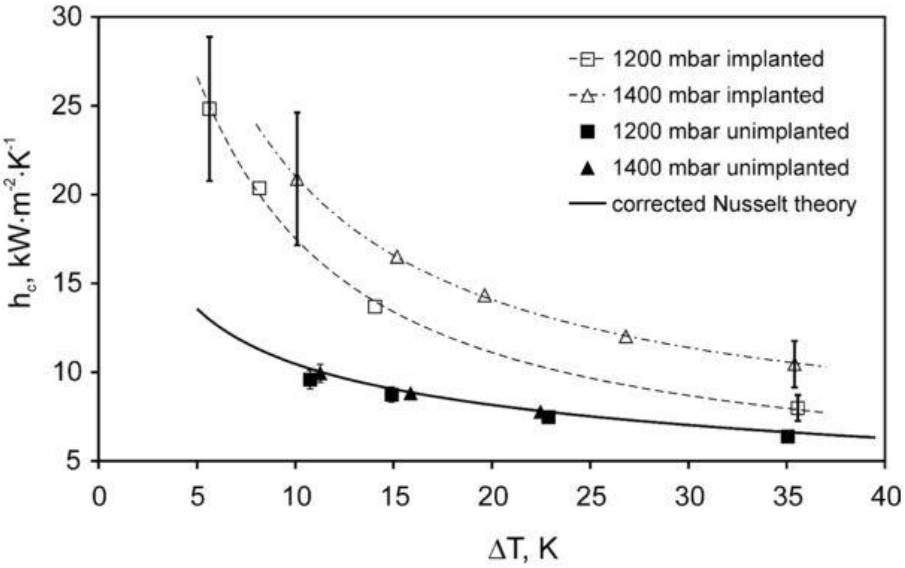

Figure 2.22: Condensation heat transfer rate on unmodified and modified surfaces at different steam pressure [41].

Dropwise condensation was obtained on titanium surfaces using ion beam implantation method at atmospheric pressure [42]. The phenomenon of condensation was completely dropwise, but it transforms to mixed filmwise and dropwise condensation after a long time of condensation. The influence of the number of ion dose and the implantation energy on condensation heat transfer performance was investigated. The visual observation for condensation is shown in Figure 2.23 for a different number of ion dose and implantation energy. The results show that the heat transfer rate for modified surfaces using ion beam implantation is 5.5 times compared to filmwise condensation model. In addition, the influence of the number of ion dose did not significantly affect the performance of condensation. The effect of ion dose numbers on condensation heat transfer rate is shown in Figure 2.24.

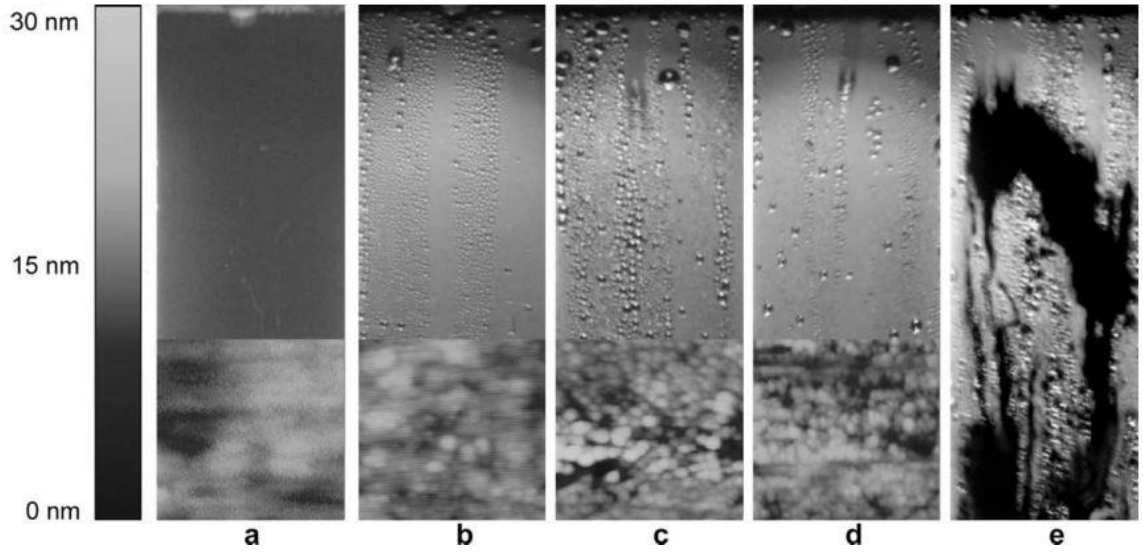

Figure 2.23: Condensation observation on titanium surfaces (a) Pure titanium (b) 10^{16} ion dose and 20 Kev implantation energy (c) 10^{16} ion dose and 60 Kev implantation energy (d) 10^{15} ion dose and 20 Kev implantation energy (e) 10^{15} ion dose and 60 Kev implantation energy [42].

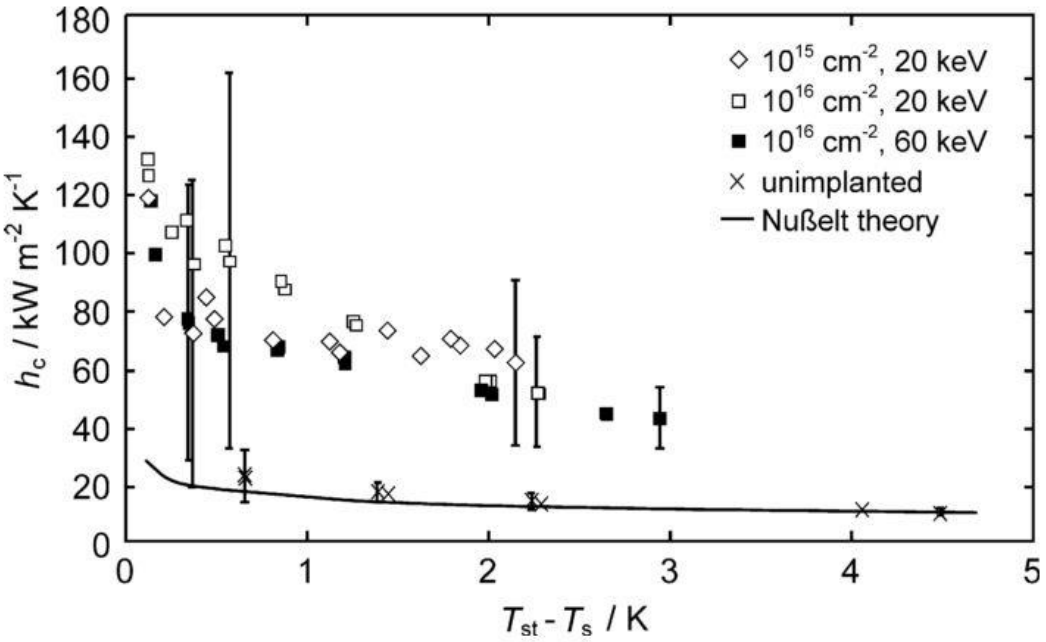

Figure 2.24: The influence of the number of ion dose and implantation energy on condensation heat transfer rate on titanium surfaces [42].

The influence of the number of ion dose on the heat transfer for dropwise condensation on stainless steel tubes is discussed [43]. The phenomenon of condensation

was completely dropwise when ion dose applied on the tube. Figure 2.25 shows the condensation phenomena on the bare stainless steel tube and modified tube with ion beam method. The heat transfer rate for dropwise condensation is three times higher than filmwise condensation model. Increasing the ion does improve the performance of the condensation heat transfer rate because it reduces the surface free energy and wettability of the surface. Figure 2.26 shows the influence of ion dose on the condensation efficiency compared to Nusselt theory where the slight effect of ion dose on condensation heat transfer was clarified.

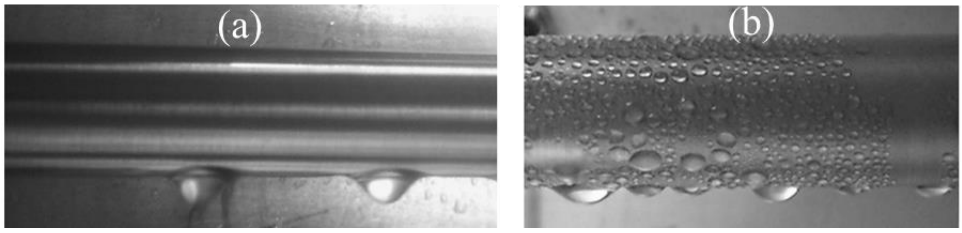

Figure 2.25: The condensation phenomena on the (a) Bare stainless steel tube (b) Modified tube with ion beam [43].

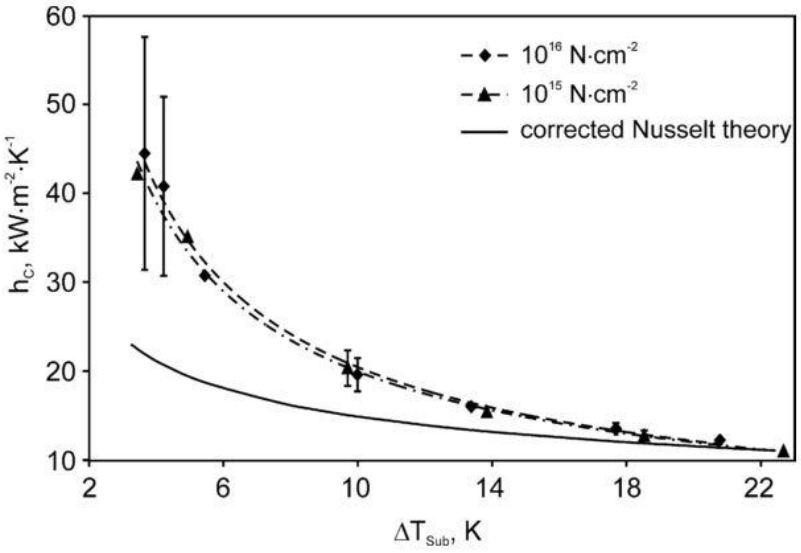

Figure 2.26: The effect of Ion Dos on the performance of dropwise condensation heat transfer rate [43].

2.2.4 Condensation on surfaces that have hydrophobic coating

Dropwise condensation can be obtained by coating the condensing surface using hydrophobic coatings because they reduce surface wettability, improve droplet departure frequency, and enhances the condensation heat transfer rate. An excellent dropwise condensation on vertical copper tubes at atmospheric pressure was obtained [44]. Condensation surfaces were modified using docosanoic acid SAM and electroless Ni-P-PTFE coatings. The condensation on SAM surface was completely dropwise, and the heat transfer rate for the surface was higher than the filmwise model. From visual observations, the droplet sizes were small and the roll off fast from the surface due to the low surface energy of condensing surface. The enhancement is mainly caused by decreasing the thermal resistance of condensing steam. Moreover, dropwise condensation was obtained on NI-P-PTFE coatings on copper tubes in this study. The high and low contents of NI-P-PTFE were used to improve dropwise condensation performance. The heat transfer rate for SAM coating was greater than NI-P-PTFE coating for both contents. Figure 2.27 shows the improvement of condensation heat transfer compared to filmwise theory. The condensation heat transfer rate was higher than complete filmwise. The heat transfer rate characteristics for high NI-P-PTFE were slightly better than low NI-P-PTFE.

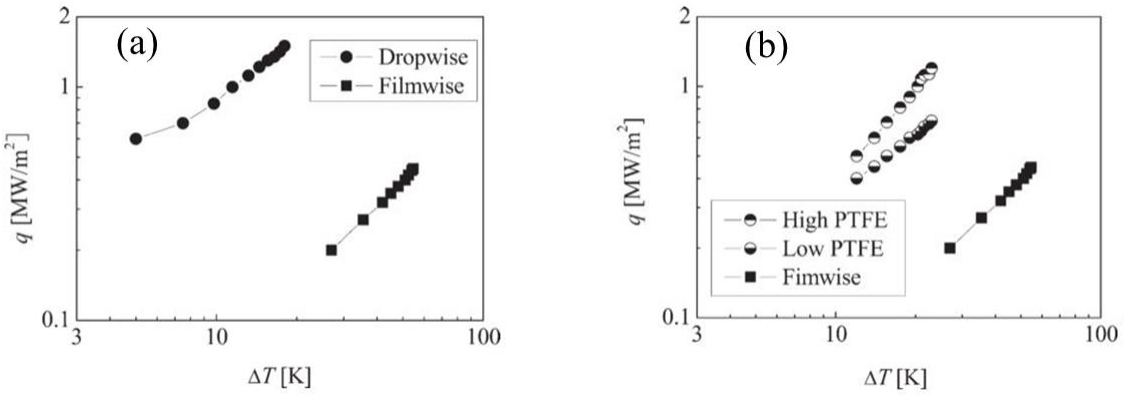

Figure 2.27: Dropwise condensation heat transfer performance compared to filmwise condensation (a) SAM surface (b) PTFE surface [44].

A sustainable and high efficiency of dropwise condensation was obtained on silver coating on copper surface with n-Heptane surfactant additives [45]. The concentration of surfactant additives was changed from 0% to 2% to study its influence on dropwise condensation performance. Figure 2.28 clarifies the heat transfer rate for bare copper tube and modified copper tube at various heptane additives concentrations. The heat transfer rate, therefore, was 50% higher compared to the bare copper tube. The durability of dropwise condensation was studied. The heat transfer and long-lasting condensation were found increased with increasing n-Heptane concentration. The optimum additives concentration that influences the heat transfer performance was existing in this study.

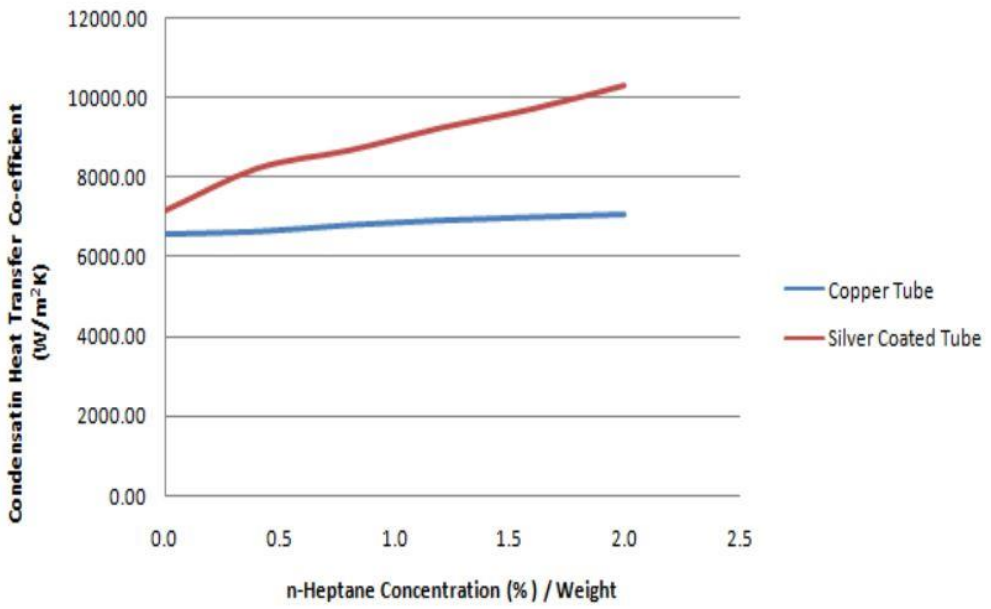

Figure 2.28: Enhancement of condensation heat transfer for bare copper tube and modified copper coated with silver at various n-heptane concentrations [45].

A study of condensation heat transfer was achieved on hydrophobic coatings which modified on copper surfaces using SAM1 and SAM2 coatings at atmospheric and vacuum conditions [46, 47]. The wettability properties and contact angle measurements were calculated before and after the condensation experiments for both surfaces. The contact angle measurements for SAM2 surface after the test was dramatically lower than the contact angle before the experiment. The contact angle measurements for the surfaces is shown in Figure 2.29 before and after the condensation tests. The performance of heat transfer for SAM1 was 3-8 times higher compared to filmwise theory at vacuum and atmospheric pressure conditions. However, the condensation performance of SAM2 coating was not qualified for enhancing condensation efficiency where its performance is almost the same with filmwise theory. The condensation heat transfer rates for the surfaces is shown in Figure 2.30 under vacuum and atmospheric pressure conditions. The

bonding of SAM2 coating on the surface was not strong enough to obtain a good dropwise condensation.

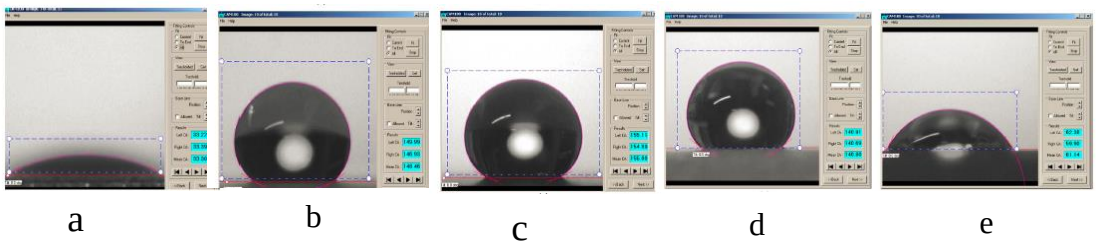

Figure 2.29: Contact angle measurement before and after the experiment. (a) bare copper tube (b) SAM1 before experiment (c) SAM2 before experiment (d) SAM1 after experiment (e) SAM2 after experiment [46].

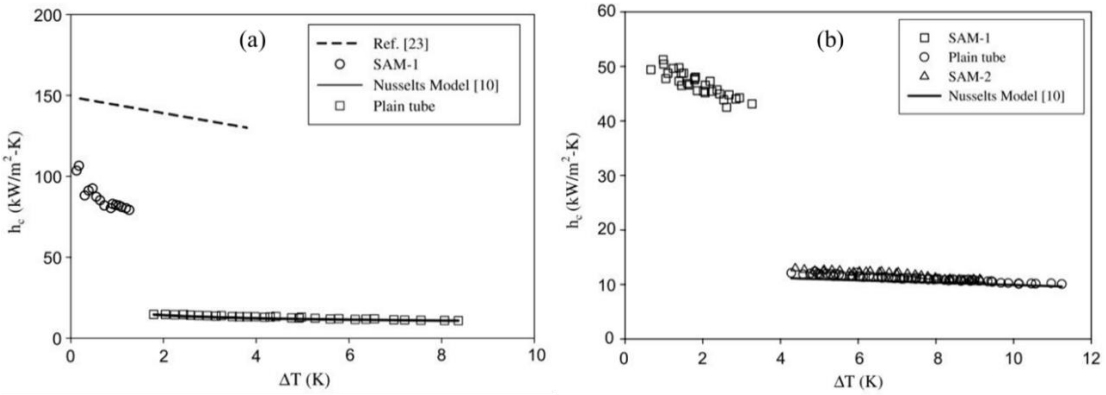

Figure 2.30: The heat transfer rate for SAM1 and SAM2 at (a) Atmospheric pressure (b) Vacuum pressure [46].

Limiting the growth rates of large droplets on condensing surfaces significantly enhances the performance of droplets departure frequency and heat transfer rate during dropwise condensation [48]. The hydrophobic coatings of the self-assembled silver SAM, super hydrophobic coating of PTFE (polyphenylene), and PPS (polyphenylene) were applied on copper tubes. The experimental investigations during condensation were under vacuum conditions. The superhydrophobic coating achieved poor condensation compared to the hydrophobic SAM coating. The condensation phenomena for all surfaces were

shown in Figure 2.31. All the modified surfaces show dropwise condensation, but the droplets size and population of droplets on the surfaces were different. Only SAM coating provides different behaviors of condensation where the droplets roll off fast from the condensation surfaces. The heat transfer rates for all surfaces are shown in Figure 2.32 where the highest heat transfer rate was on SAM surface. The enhancement of condensation rate on SAM surface caused by high nucleation rate, small droplet sizes, and lower thermal resistance compared to other surfaces.

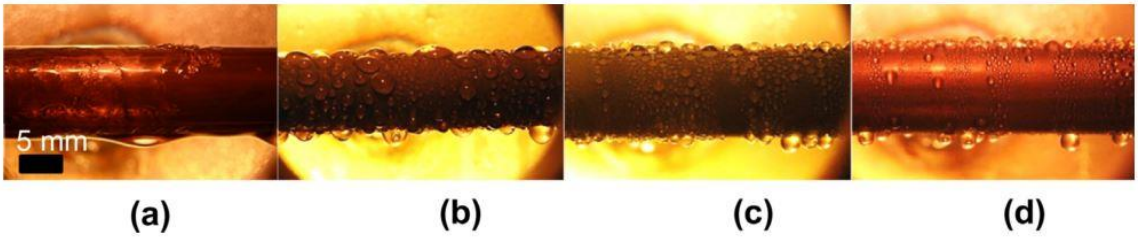

Figure 2.31: Dropwise condensation phenomena on (a) Bare copper (b) PPS coating (c)PTFE coating (d) SAM coating [48].

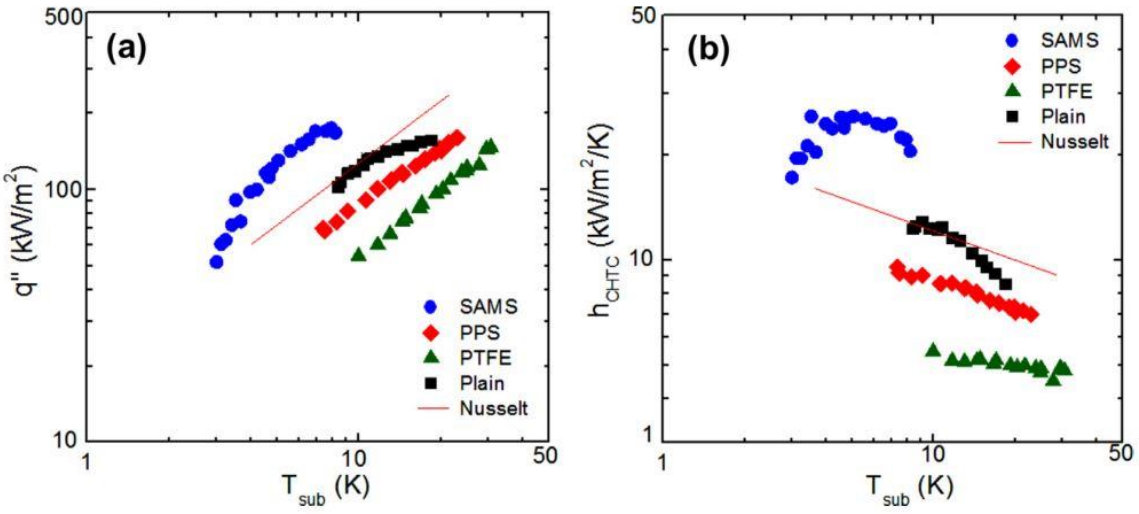

Figure 2.32: Heat transfer performance on various coating compared to filmwise condensation under (a) Atmospheric conditions (b) Vacuum conditions [48].

Dropwise condensation was achieved on iron tubes using Teflon coating [49] at atmospheric pressure. The condensation phenomenon was completely dropwise during the experiment compared to the bare tube. The condensation heat transfer rate increased by 20% to 60% in relation to condensation on the bare iron tube. The visual image of condensation and the improvement in heat transfer rate is shown in Figure 2.33. The transformation of the condensation modes caused by the lower surface energy of the modified surface compared to the pure iron surface.

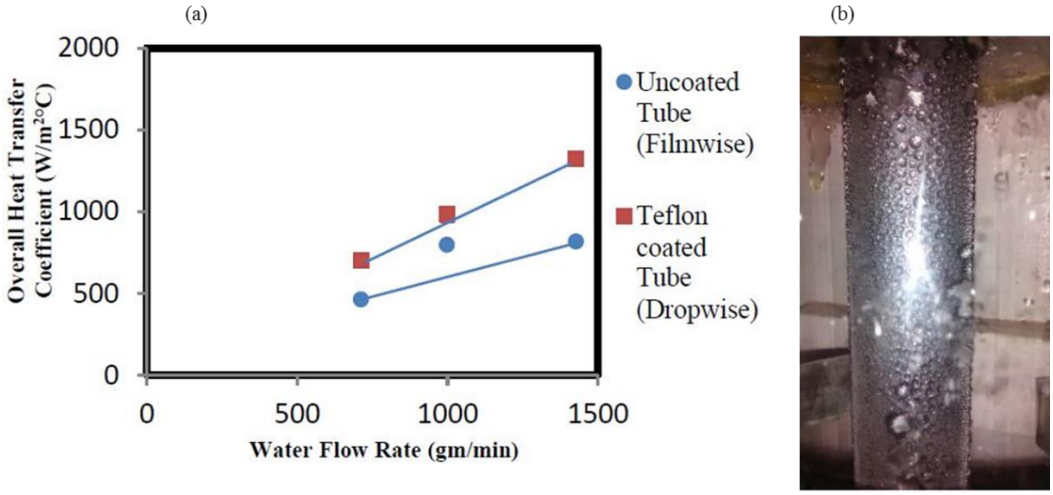

Figure 2.33: (a) Dropwise condensation heat transfer performance on Iron coated with Teflon compared to bare iron. (b) The phenomena of dropwise condensation on the iron tube [49].

Dropwise condensation on carbon steel tube coated using nickel-based coating tube was obtained experimentally [50]. The temperature distribution around the tube was smaller for carbon steel tube compared to modified Ni-based tube as shown in Figure 2.34. The heat transfer performance was 13 times higher than carbon steel tube because of the lower surface energy of nickel-based coated tube. The dropwise condensation can be maintained for a long time. The enhancement in heat transfer rate for Ni- coated surface comes from that the low thermal resistance compared to carbon steel surface.

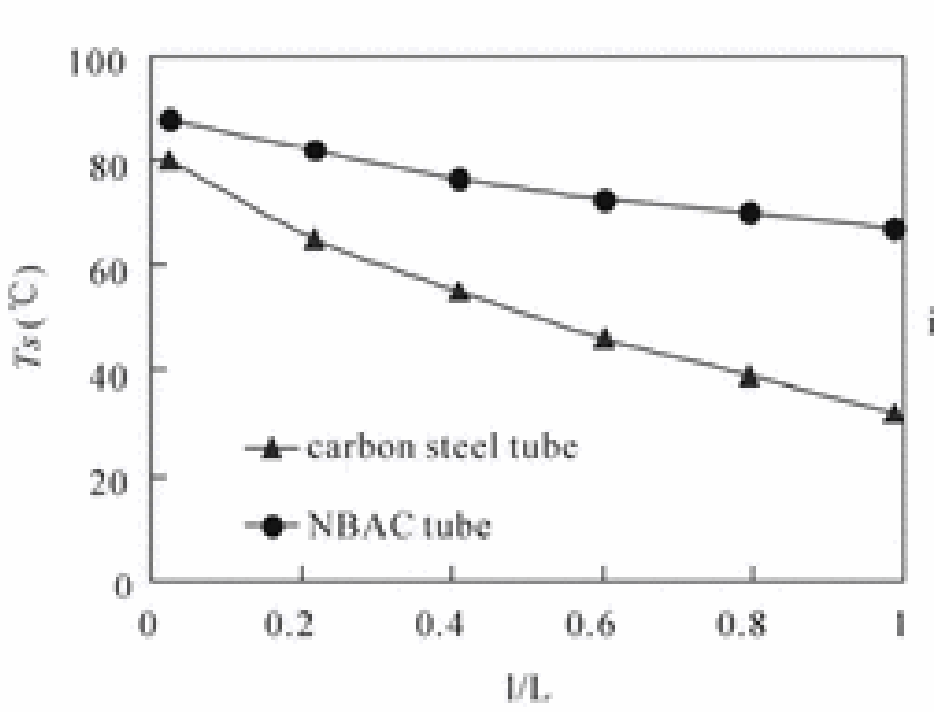

Figure 2.34: The temperature distribution around the tube compared to carbon steel tube compared to the Ni-based tube [50].

Small hanging droplets at the bottom of the condensing tube surfaces can reduce thermal resistance and promote condensation efficiency. Different micro/nanoscale porous surfaces that have different wettability characteristics (PPS, CNT, etched surface and SAM) were tested [51] at atmospheric pressure. The modes of condensation were dropwise for all the surfaces, but the size of condensing droplets beneath the tubes was quietly different. The visualization study of condensation is shown in Figure 2.35. The porous surfaces can reduce the growth of large droplets and then improve the surface renewal rates during condensation. The condensation heat transfer performance of porous surfaces increases with decreasing the size of droplets that hang on the bottom of the tubes. Decrease the droplet's size beneath tubes increases the droplet departure frequencies and reduces the thermal resistances. The heat transfer rates for porous surfaces are shown in Figure 2.36. The condensation heat transfer rates are lower than

complete filmwise on some porous surfaces because of the large thickness of the coating which produces additional thermal resistance and the large droplets size that hanging beneath the tubes.

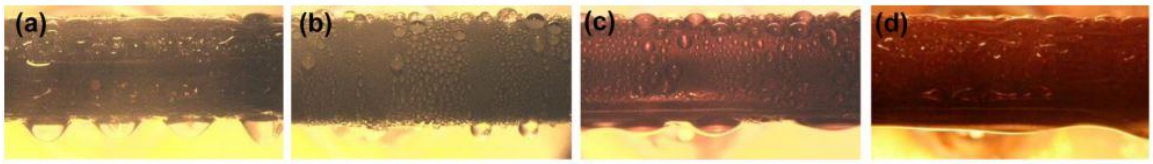

Figure 2.35: Steam condensation phenomena on (a) PPS/CNT (b) PTFE coating (c) SAM coating (d) Etched surface [51].

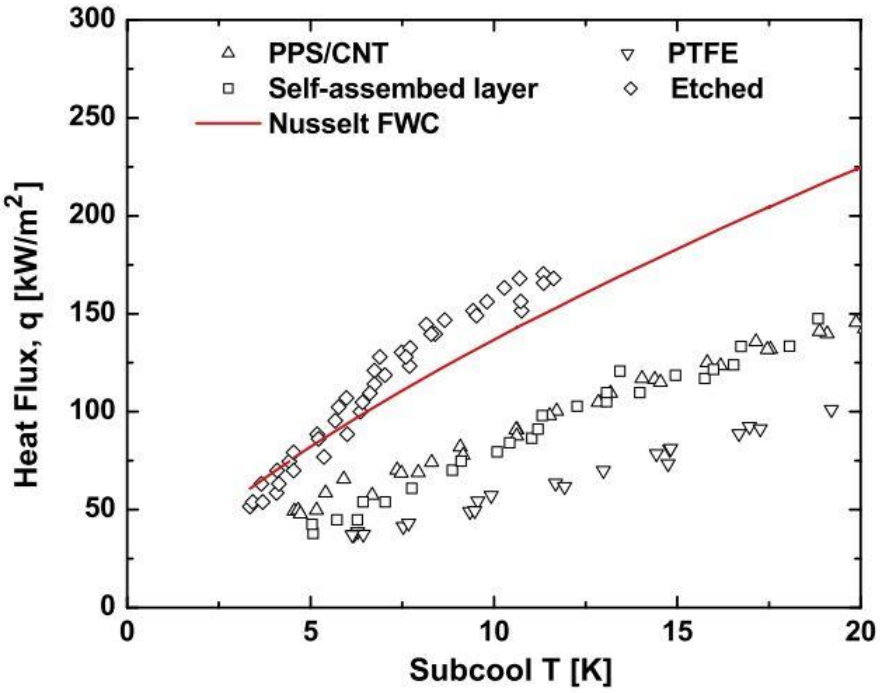

Figure 2.36: Heat transfer rate for different porous tube surface [51].

A hydrophobic and organic self-assembled monolayer (SAM) coating was applied on gold that coated the aluminum surface, copper surface and, (90/10) copper-nickel alloy [52] to verify condensation performance. The condensation experiments were operated under vacuum and atmospheric conditions. The visual observations of

condensation were similar for all surfaces. The condensation heat transfer rate was enhanced for all surfaces compared to filmwise condensation model. The performance of condensation on copper and copper-nickel alloy were the highest because the droplet sizes were smaller than other surfaces. Figure 2.37shows the heat transfer rates for all surfaces under vacuum and atmospheric pressure conditions. The heat transfer rate was enhanced by 14 times than filmwise for copper and copper-nickel alloy and nine times for gold –coated aluminum.

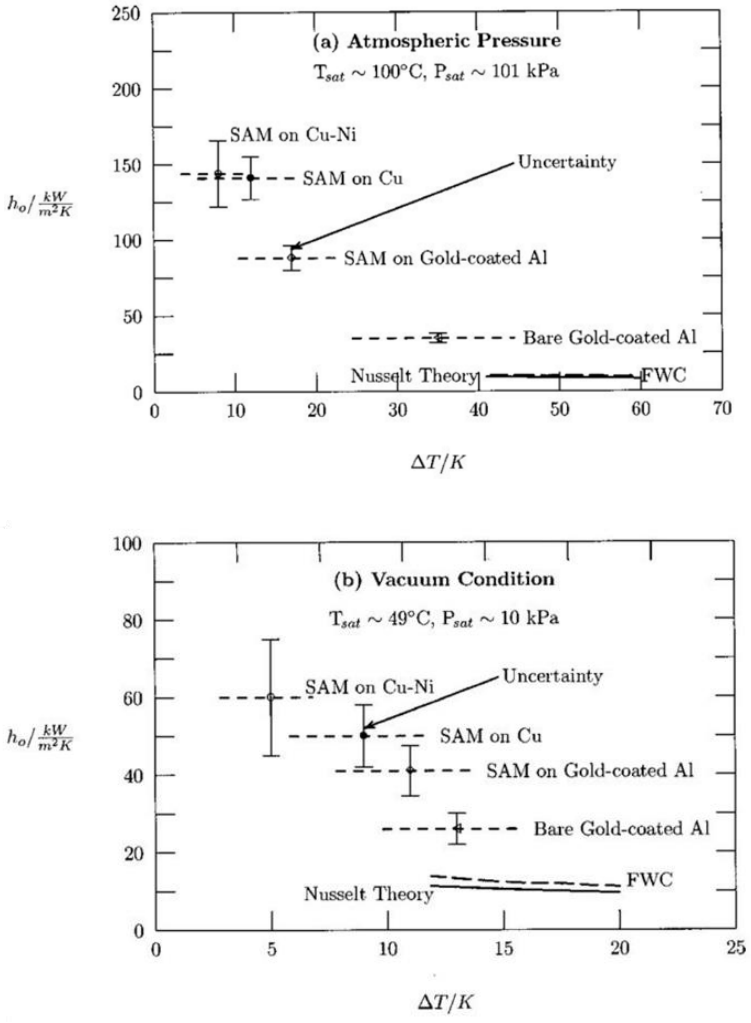

Figure 2.37: Heat transfer enhancement under (a) Atmospheric and (b) Vacuum conditions [52].

A durable dropwise condensation of steam was obtained on electroplated silver surface [53] at atmospheric pressure. The plating thickness was changed until the optimum thickness that enhances condensation heat transfer rate was found. The condensation behavior was dropwise, and its durability depends on the thickness of the coating. The influence of the coating thickness on condensation heat transfer is shown in Figure 2.38a. The condensation phenomenon is shown in Figure 2.38. The dropwise condensation can last for 2400h with 300 nm coating thickness.

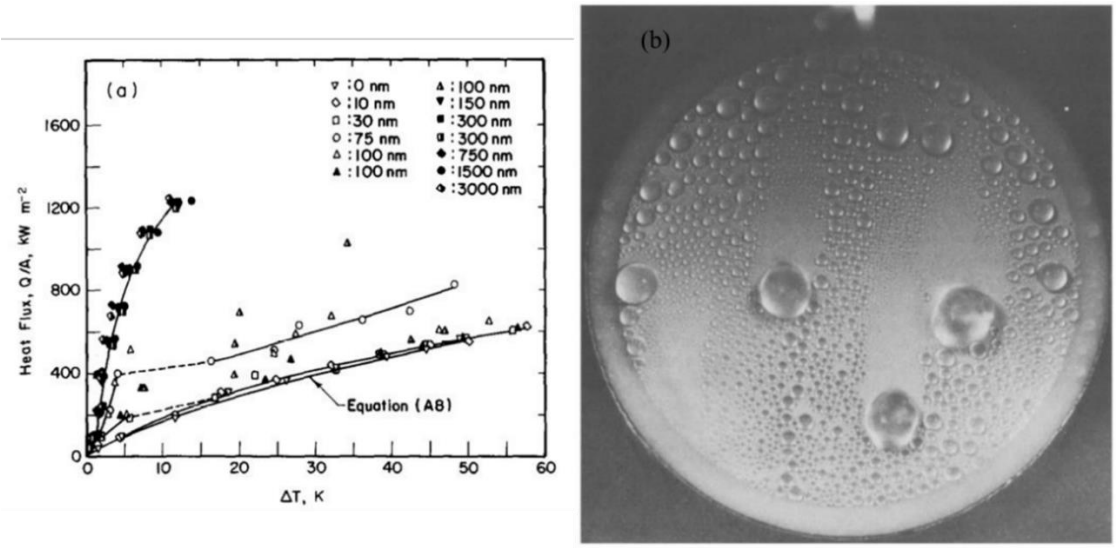

Figure 2.38: (a) Effect of silver coating thickness on heat transfer rate. (b) Dropwise condensation phenomena on silver coating [53].

Dropwise condensation was achieved using chromium coating and oleic acid promoter on the vertical copper surface at atmospheric pressure [54]. In this study, solid chromium coating does not enhance condensation compared to chromium electroplated coating because complete filmwise condensation was obtained on solid chromium surface and oleic acid. However, dropwise condensation is achieved using electroplated chromium surface with oleic acid, but it was lasting for a short time. The condensation

became mixed filmwise and dropwise after 24 hours. Figure 2.39 shows the performance of condensation for chromium coating with oleic acid on the copper surface.

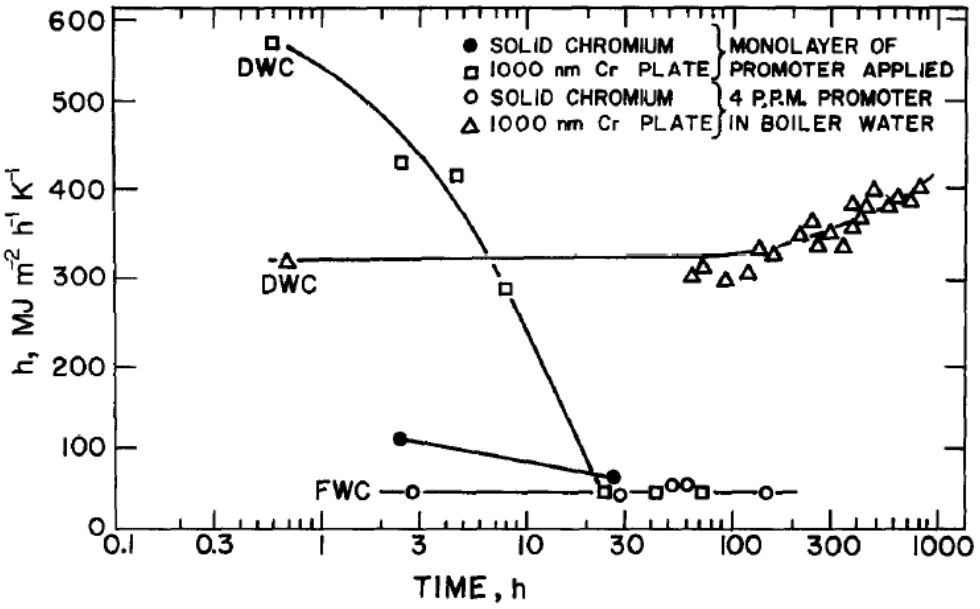

Figure 2.39: The performance of condensation for chromium coating with oleic acid on the copper surface [54].

An excellent dropwise condensation of steam on copper surface which coated by an amorphous hydrogenated carbon (DLC) using chemical vapor deposition CVD coated materials [55]. The dropwise condensation heat transfer for modified surface enhanced by 11 times than filmwise condensation when the contact angle is 90 degrees. However, both filmwise and dropwise condensation can be observed when the contact angles are 74 degrees. The heat transfer rate for modified surface is seven times higher than filmwise when the contact angle is 74 degrees. The increase in the heat transfer rate comes from surface characteristics and their wettability effect. Figure 2.40 shows the condensation heat transfer performance on modified copper surfaces.

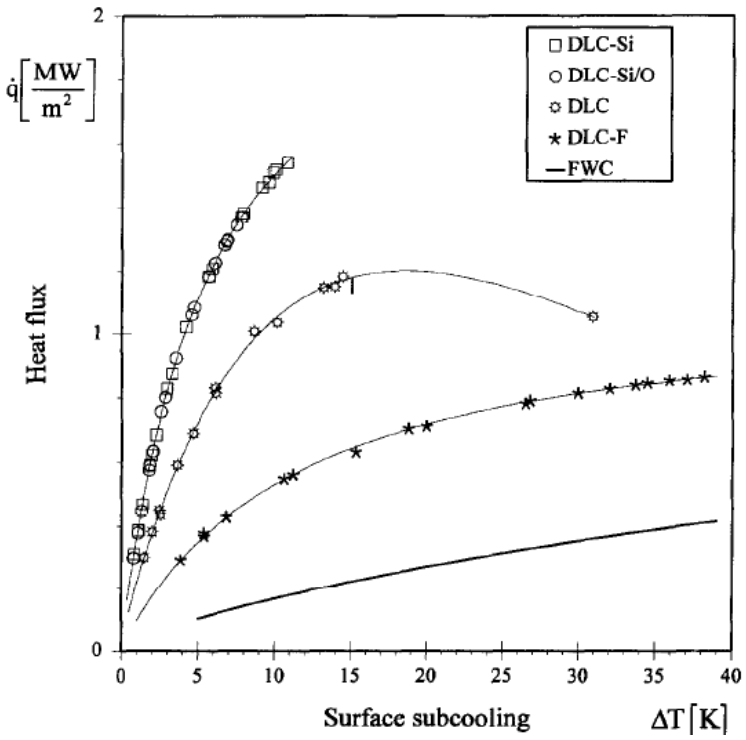

Figure 2.40: Heat transfer rate for dropwise condensation on different coatings on copper compared to filmwise condensation [55].

2.2.5 Dropwise condensation heat transfer versus wettability

The low surface wettability promotes the droplet departure frequency and condensation heat transfer since the steam condenses as droplets on the low wettability surfaces. However, some of the condensing surfaces which have low wettability in the air environments turn to high wettability in the condensation environments. Numerous methods were analyzed and studied the effect of surface wettability on condensation phenomena and heat transfer performance.

Condensation heat transfer on modified and unmodified vertical titanium surfaces was discussed [56]. Both dropwise and filmwise condensation was existing on the unmodified titanium surface where the filmwise region flowed down in the form of rivulets while the droplets were sucked into the rivulets before they grow to the departure

size. The heat transfer decreases with increasing the area of the rivulets, but it is still higher than complete filmwise condensation. Then, the titanium surface was modified using chemical etching process, but the contact angle was small, and the condensation was completely filmwise. However, dropwise condensation obtained on titanium surface after treating the surface chemically with 30wt% hydrogen peroxide solution. The condensation phenomena for the unmodified and the modified surfaces are shown in Figure 2.41. The heat transfer rate for the unmodified surface was little higher than filmwise theory. However, the heat transfer rate for modified surface with etching process was the same performance as filmwise condensation theory. The significant influence on the heat transfer rate on the modified surface with hydrogen peroxide solution was obtained. The highest performance for condensation heat transfer was obtained on the modified surface with hydrogen peroxide solution compared to compete filmwise condensation. Figure 2.42 shows the performance of condensation on the modified and unmodified titanium surfaces.

Figure 2.41: Condensation phenomena on (a) Unmodified surface mixed filmwise and dropwise. (b) Modified surface using etching process complete filmwise. (c) Modified surface using chemical treatment complete dropwise [56].

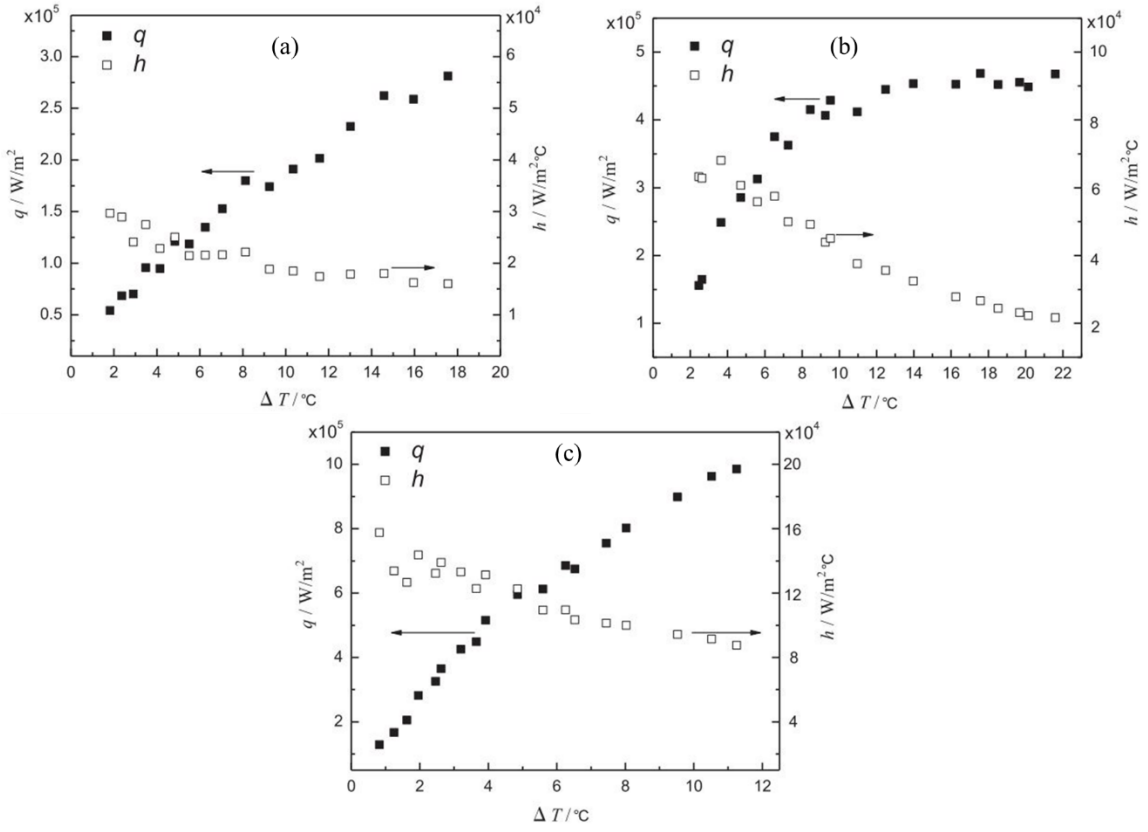

Figure 2.42: Condensation heat transfer rate on (a) Unmodified surface mixed filmwise and dropwise. (b) Modified surface using etching process complete filmwise. (c) Modified surface using chemical treatment complete dropwise [56].

Moreover, droplet surface tension forces affect dramatically the droplet departure frequency and heat transfer rate during condensation [57]. The condensation phenomena for various droplet surface tension forces on three types of modified silicon omniphobic surfaces was discussed. The surfaces are smooth oleophobic (fluoro silane) surface, re-entered superomiphobic surface and lubricant-impregnated surface (nano-LIS). Depending on the surface free energy and the value of liquid's surface tension, some surfaces enhance dropwise condensation for different kinds of droplet surface tension while some surfaces became flooded and reverted to filmwise The enhancement of heat transfer rate on modified surfaces was eight times compared to bare silicon surface. Figure 2.43 shows the enhancement of condensation on different types of fluid. The

declining in the performance of condensation heat transfer rate caused by the increase in thermal resistance due to the flooding of condensing steam on the surface.

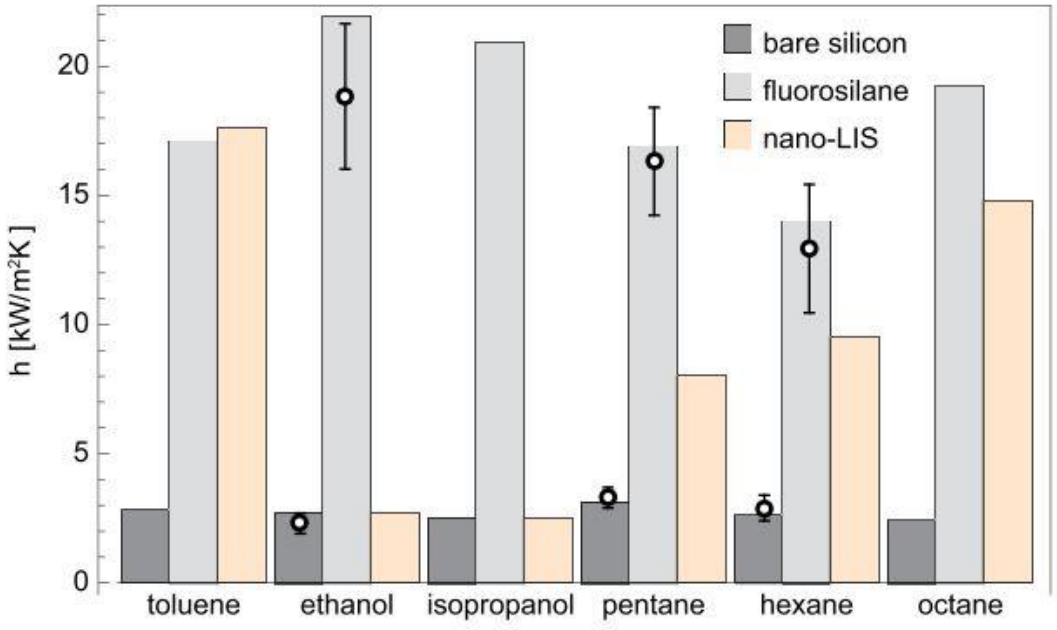

Figure 2.43: The enhancement of condensation heat transfer for various types of fluid on different modified surfaces [57].

The influence of roughness, wettability and contact angle hysteresis of the polymeric surface on droplet size and condensation rate was experimentally evaluated during dropwise condensation [58]. Five polymer surfaces which have different roughness have been tested. The results show that the roughness and contact angle hysteresis affect the droplets nucleation, droplets growth efficiency, and condensation rate significantly at the beginning of condensation. However, the droplets size and the surface flooding increase with increasing the surface roughness. The number of nucleation sites which are generated during condensation was high on high roughness surfaces. However, most of the small droplets pinned by the structure of the rough surface. Then, the droplets sizes increase cover the vast region from the condensing

surface. The influence of surface roughness on the surface flooding and the droplets size during condensation is shown in Figure 2.44.

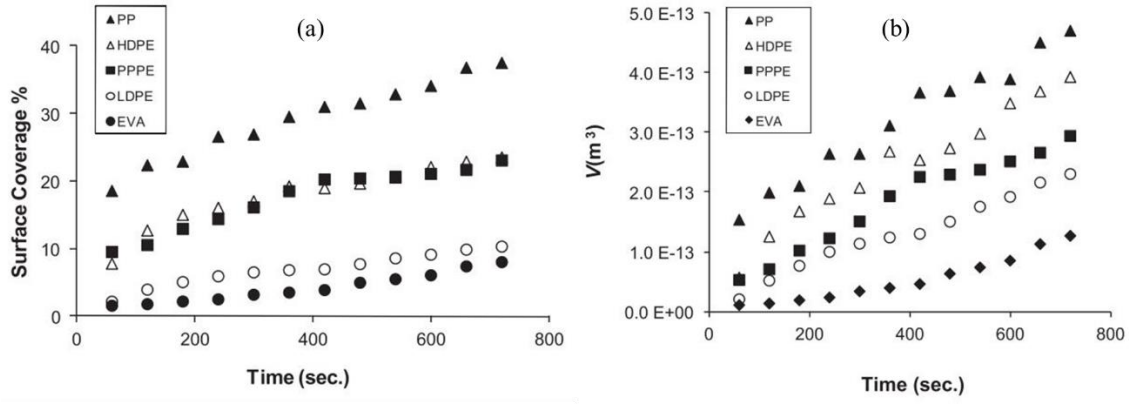

Figure 2.44: The influence of surface roughness on (a) The surface coverage (b) The droplets size with condensation time [58].

The effect of complete and partial titanium coatings on droplets drainage rates and heat transfer performances during dropwise condensation on (PVDF) condenser was investigated [59]. Three condensers have been tested: (i) plain (PVDF), (ii) plain (PVDF) coated using titanium, and (iii) plain (PVDF) partially coated using titanium tracks. The behavior of condensation was dropwise for all the condensers. The condensation phenomena on the three condensers are shown in Figure 2.45. However, the performance of droplets drainage rates and condensation heat transfer rates were completely different. The titanium tracks improve the condensation heat transfer 50% compared to plain (PVDF). The width of the titanium track which promotes the heat transfer rate would be the same of maximum droplets diameter on complete titanium coated condenser.

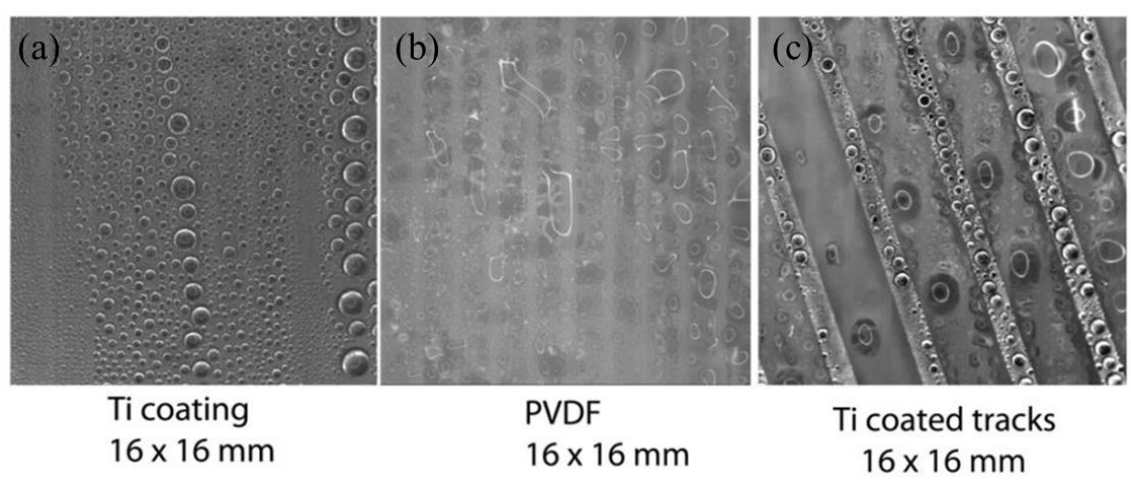

Figure 2.45: The condensation phenomena on the three condensers (a) Complete titanium coating on (PVDF) (b) Plain (PVDF) (c) Titanium tracks coating on (PVDF) [59].

The influence of condensation environment on surface wettability of copper surface and modified copper surface have been explained [60]. The surfaces (bare copper and copper coated with SU-8 (Microchem Permanent Epoxy)) have same wettability behaviors and same contact angles in ambient conditions. However, the surfaces present deferent wetting behaviors and droplets growth in condensation environment. The condensation phenomena are shown in Figure 2.46. Large droplet's sizes grow on bare copper surface, but small droplet's sizes grow on modified copper surfaces during condensation because the bare copper surface has high surface wettability. Due to the change of droplet dynamic during condensation as shown in Figure 2.46, the heat transfer rate is completely different. The copper surface with SU-8 coating has a high heat transfer rate compared to the bare copper surface because the condensed droplets grow faster on modified surface compared to the droplet's growth on bare copper surface. Figure 2.47 shows the heat transfer rate for bare copper and modified copper surfaces.

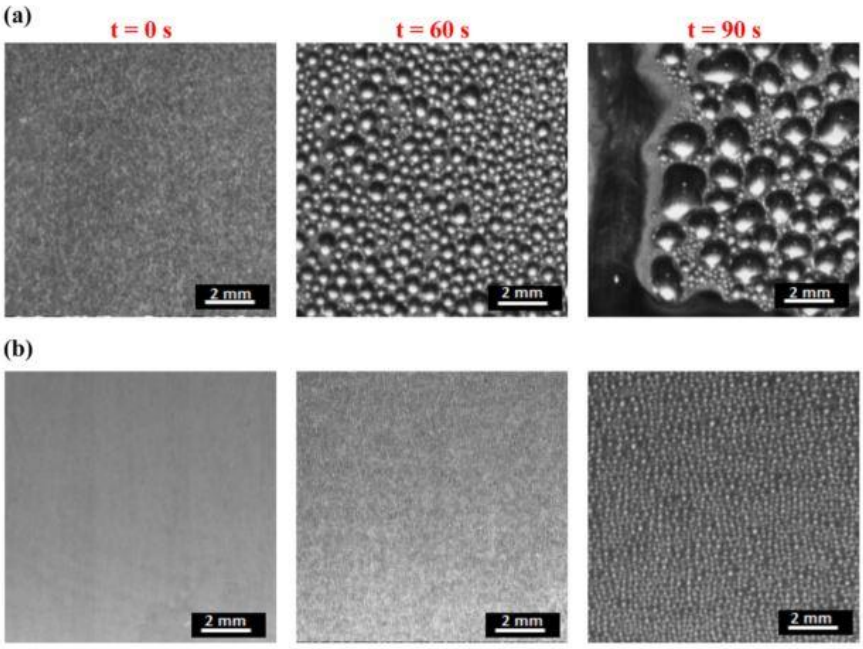

Figure 2.46: Growth rate stages for condensed droplets on (a) Bare copper (b) Copper with the SU-8 coating [60].

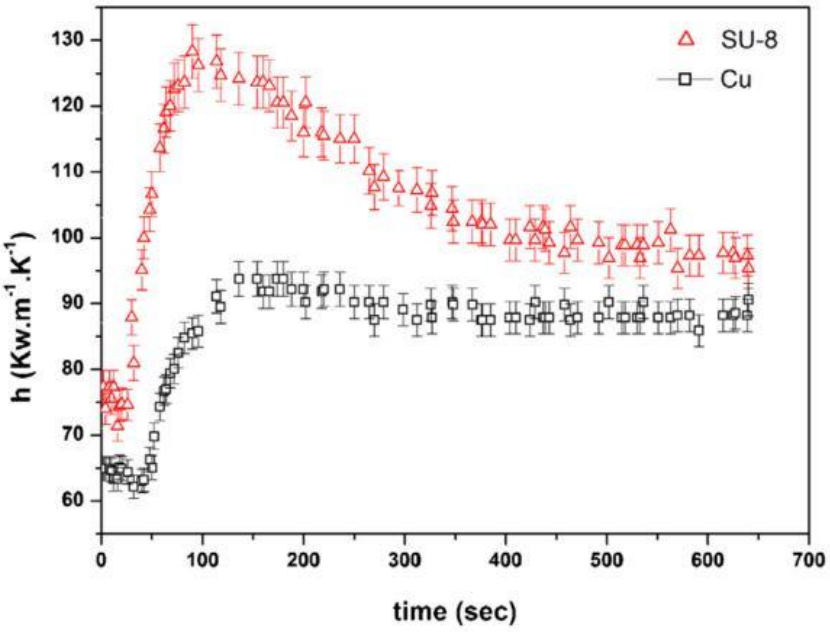

Figure 2.47: Heat transfer coefficient for (a) Bare copper. (b) Copper modified with the SU-8 coating [60].

In addition, the effect of surfaces nanostructures on dropwise condensation heat transfer performance has been experimentally studied [61]. Chemical treatment of self-assembled monolayer SAM was prepared on smooth copper (SAM2) surface and nanostructured copper (SAM1) surface to enhance dropwise condensation. The condensation was dropwise on both surfaces, but the SAM2 surface has lower droplet growth rate than the SAM1 surface. The visual observation of condensation phenomena is shown in Figure 2.48 for both surfaces. The small droplets pinned by the nanostructure of the SAM1 surface and coalescence with other droplets. The large formed droplets size cover large regions on the condensing surface and delay the droplet departure from the surface as shown in Figure 2.48. The heat transfer rate for a smooth surface with SAM1 is higher than nanostructure surface with SAM2 even the surface area of the nanostructure is bigger than a smooth surface. Figure 2.49 shows the heat transfer rate for smooth and nanostructure surface compared to filmwise theory. The heat transfer rate for smooth is enhanced by a factor 3 compared to filmwise while the heat transfer rate for smooth with nanostructure surface is improved by a factor of 1.8 compared to filmwise condensation. The large droplets fill the cavities between the nanostructures and create a liquid film on condensing surface. The liquid film provides thermal resistance which reduces the heat transfer rate and droplet's velocities on the surface.

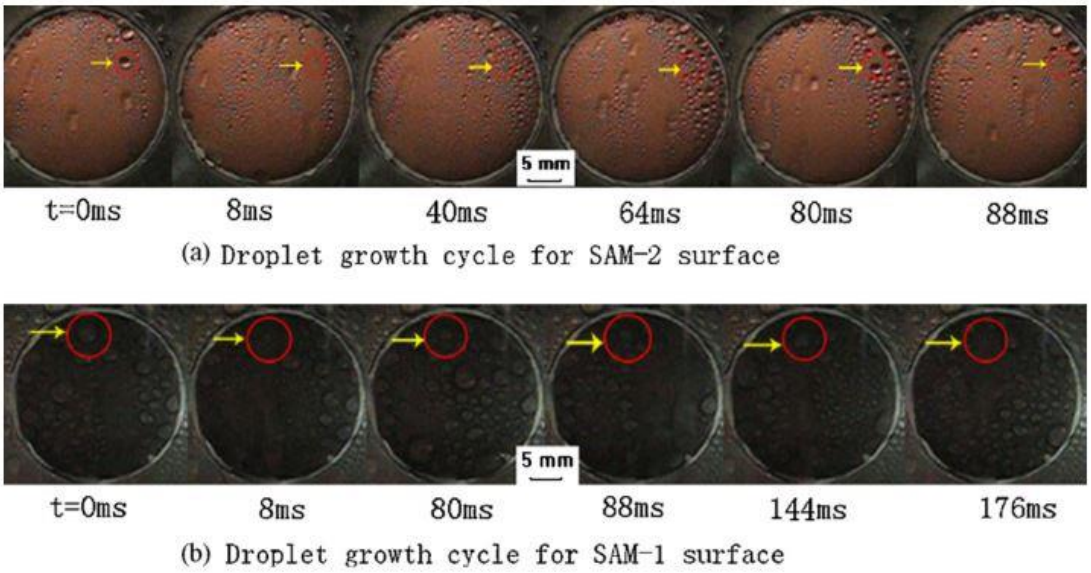

Figure 2.48: Droplet growth cycle during dropwise condensation for both surfaces SAM1 and SAM2 [61].

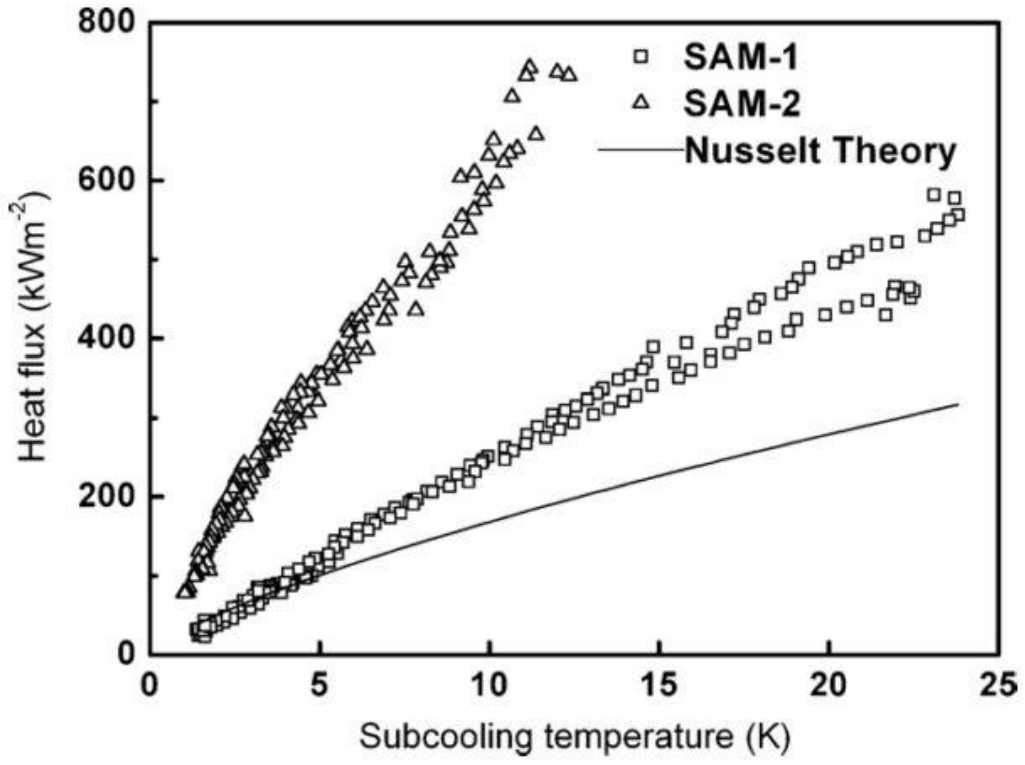

Figure 2.49: Heat transfer rate during dropwise condensation for both nanostructures surfaces SAM1 and smooth SAM2 [61].

2.2.6 Condensation on gradient surfaces

Gradient surfaces improve the droplets removal from the condensing surfaces without depending on the body forces such as gravity. The energy gradient causes a difference in contact angles which increases the droplet's motion and allow condensation for new droplets to condense on the surfaces. Condensing surfaces which have gradient wettability features have a powerful ability to enhance the droplet dynamics and the heat transfer rate for dropwise condensation [62, 63]. Efforts have been taken to fabricate gradient wettability surfaces to increase the droplet velocity and drainage rate during condensation.

Condensation on copper surfaces have gradient wettability characteristics was discussed regard to condensation on complete dropwise surfaces [64]. The influences of surface orientations at different positions were discussed. The gradient of the surface wettability causes the droplets move to the high wettability region without depending on any additional forces. The physical mechanism of droplets movement on gradient surfaces is shown in Figure 2.50. The heat transfer rates were improved for all surface orientations compared to traditional dropwise condensation heat transfers rate. The heat transfer rate for vertical gradient wettability surface is 35% higher than traditional dropwise condensation. Figure 2.51 shows the heat transfer rate on vertical gradient surface compared to filmwise and dropwise condensation surfaces. In addition, the heat transfer rates for gradient surfaces still gives a high performance for both horizontal and against the gravity direction.

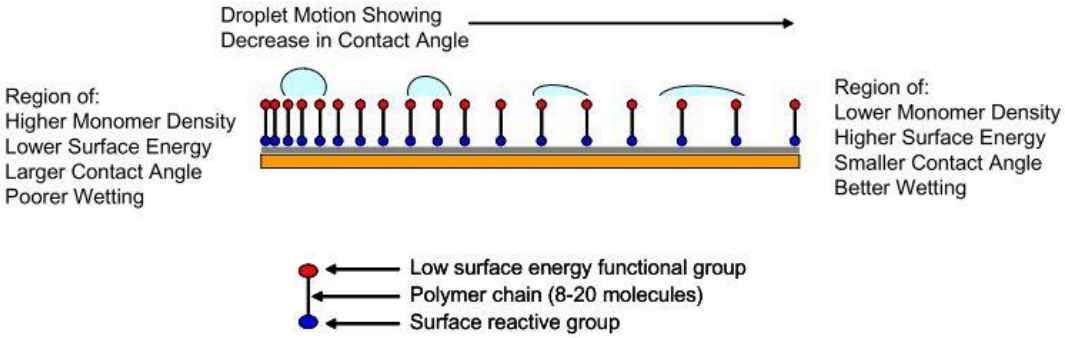

Figure 2.50: The physical description on how the droplet's motion on graded wettability surface [64].

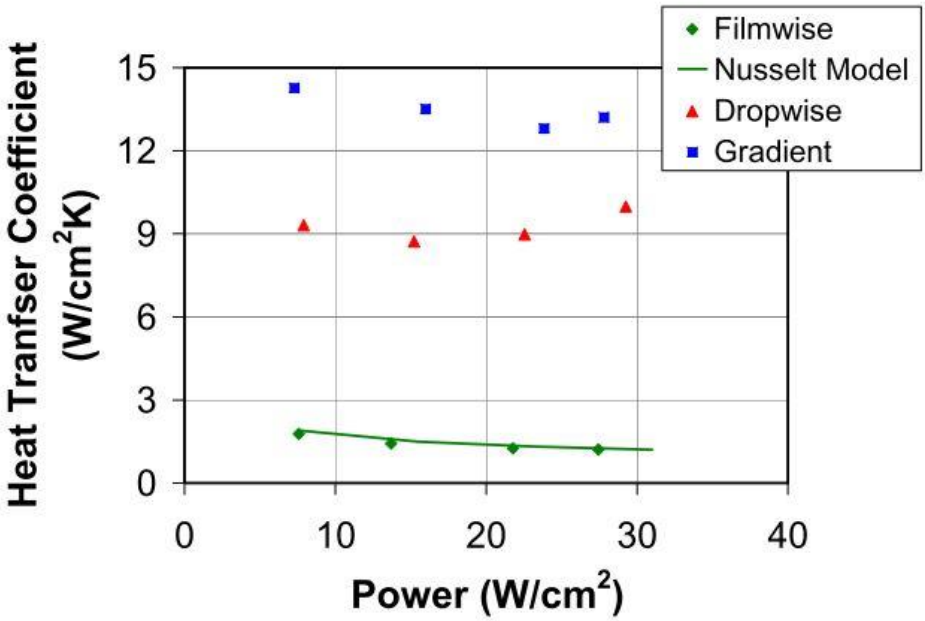

Figure 2.51: Heat transfer rate on vertical gradient surfaces compared to complete filmwise and traditional dropwise surfaces [64].

Wettability gradient was applied on copper surfaces to predict the improvement of droplets dynamics behavior during condensation [65]. The velocity of droplets on condensing surfaces was improved by enhancing the coalescence of droplets on gradient surfaces. However, the gradient wettability reduced the condensation performance due to the thermal conduction that caused by the liquid film from the hydrophilic side.

Figure 2.52 shows the droplets dynamic mechanisms on gradient regions. The attention should be taken to remove the droplets while they are small on the gradient surfaces to reduce the thermal resistance. Then, the liquid film thickness reduced and the heat transfer rate improved on gradient surfaces.

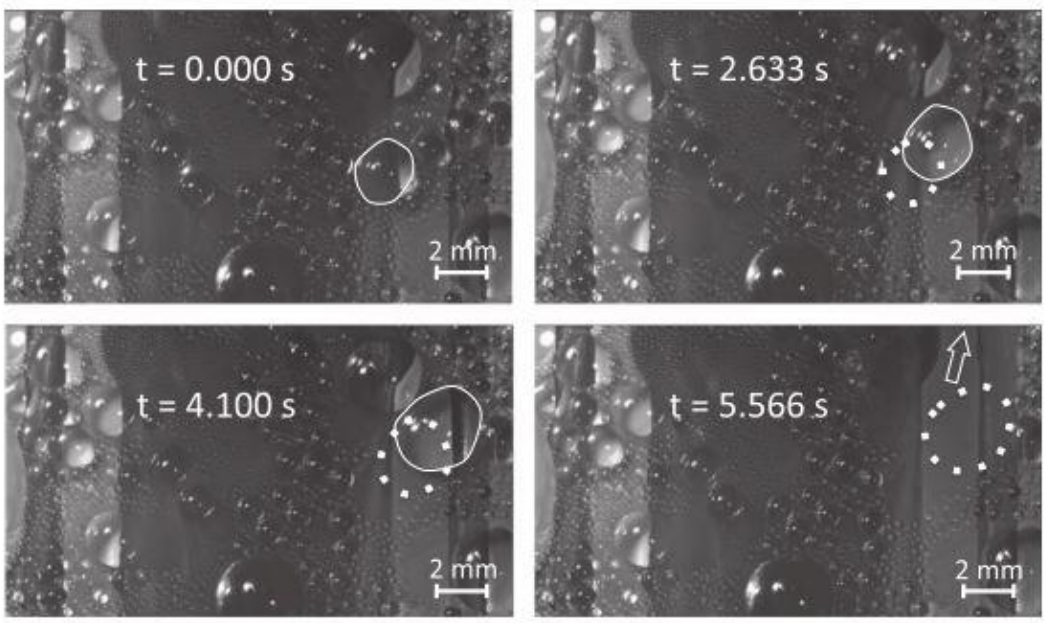

Figure 2.52: The droplets movement on gradient surfaces at a time [65].

Superhydrophobic and super hydrophilic modifications were applied on copper surface to create gradient wettability and improve the droplets velocity during condensation [66]. The super-hydrophilic regions obtained using H_2O_2 solution while superhydrophobic regions achieved using Teflon coating. The droplets move on gradient surface with high momentum. As shown in Figure 2.53, different gradient lengths were used during the experiment to optimize the maximum length and improve the droplets dynamic. The optimum width which obtains the maximum droplet's velocity on the surface was 1mm. Therefore, gradient surface is expected to improve droplet's dynamics and condensation heat transfer performance.

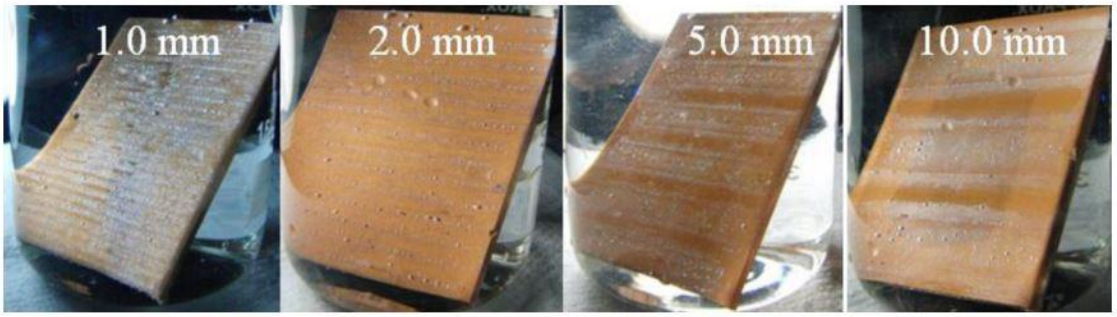

Figure 2.53: Wettability gradient on copper surfaces with different gradient lengths [66].

Multiple hydrophilic aluminum strips have been fabricated using metal deposition techniques on a hydrophobic copper plate to enhance the droplets velocity and water droplets migration [67]. The droplets on the hydrophilic regions are pinned at the beginning of the hydrophobic regions due to the sharp difference in surface tension forces. The droplets will not spill onto the copper until the contact angle becomes higher than copper surface contact angle. Figure 2.54 shows the droplets dynamic behaviors on different shapes of aluminum and copper gradient surfaces. Moreover, the water collection on the modified surfaces is improved, and the heat transfer is predicted to be enhanced.

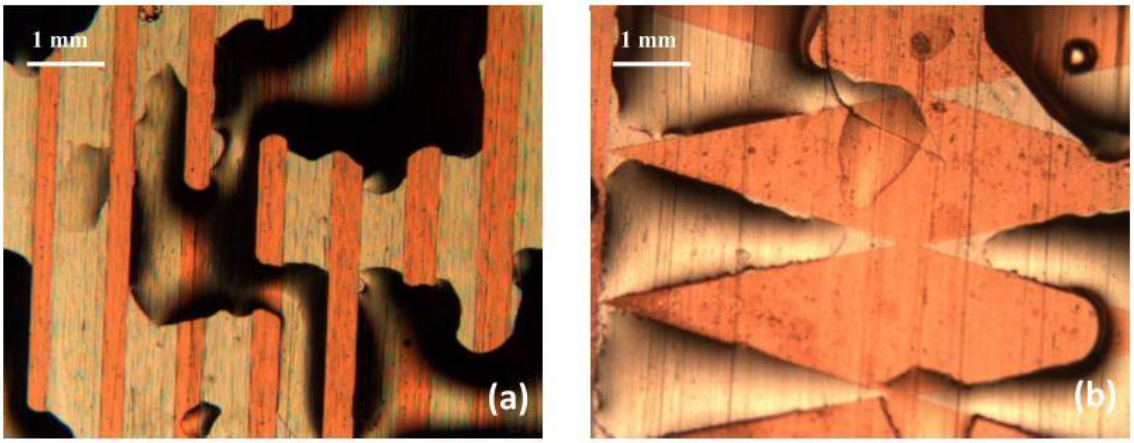

Figure 2.54: Water movement behavior on aluminum-copper gradient surface [67].

2.2.7 Condensation on hybrid surfaces

The performance of condensation heat transfer and droplet dynamics can be improved using hybrid surfaces by quickly removing the condensate's steam and minimizing the size of droplets on the condensing surface. However, not all hybrid surfaces can promote the heat transfer rate and droplet departure frequency during dropwise condensation since there are numerous parameters that influence's hybrid surface performance and should be taken into account. The parameters that influence the hybrid surface performance during condensation are the drainage droplet rates, droplet departure frequencies, maximum droplet diameters, and droplets mobility i.e. Researchers modified hybrid surfaces where those factors can be controlled and designed in ways the heat transfer rates can be enriched. Hybrid surfaces are prepared by combining both hydrophobic and hydrophilic regions where the condensate removal, droplets mobility and droplets departure frequency is increased during condensation.

A promotion of condensation heat transfer rates was achieved experimentally using hydrophilic-hydrophobic vertical stripes [68] on vertical copper discs. The widths of hydrophobic and hydrophilic regions were changed until the optimum widths that maximize the condensation performance were obtained. The design of hybrid surfaces on copper discs is shown in Figure 2.55. The heat transfer rates increase with decreasing the hydrophobic and hydrophilic widths. However, the heat transfer rates decrease with a further hydrophobic and hydrophilic widths decreasing. Therefore, the optimum width for both the hydrophilic and hydrophobic regions that enhance dropwise condensation was found. The heat transfer rate was promoted by 23 % compared to complete dropwise condensation when the hydrophobic width is 0.55 mm, and the hydrophilic width is 0.45

mm. Figure 2.56 shows the enhancement of condensation using hybrid surfaces compared to complete dropwise surface. In addition, the analysis of the droplets sizes and droplets distributions on the strips patterns for the hybrid surface was investigated theoretically [69]. The enhancement of condensation on hybrid surfaces was significantly controlled by the maximum droplets radius on the condensing surface. The maximum droplet radius depends mainly on the width of hydrophobic and hydrophilic regions. The maximum droplet radius that improves the condensation and droplet departure frequency existed in this study.

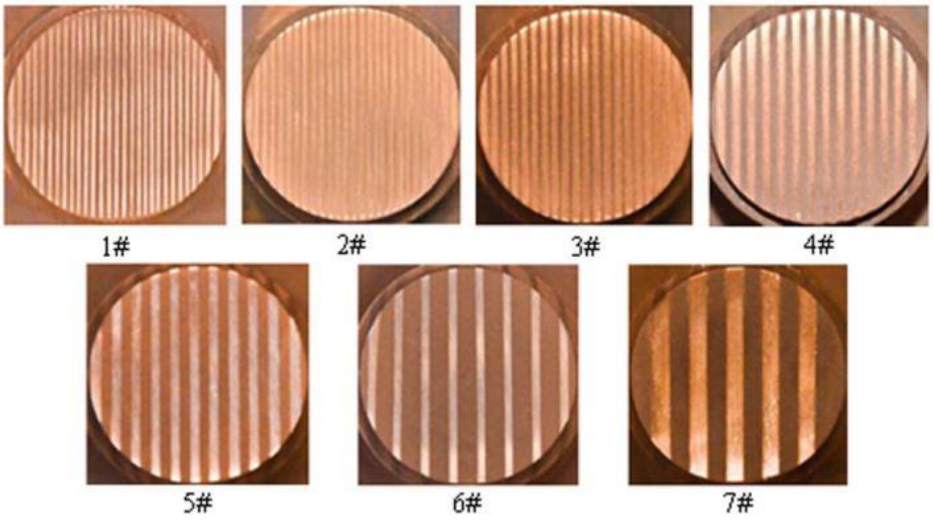

Figure 2.55: The design of hybrid surface on copper discs [68].

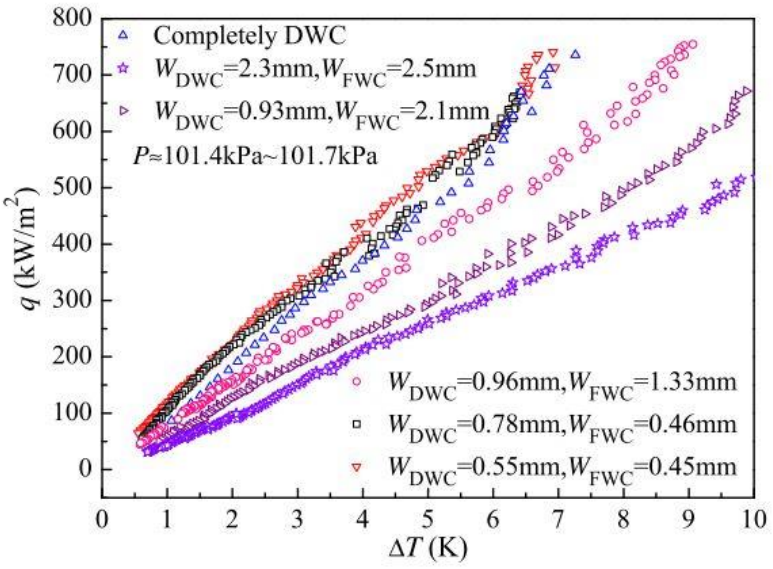

Figure 2.56: The enhancement of condensation using hybrid surfaces compared to complete dropwise surface [68].

Using hybrid surfaces to control the water drainage rate, droplets departure frequency improves the total performance of condensation. Super-hydrophilic tracks like wedge-shaped patterns and straight patterns have been fabricated on aluminum surfaces to improve the condensate collection rate and the heat transfer rate for condensation [70]. The design was inspired by the network that found in banana leaves. Figure 2.57 shows the design of the patterns on aluminum surface. The experiment was implemented at different saturation temperatures and relative humidity. The improvement of condensate collection and heat transfer rate was achieved at high humidity although the patterns occupy 40% from the total area of the surface. The enhancement in the condensate water collection and heat transfer rate for hybrid surfaces is shown below in Figure 2.58 at different condensation conditions. The heat transfer rate enhanced due to the increasing the condensate collection rates and minimizing the droplet diameters on the surface.

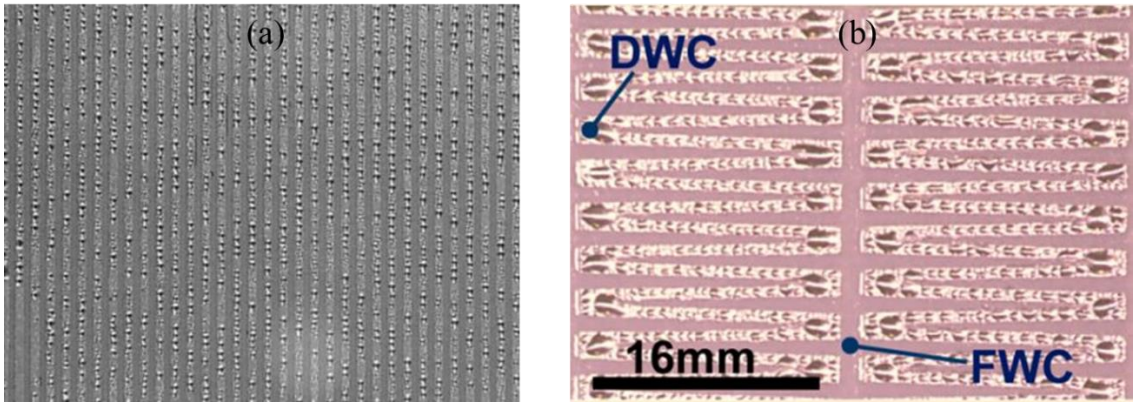

Figure 2.57: The design of the patterns (a) Straight patterns on aluminum surfaces (b) Wedge-shaped patterns [70].

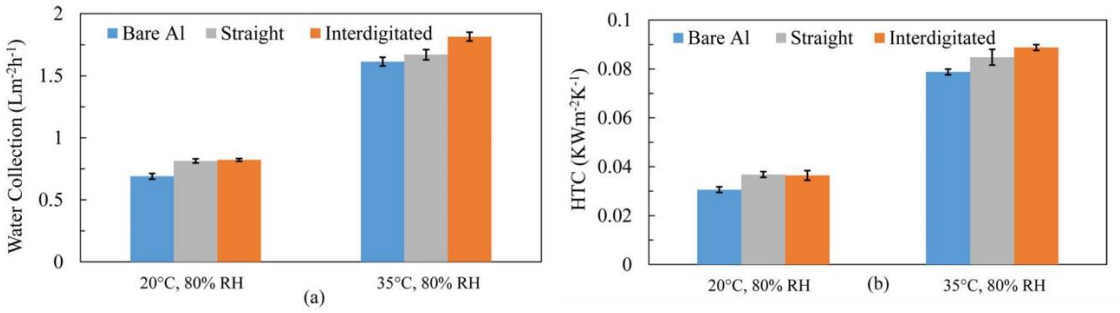

Figure 2.58: The enhancement in the condensate water collections and heat transfer for hybrid surfaces at different condensation conditions [70].

Condensation heat transfer rate was enhanced on hybrid surfaces using super hydrophilic staggered interdigitated patterns on aluminum surfaces at various experiment conditions [71]. The experiments performed at 20, 35 C^{o} bulb temperatures and 80% relative humidity. The hybrid surface design improves the drainage rate of condensing water and droplets removal from the surface. The condensation phenomenon on hybrid surface is shown in Figure 2.59. The area percentage of the patterns regards to the total surface area was changed until the optimum area percentage that maximizes the water drainage and condensation heat transfer rate obtained. The enhancement of 34.4% in heat transfer rate and 30.5 in drainage water rate was achieved compared to the bare

aluminum surface when the percentage of hydrophilic area is 29.9% from the total surface area. In addition, the improvement of 18% in heat transfer rate and 15.4 in drainage water rate was obtained compared to the bare aluminum surface when the percentage of hydrophilic area is 35.9% from the total surface area. Figure 2.60 shows the water drainage rate and heat transfer rate enhancement at different working conditions and various area percentage of hybrid surfaces.

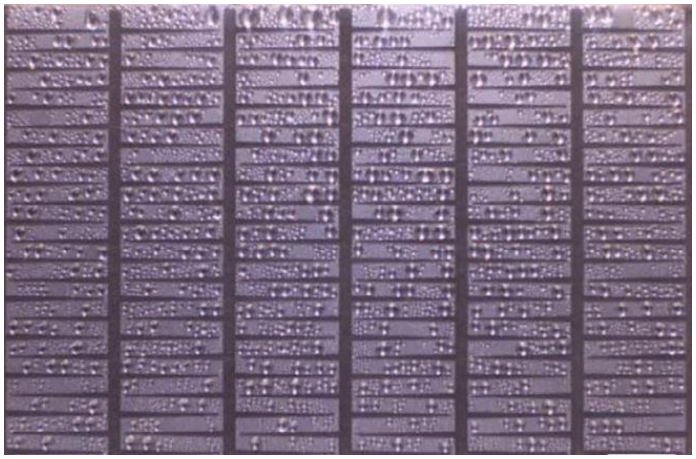

Figure 2.59: The surface design and condensation phenomenon on staggered patterns [71].

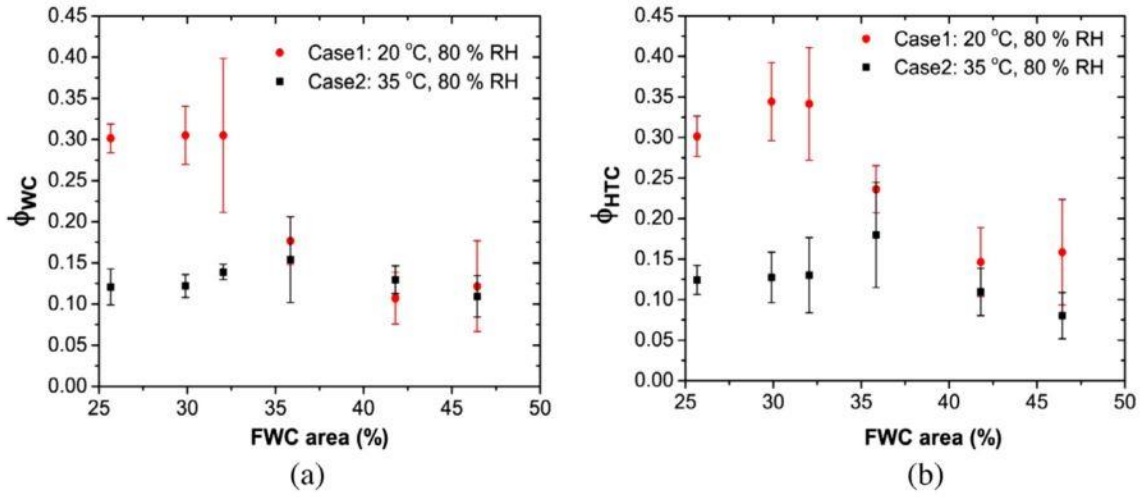

Figure 2.60: The water drainage and heat transfer rate enhancement at different working conditions and various area percentage for hybrid surfaces [71].

A spontaneous and fast movement of condensate droplets were achieved on vertical hydrophilic and hydrophobic strips patterns which fabricated on a solid surface [72]. During condensation, the droplets nucleate from the hydrophobic stripes, and then they move smoothly with high momentum to the hydrophilic regions. The images of condensation phenomena of on complete hydrophilic, complete hydrophobic, and hybrid surfaces is shown in Figure 2.61. During condensation on hybrid surfaces, the droplets nucleate, grow on hydrophobic regions to the certain size and migrate to the more hydrophilic regions. The optimum stripe's width that improves droplets velocity and achieves high condensation efficiency is found in this study. The optimum width that enhances condensation heat transfer rate is 1mm for both hydrophobic and hydrophilic strips. The heat transfer increased by 20% compared to complete hydrophobic surfaces. The enhancement of condensation is shown in Figure 2.61 compared to complete dropwise surface.

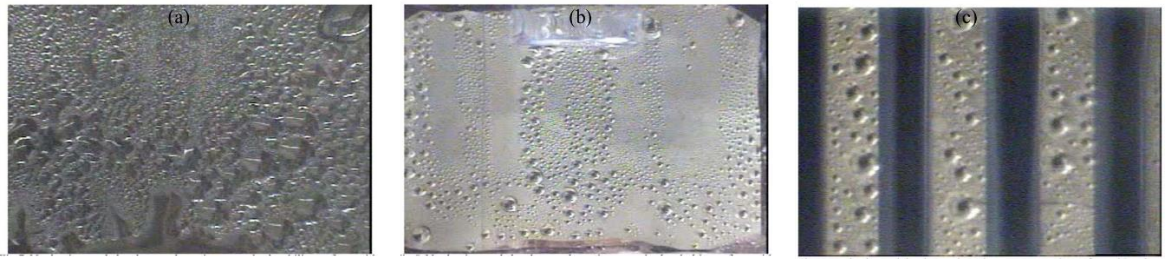

Figure 2.61: The phenomena of condensation on (a) Hydrophilic, (b) Hydrophobic, and (c) Hybrid surfaces [72].

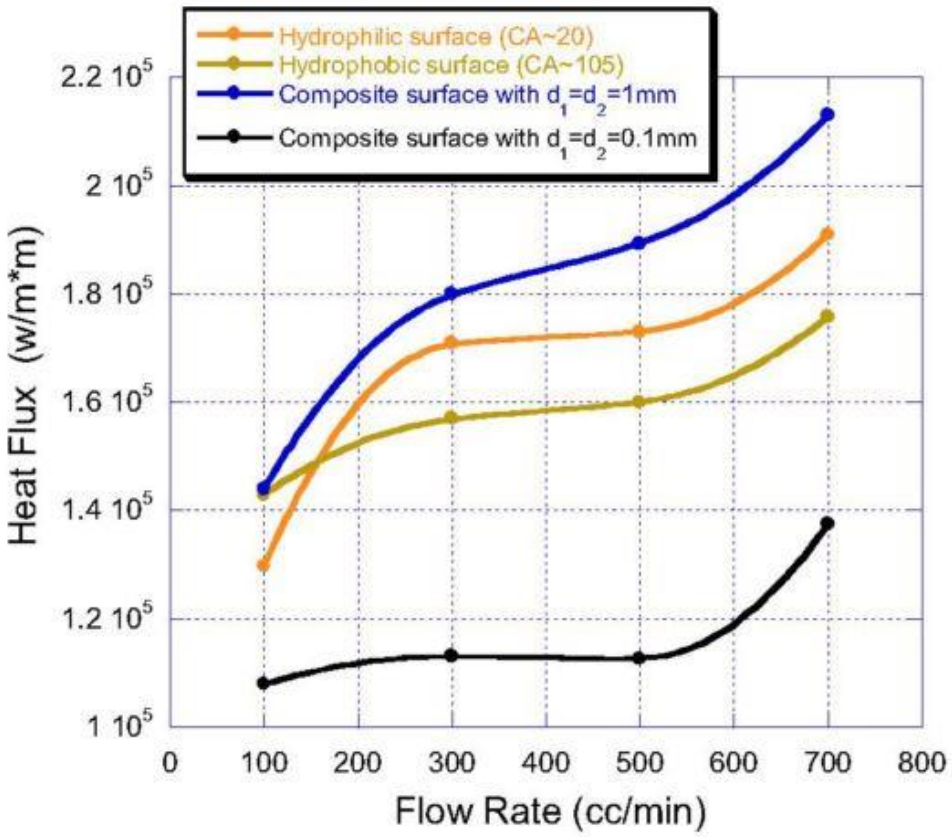

Figure 2.62: The enhancement of condensation on hybrid surfaces [72].

Hydrophilic tree patterns and hydrophilic islands patterns were performed on a vertical copper plate to enhance dropwise condensation heat transfer [73, 74] at atmospheric pressure. Figure 2.63 shows the patterns design that has been evaluated by condensation experiments. In each design of hybrid surfaces, the hydrophilic patterns occupied 25% from the total area of condensing while 75% from the rest of area is hydrophobic regions. For island patterns case, the droplets departure frequency increases with decrease the size of the patterns, and the heat transfer rate was enhanced by 25% compared to complete dropwise surface. For tree patterns case, the droplet departure frequency and heat transfer rate are lower than the complete dropwise surface because the surface was flooded during condensation.

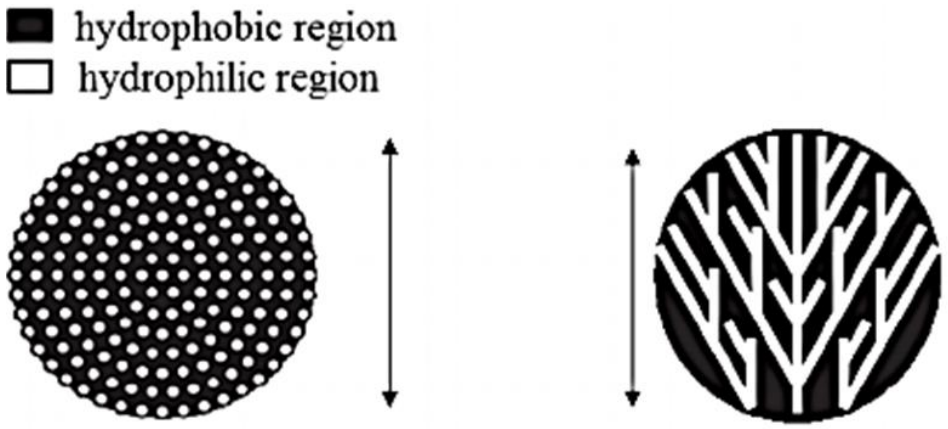

Figure 2.63 Hydrophilic island and hydrophilic tree on hydrophobic copper [73].

In addition, the influence of hydrophobic stripe's widths on condensation heat transfer on copper plates has been experimentally investigated [75]. The width of the hydrophobic stripes changed while the width of hydrophilic strips maintained constant. The effect of the surface orientation on condensation heat transfer performance was clarified. The visualization of dropwise condensation on horizontal and vertical hybrid surfaces is shown in Figure 2.64. In the case of horizontal orientation, the heat transfer rate increases with increasing the width of hydrophobic stripes since the sweeping droplets rate improved. The heat transfer coefficient increases by 1.2 compared with the complete hydrophobic surface. On the other hand, the trend becomes opposite for vertical surface where the heat transfer rate increases with the decrease strip's width because of the flooding which occurs with increase the stripe's width. Figure 2.65 explain the improvement of the condensation heat transfer rate for horizontal and vertical hybrid surfaces for various stripe's width.

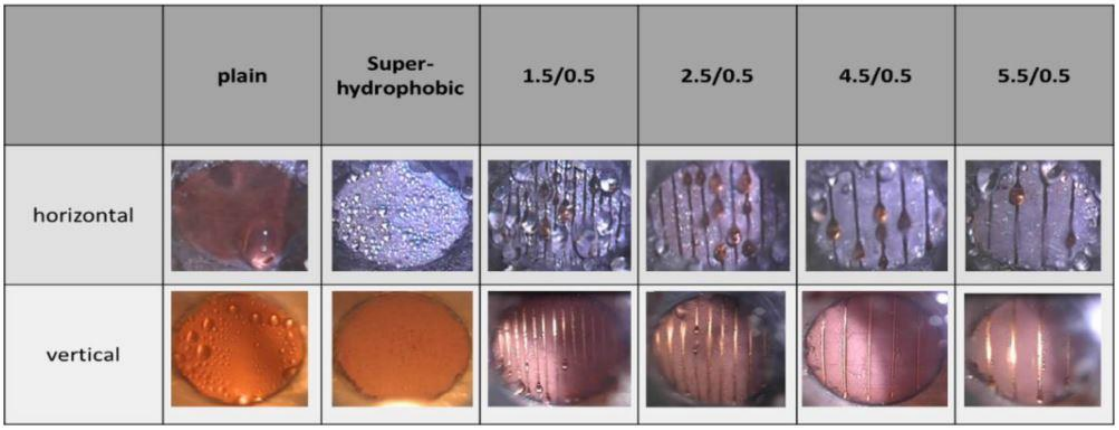

Figure 2.64 The dropwise condensation behavior on hybrid surfaces for different orientations and various hydrophobic strips width [75]

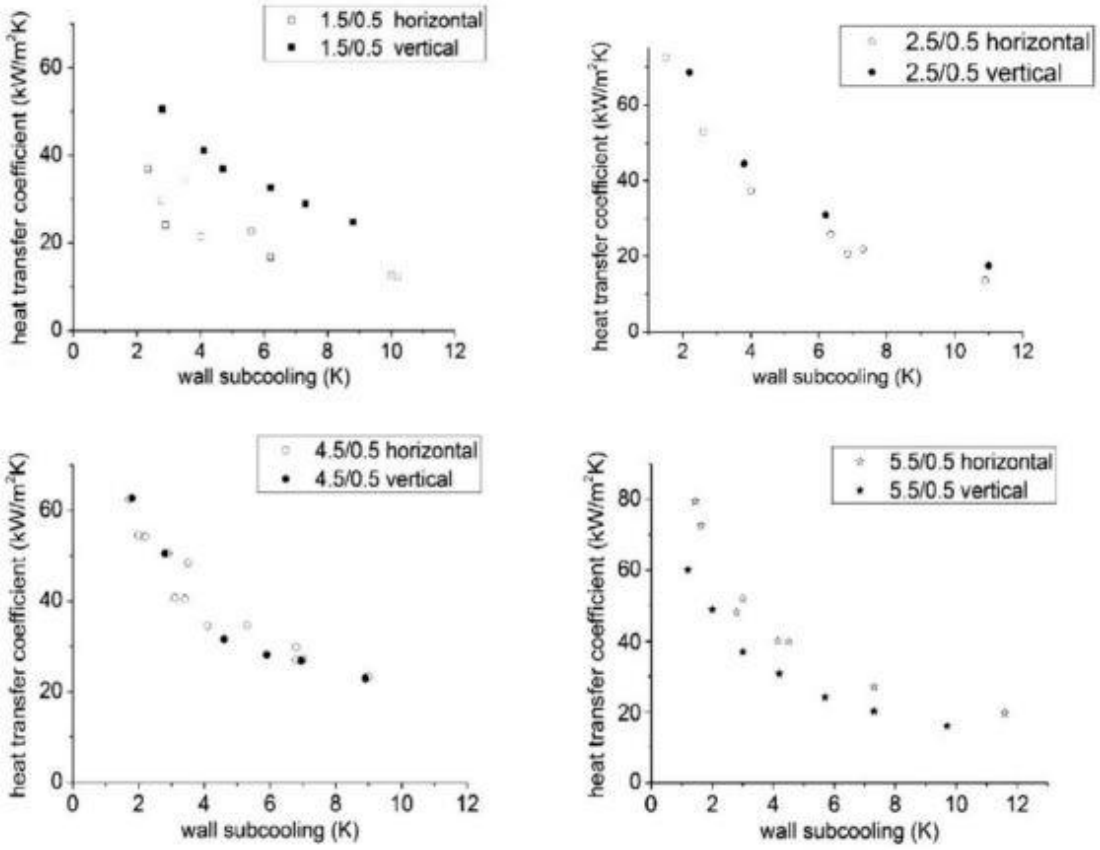

Figure 2.65: The improvement of condensation heat transfer rate for hybrid surfaces for both surface orientations [75].

2.3 Summary and conclusions from literature review

The above section reviews the work and research that have been performed to enhance the droplets dynamic, droplet departure frequency, and heat transfer rate during the condensation. Moreover, different methods have been explained to enhance condensation efficiency. Based on the previous research and literature review, the below conclusions can be obtained:

Droplet dynamic and droplets departure frequency highly influence the performance of heat transfer during dropwise condensation. Introducing super-hydrophobic surfaces for condensation can enhance droplet speed and coalescence because they have low surface energy. However, some super-hydrophobic surfaces do not enhance droplet dynamic during condensation because the surface structure pinned the small droplet and grew larger on the condensing surfaces.

Dropwise condensation is affected strongly by the surface geometry modifications. Grooves can promote the behavior of falling droplets from the condensing surface and increase the surfaces area that exposed to the steam. However, some geometries reduce the heat transfer during dropwise condensation because they cause flooding of droplets even though dropwise condensation still exist. Therefore, more attention should be taken in account when updating the geometry of the condensing surfaces.

Condensation of a mixture of steam is affected by the concentrations of steam in the mixture. The influence in condensation efficiency comes from surface tension differences that introduced temperature gradients. Dropwise condensation on some

surfaces became filmwise condensation when the concentration of the mixture changed. Therefore, the optimum concentration which can achieve dropwise condensation was clarified.

Different methods and research have been made to introduce hydrophobic surfaces that obtain dropwise condensation since they have low wettability characteristics. Chemical treatment can reduce the surface energy and thereby enhance droplet dynamic, droplet departure frequency, and heat transfer rate. However, the durability of the long lasting of dropwise condensation has not been yet achieved.

Gradient surfaces enhance dropwise condensation performance compared to the hydrophobic surfaces because they increase droplet migration velocity, droplet coalescence, droplet departure frequency without depending on body forces such as gravity.

Hybrid surfaces improve dropwise condensation heat transfer rate because they improve the velocity of removing droplet from condensing surfaces. In addition, hybrid surfaces can minimize droplet size and increase the departure frequency. The heat transfer rate of condensation on hybrid surfaces is higher than complete dropwise since the departure frequency enhanced. However, some hybrid surfaces reduce condensation efficiency because they cause flooding which increases the thermal resistances and reduce the heat transfer rates.

CHAPTER 3

EXPERIMENTAL INVESTIGATION

3.1 Experimental setup

To obtain the heat transfer rates during condensation on horizontal tubes at saturation conditions, condensation experiment setup was conducted. The experimental setup consists of four main sections: (i) steam generator, (ii) cooling system, (iii) condensation chamber, and (iv) data acquisition system. Figure 3.1 shows the schematic design of the experimental condensation system. The steam generator consist of a water reservoir which is heated by two electric heaters. The first heater 3500 W (AVANTCO) is operated during the experiment, while the second heater 550 W (Brisk Heat) is operated when the condensation rate was high, and the steam was insufficient. The steam is flowed into the condensation chamber through a flexible stainless steel tube (0.75”D, 5”L). A wrapped heater (Brisk Heat HTC451003) heated the flexible tube at a controlling temperature which is controlled using a heater controller (Brisk Heat SDC120KC-ASDC) to make sure no condensation for steam before entering the chamber. Three calibrated T-type thermocouples with an accuracy of 0.1% were used to measure the steam temperature, and a calibrated pressure transducer (Omega PX01C1- 050A5T) located at the top of the condensing chamber used to measure the steam pressure. The condensing chamber is made from aluminum compositions. The chamber is fabricated with four cartridge heaters inserted from the bottom corners of the chamber. The chamber has two openings at the upper side and lower side of condensing chamber to maintain the

chamber's atmospheric pressure. The four cartridge heaters were used to prevent condensation at the chamber's wall during the condensation process. The condensation chamber is insulated to diminish the effect of unwanted condensation, reduce heat losses and condensation occurring at other places. The chamber has a 6-inch-diameter circular glass window for visual observation of the condensation process. A high-speed camera (Phantom v7.3) is used to visualize the condensation process. The excessive and condensed steam flowed out of the chamber from the openings located at the top and bottom of the chamber.

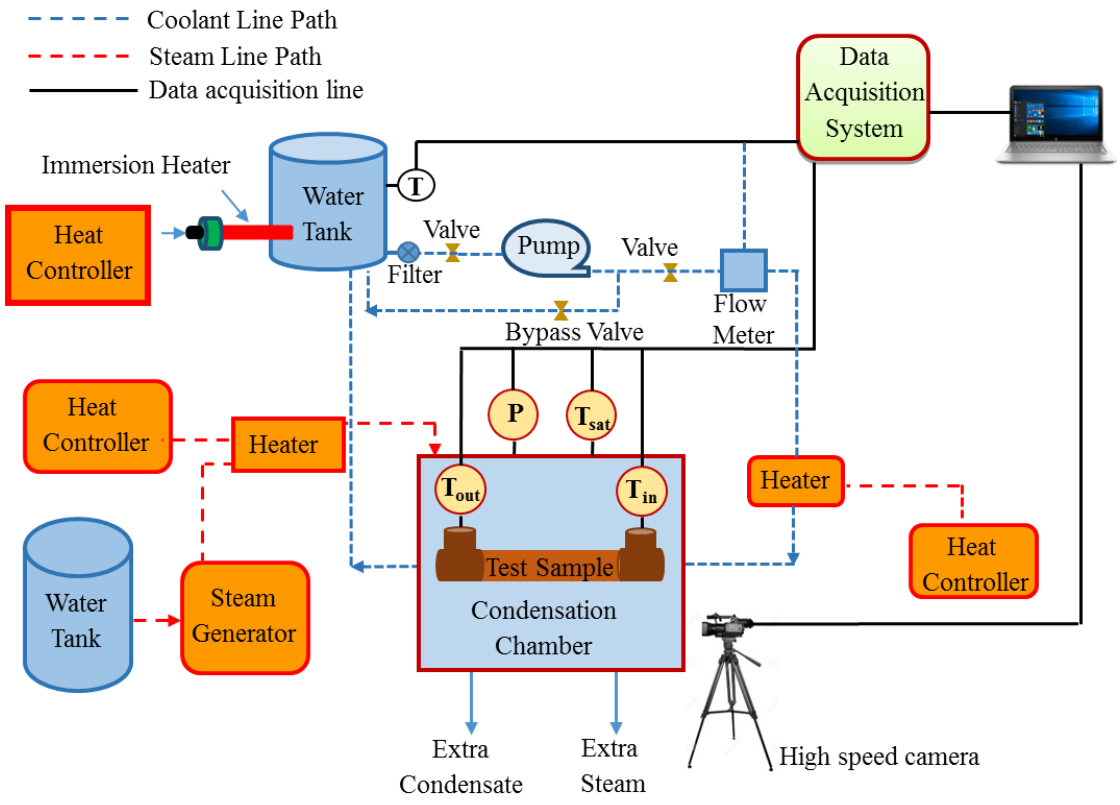

Figure 3.1: Schematic diagram of experimental setup on tubes at atmospheric pressure.

The cooling system consisted of a water tank (galvanized steel, 56 liters), pump (SHURFL-GMBN4VA53-9.7GPM at 124 psi), and flow meter (Omega FMG 92-0.62-

6.6 GPM with 0.1% accuracy). The water is pumped at a constant flow rate while immersion heat (2000 W) inserted into the water tank to change the water temperature. Before the water is entered the condensation chamber, it was heated again using a wrapped heater (Brisk Heat HWC1240–24’ and 1440 W). The water was returned to the water tank to be pumped again. Two calibrated Type K thermocouples were used to measure the inlet and outlet temperatures for the test sample. The data were monitored and recorded using the Agilent 34972A data acquisition system. Figure 3.2 shows an image of the condensation experiment setup on horizontal tubes.

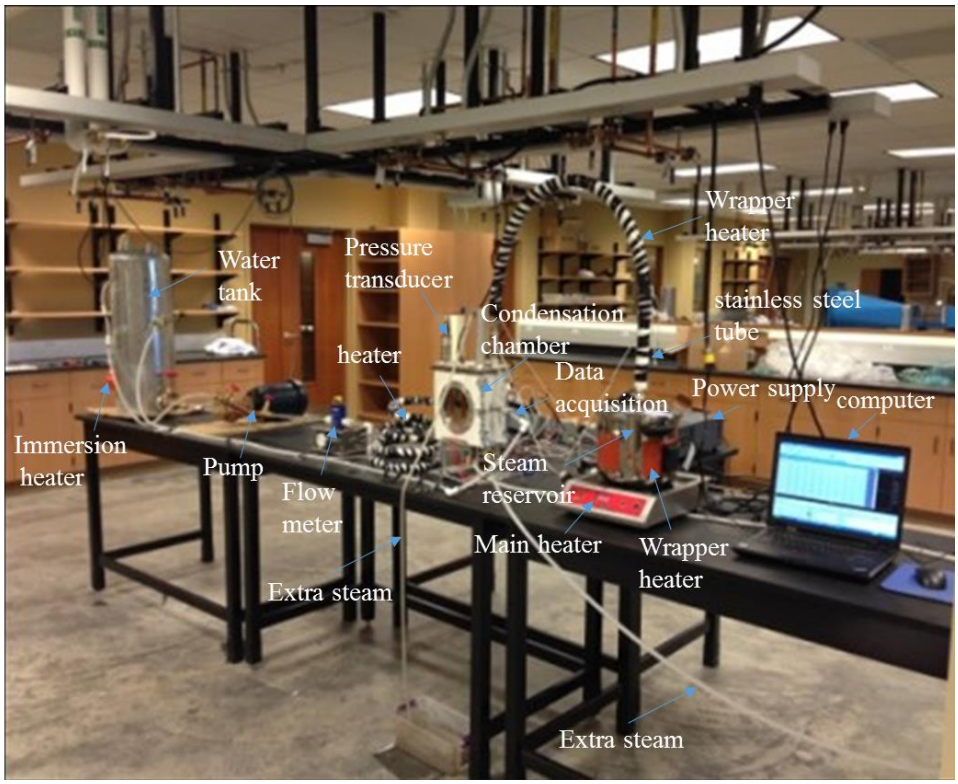

Figure 3.2: Experimental setup on tubes at atmospheric pressure.

3.2 Experiment procedure

The coolant water was pumped inside the test sample in steady flow which was maintained around 3±2% L/min for all experiments. The inlet temperature of the coolant was varied from about 28ºC to 85ºC, with regards to Reynold’s number it was varied

within a range of approximately from 18,000 to 48,000. The inlet temperature was continuously increased during the experiment using three heat sources, the water tank's immersion heater, the inlet heater, and the heat transfer from the vapor condensation. The steam was delivered to the condensation chamber before the coolant water pumped to the tube for at least ten minutes to assure steady state saturation conditions. The inside of the chamber's temperature, pressure, and the chamber wall temperatures were monitored to confirm the steady state saturation conditions. For each tested sample, three condensation experiments were performed. The first experiment was performed for the heat transfer calculations, the second experiment was applied to visualize the condensation phenomena, and the third experiment was implanted heat transfer calculations. The repeating condensation experiments allow more observation change in the heat transfer. During the visualization experiment, the window's heaters were operated to prevent condensation on the window. The LED light source was applied during visualization experiment to visualize the condensation phenomena. Moreover, during the heat transfer measurements experiments both the window heaters and the LED light source were not operated to avoid any radiation effects on the heat transfer measurements.

3.3 Data reduction

The overall heat transfer coefficient H_o of a condensing on tube test can be determined by

$$H_o = \frac{\dot{Q}}{A \times \Delta T_{LMTD}} \quad . \qquad (3.1)$$

Where $\dot{Q}$ is the total heat flow, ΔT_{LMTD} is the log mean temperature difference and A is the outer tube surface area. The ΔT_{LMTD} can be calculated by

$$\Delta T_{LMTD} = \frac{T_{cw,out} - T_{cw,in}}{Ln\frac{T_{sat} - T_{cw,in}}{T_{sat} - T_{cw,out}}} . \quad (3.2)$$

Where T_{sat} is the saturated steam temperature and $T_{cw,out}$ and $T_{cw,out}$ are the inlet and outlet temperatures of the cooling water. Total heat flow can be determined as

$$\dot{Q} = \dot{m}_c \times c_p \times \left(T_{cw,out} - T_{cw,in}\right) - \dot{Q}_{losses} \quad (3.3)$$

Where m_c is the mass flow rate of cooling water in (kg/s) and C_p in (J/kg.K) is the specific heat. The equation below calculates the convective heat transfer coefficient for cooling water inside the tube h_i in W/m^2.K:

$$h_i = \frac{N_u \times K_w}{D_i} . \quad (3.4)$$

Where K_w is the thermal conductivity of water, and D_i is the inside diameter of the tube, and Nu is the Nusselt number. The Nusselt number can be calculated from the equation below for turbulent flow:

$$N_u = C \times R_e^{0.8} \times P_r^{0.353} \times \left(\frac{\mu_c}{\mu_{c,w}}\right) . \quad (3.5)$$

Where Re is the Reynolds number, Pr is the Prandtle number, and C is constant and equal to 0.035 in this study [76]. The overall heat transfer coefficient is related to the inner and outer heat transfer coefficients, as below:

$$\frac{1}{H_o \times A_o} = \frac{1}{h_i \times A_i} + \frac{Ln\frac{D_o}{D_i}}{2 \times \pi \times l \times K_{tube}} + \frac{1}{h_c \times A_o} . \quad (3.6)$$

The equation above gives us the heat transfer coefficient outside the tube. During the experiment, the subcooling temperature difference (the difference between the steam and the outer temperature of the tube) cannot be measured, but it can be calculated it from the following equation:

$$\Delta T_{sub} = T_{sat} - T_s = \frac{\dot{Q}}{h_o \times A_o} . \quad (3.7)$$

The experimental results of the heat transfer coefficient were compared with the filmwise condensation from the Nusselt model for the horizontal tube. The Nusselt model for the horizontal tube for the filmwise condensation is [77]:

$$h_{FWC} = 0.728 \times \left[\frac{h_{fg}^{\sim} \times \rho_c \times (\rho_c - \rho_s) \times g \times k_c^3}{\mu_c \times (T_{sat} - T_s) \times D_o}\right]^{1/4} \quad (3.8)$$

Where ρ_c, ρ_s, μ_c, k_c, and $h_{gf}^{\sim}$ are the liquid properties and can be found at average fluid temperature.

The corrected enthalpy can be calculated from [77]:

$$h_{gf}^{\sim} = h_{fg}\left[1 + 0.68\left(\frac{c_{p,l}(T_{sat} - T_w}{h_{fg}}\right)\right]. \quad (3.9)$$

3.4 Heat loss calculations

The heat losses $\dot{Q}_{losses}$ calculations are important to ensure that the calculated $\dot{Q}$ in Eq. (3) was due to the heat transfer rate through only the tested tube's surfaces. Therefore, a calibration test was needed to confirm the heat transfer results are accurate. The copper tube which is thermally insulated and has the same basic dimensions of the other tested tubes was installed in the test chamber. Then regular condensation experiment procedure was performed to obtain the heat transfer rate. The obtained heat transfer rate represents the heat loss ($\dot{Q}_{losses} = \dot{m}_c\ C_{p.c}\ (T_{out.c} - T_{in.c})$) in Eq. (3). Figure 3.3 shows the copper tube which is thermally insulted to calculate the heat losses $\dot{Q}_{losses}$. More details for experimental procedure, heat losses calculation and data reduction can be found in [78]. This calibration method allows to measure accurate results for the heat transfer rate on the exposed tube outer surface area. The results of heat losses for different Reynolds numbers is illustrated in Figure 3.4 for thermally insulated tube.

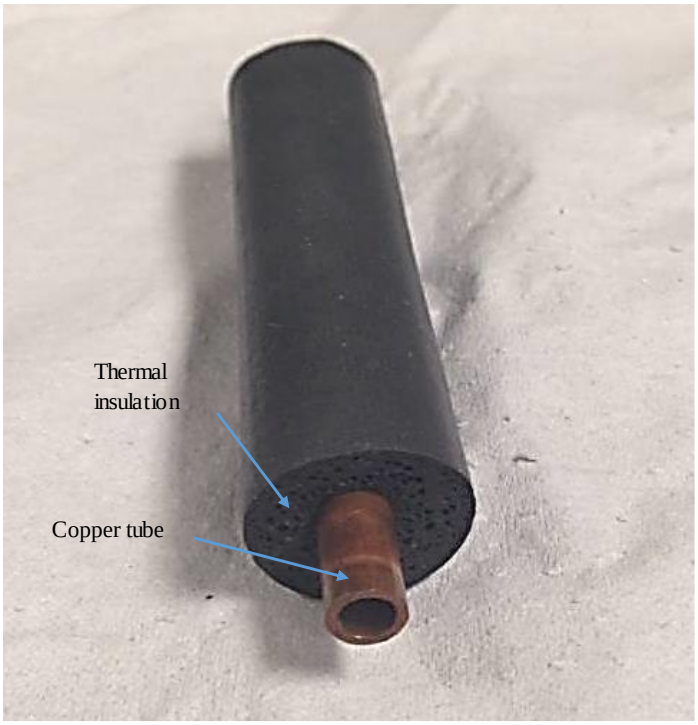

Figure 3.3 copper tube which is thermally insulated.

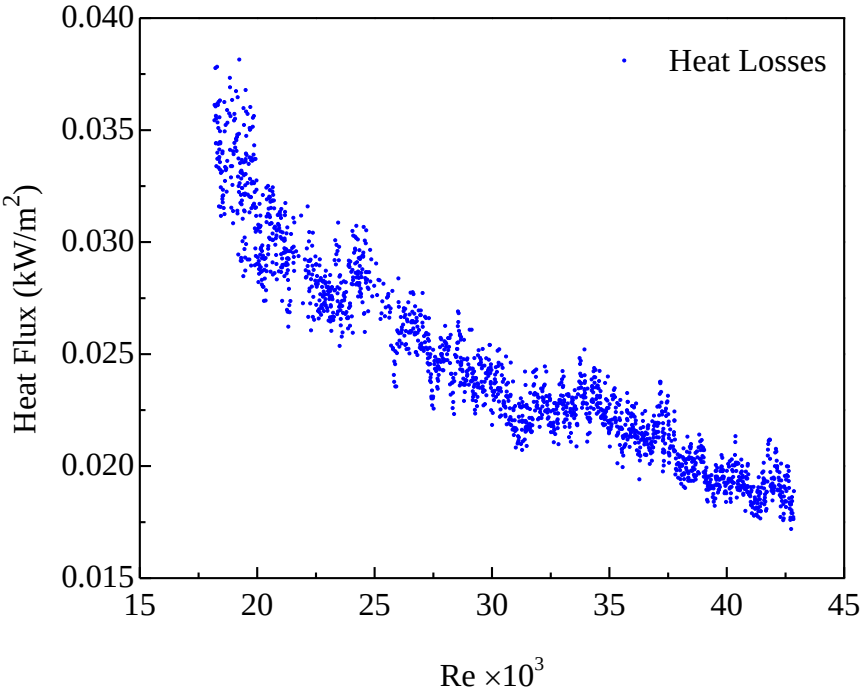

Figure 3.4: The heat losses results versus Reynolds numbers for the insulated copper tube.

3.5 Experimental set up calibration

The experiment results were validated with the theoretical results for filmwise condensation Nusselt model on horizontal tube to ensure the proper functioning of the experimental setup. Condensation experiments were performed in the lab on a horizontal copper tube coated with H_2O_2 to obtain complete filmwise condensation. The condensation was completely filmwise, as Figure 3.5 shows. Figure 3.5 shows filmwise condensation on copper tube at saturation condition when the subcooling temperature difference (ΔT) is 12 ℃. Figure 3.6 and Figure 3.7 show the reduced data after considering the heat loss in the system for heat flux and heat transfer coefficient, compared with the theoretical results for filmwise condensation Nusselt model. In addition, the surface temperature of the tube was directly measured during condensation using thermocouple T-type which inserted in 0.5mm deep in the center of tube length. The hole in the tube wall was performed carefully using a drill bit, and the thermocouple was fixed inside the tube wall. To assure that the thermocouple does not move during the experiments, the soldering process was performed. The condensation heat transfer results for calculated surface temperature and direct measurement surface temperature have a good agreement with Nusselt model for complete filmwise condensation.

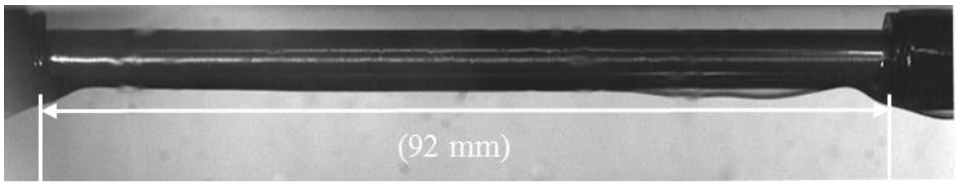

Figure 3.5: Filmwise condensation for calibration.

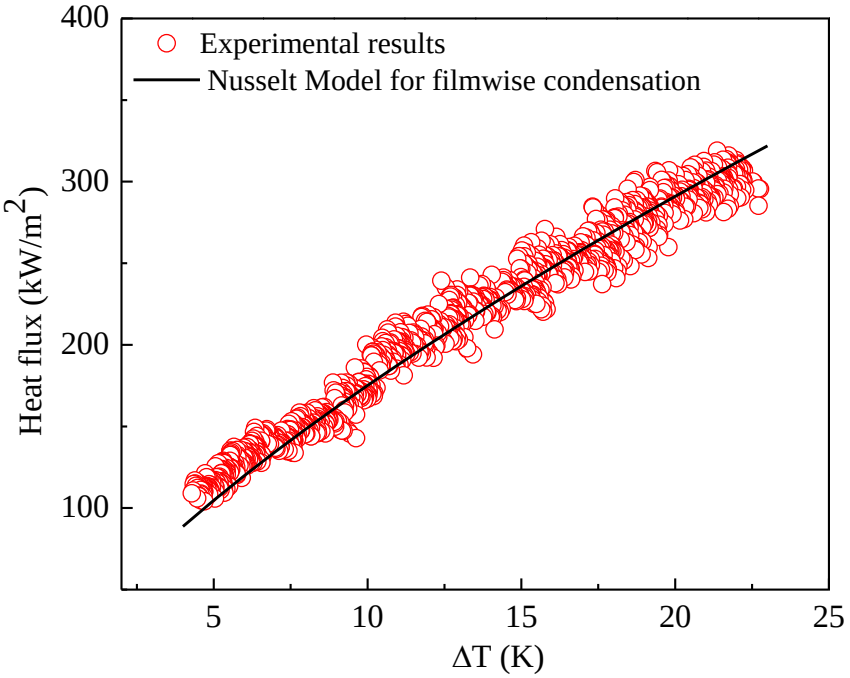

Figure 3.6: Calibration test results for heat flux compared with Nusselt theory.

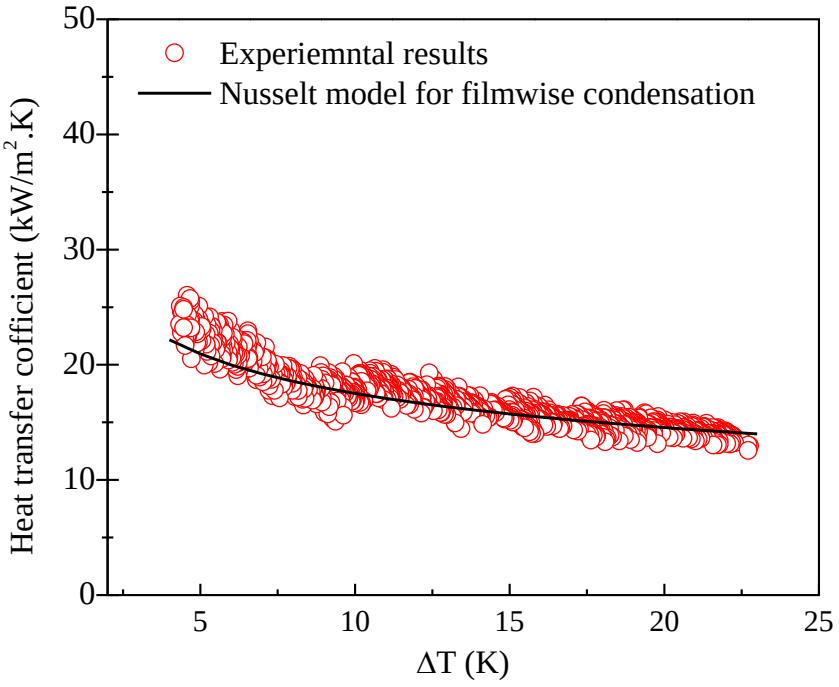

Figure 3.7: Calibration test results for heat transfer coefficient compared with Nusselt theory.

In addition, the results were refined by taking the average for mass flow rate that was constant during the experiment and by taking the average and curve fitting for both inlet and outlet water temperatures. In general, the same refining process was applied to all experimental results. Figure 3.8 shows the condensation heat transfer rate and heat transfer coefficient after the refining process.

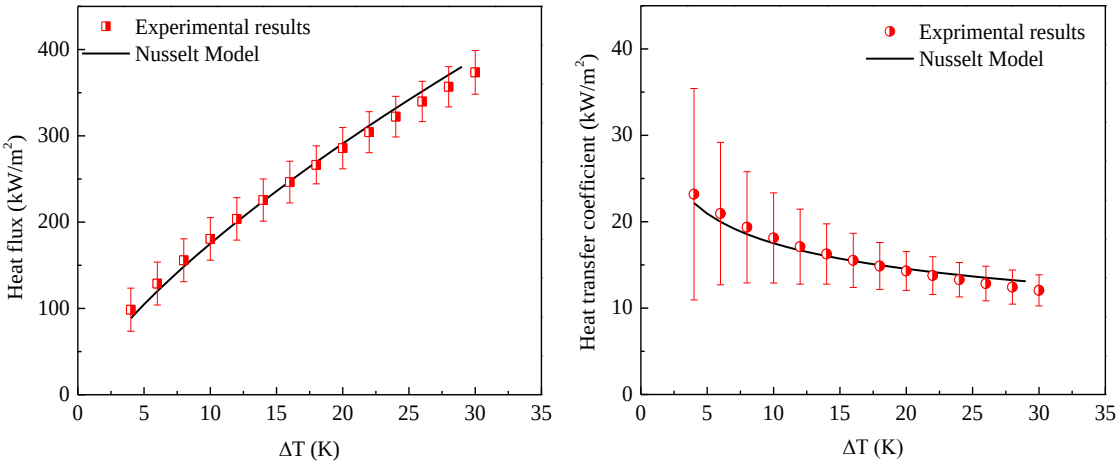

Figure 3.8: Calibration test after refining the results compared with Nusselt theory.

3.6 Uncertainty quantification

The uncertainties in the data measurements (Q_Z) are considered for the heat flux, the overall heat transfer coefficient, and the condensation heat transfer coefficient in the following data analysis. Uncertainties propagation in the calculated values is estimated using Kline and McClintok method [79]:

$$Q_Z = \left[\left(\frac{\partial Q}{\partial q} Z_1\right)^2 + \left(\frac{\partial Q}{\partial q} Z_2\right)^2 + \cdots + \left(\frac{\partial Q}{\partial q_n} Z_n\right)^2\right]^{\frac{1}{2}}, \qquad (3.10)$$

Where ($Q = Q(q_1, q, \ldots\ q_n)$) is a function of independent variables (n) and Z_i is the uncertainty in the variable (q_i). The uncertainties of experimental parameters are listed in Table 3.1.

Table 3.1: Uncertainties of key parameters.

Experimental measurements	Uncertainty
Coolant inlet and outlet temperature T_{in}, T_{out}	0.5 K
Flow rate of coolant ($\dot{m}$)	1 %
Saturated steam temperature T_{sat}	2%
Condensing surface area (A)	4%
Heat flux (q)	(3-9) %

3.7 Surface preparation procedure

In this study, the test sample is a copper tubes (Cu-101 from McMaster-Carr, 99.99% purity) of length 92 mm. The outside diameter is 6.35 mm, and the thickness is 0.9 mm. Initially, the copper tube first polished used three types of sandblasting papers of roughness grades 600, 800, and 1200 respectively. Then, the tube was cleaned with acetone, ethanol, and deionized water using an ultrasonic cleaning device. The copper tube was dried with nitrogen. Using Cero 3 software, preparing the hybrid surface which has hydrophilic or hydrophobic pattern's design created and printed on a white transparent paper. Then the design was transferred to the green photoresist sheet (IKONICS Imaging-Rapid - Mask High Tack-2 mil thickness) using an exposed rapid mask high-tack (IKONICS Imaging-Letralite-15 W) ultraviolet light. The sample of design of patterned hybrid surface on white plastic sheet and the green photoresist sheet is shown in Figure 3.9.

(a)

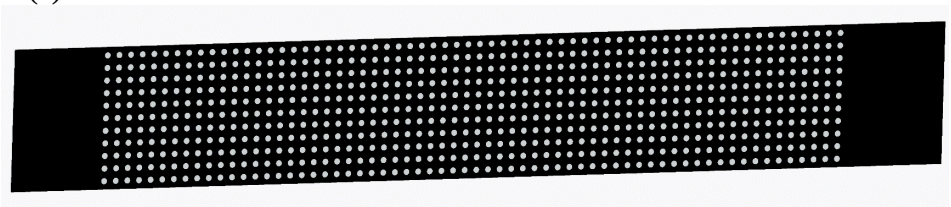

(b)

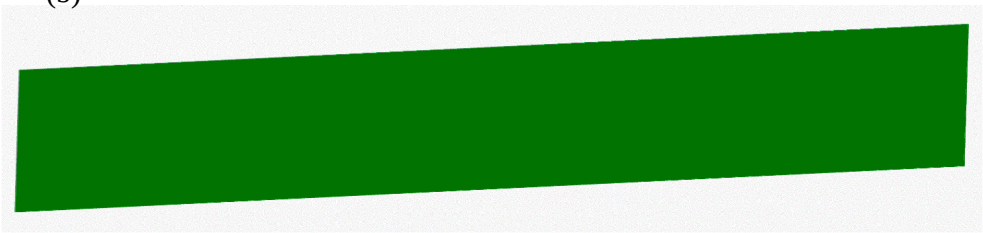

Figure 3.9: (a) The sample of design of hybrid surface (b) The transparent green film.

The green photoresist sheet was contacted to the designed white plastic sheet and then exposed to the ultraviolet light. The patterned hybrid surface design transfers to the green photoresist sheet in specific time during ultraviolet light operation. The time of transition from white plastic sheet to green photoresist sheet was changed until the optimum time of transition was found. The time of transition was 3 minutes that certain complete transition of the design to the green photoresist sheet. The separation of the designed white plastic paper from the green photoresist sheet occurs after the design is transferred. The hybrid surface design which transferred to the green photoresist sheet is shown in Figure 3.10. Then, the green photoresist sheet was wrapped carefully on the polished copper tube as shown in Figure 3.11. The wrapped tube was covered and maintained in a dark place for 12 hours to ensure that the green photoresist sheet completely adhered to the tube.

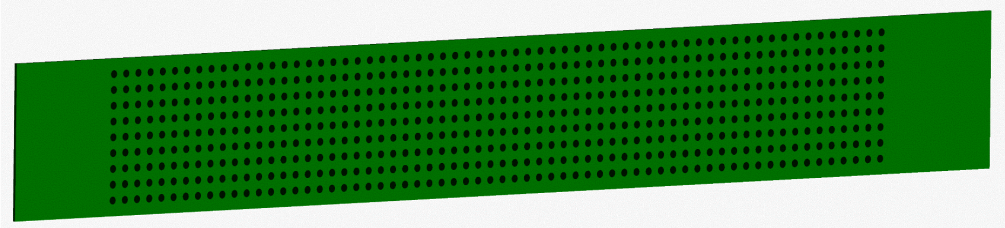

Figure 3.10: Transferring the design to the green photoresist sheet.

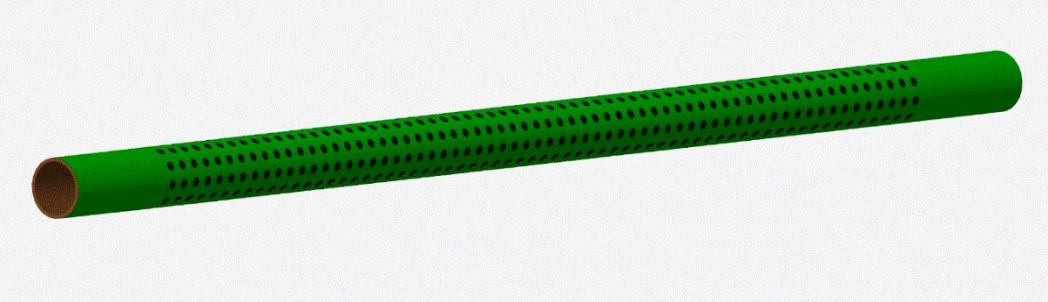

Figure 3.11: The wrapped copper tube with green photoresist sheet.

The wrapped tube was exposed to the abrasive sandblasting jet machine (Abrasive Jet Technologies, LLC, Micro Abrasive Blasting Unit-Model K) using 50-micron silicon carbide particles (SiC). The sandblasting process performed using micro jet nozzle (Abbrasive Jet Technologies, LLC, nozzle Type C, 1.14 mm in diameter). Due to the design of hybrid patterned surface design, only the dark green regions were sandblasted. However, the light green regions covered by the film during the sandblasting process. Figure 3.12 shows the wrapped tube after the sandblasting process. The tube was immersed in DI-water, and then the green mask was removed completely from the tube.

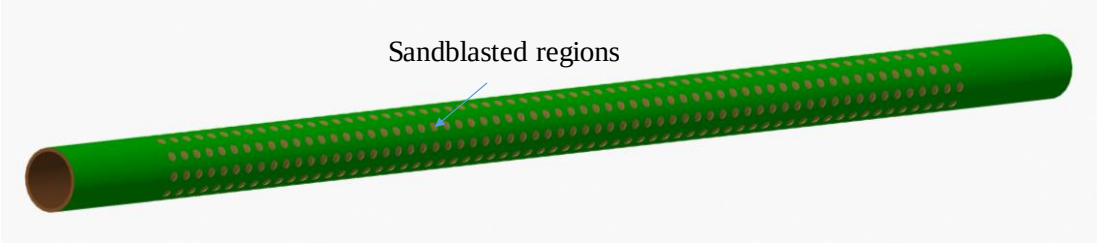

Figure 3.12: The wrapped tube after the sandblasting process.

The tube is cleaned with acetone and DI-water and then dried in nitrogen. Then, the tube is immersed in 0.0025 mol/L of n-octadecyl mercaptan solution for 1 hour at 75℃ to create the hydrophobic regions. Figure 3.13 shows the copper tube with two wettability regions where the sandblasted regions are hydrophilic, and plain regions are hydrophobic regions. The preparation of various patterns with different sizes and different gap distances was achieved to study the effect of the sizes and gaps on the heat transfer rate for dropwise condensation. The tube was identified to find the surface wettability for both regions by measuring the contact angles for the regions before and during the experiment. The surfaces' structure and roughness were studied with SEM images for copper surface coated using SAM and sandblasted surface which coated using SAM and hybrid surface as shown in Figure 3.14.

Figure 3.13: The copper tube with two wettability regions.

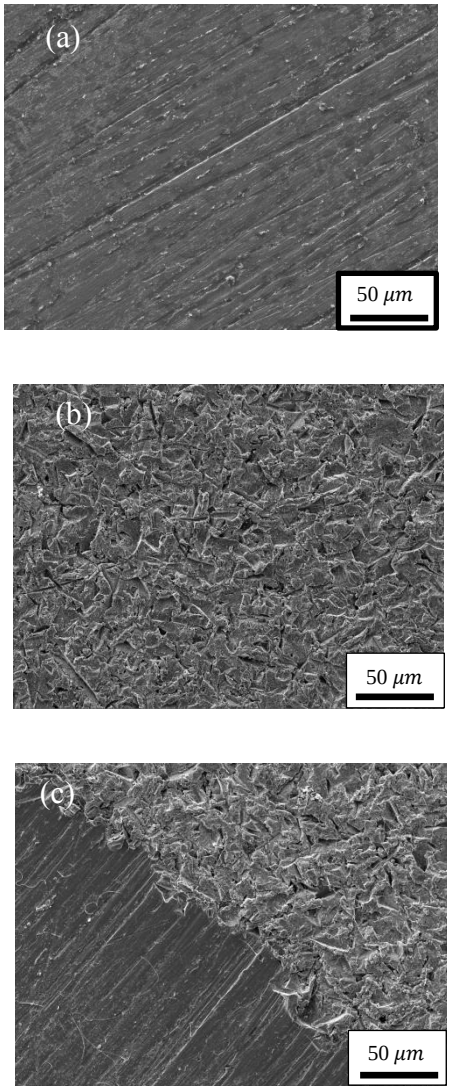

Figure 3.14: SEM images for (a) Cu with SAM (b) Cu sandblasted and SAM (c) Hybrid surface.

The average contact angles before the condensation experiments for smooth surface which coated SAM coating was 120 $\pm$ 0.5 degree and 135 $\pm$ 0.5 for complete sandblasted surface. Figure 3.15 shows the contact angle measurements for the surfaces in air conditions before condensation experiments.

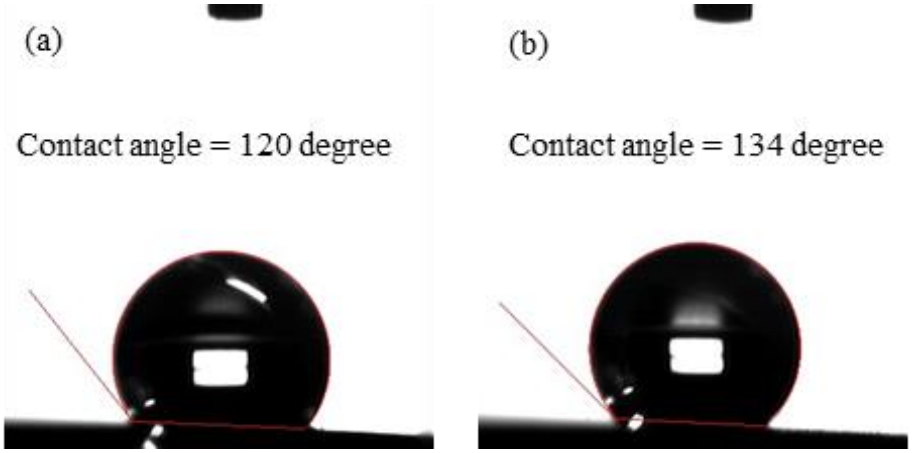

Figure 3.15: The contact angle measurements for the surfaces in air conditions (a) Smooth copper with SAM (b) Sandblasted copper with SAM.

However, the contact angles were changed during condensation experiments. The contact angle for complete dropwise which coated with SAM was 95 $\pm$ 1 degree while it is 62 $\pm$ 1 degree complete sandblasted surface during the experiments as shown in Figure 3.16.

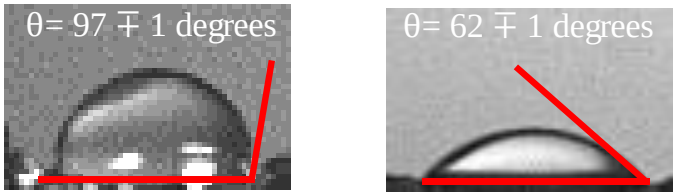

(a) Hydrophobic regions (b) Sandblasted regions

Figure 3.16: Wettability of hydrophobic and hydrophilic regions for hybrid surface.

The preparation of hybrid surfaces which have hydrophobic patterns was performed to investigate the influence of patterns' size on condensation heat transfer performance and droplets' dynamics. Moreover, hybrid surfaces which have hydrophilic patterns with different diameters and different gap distances were achieved on copper tubes. The effect of the patterns' sizes and gaps between the patterns on the heat transfer rate and droplets dynamics were discussed for dropwise condensation. In addition, the

patterns geometry influence on condensation and droplets dynamics behavior is discussed in this study.

CHAPTER 4

RESULTS AND DISCUSSIONS

In this study, condensation heat transfer on complete hydrophobic surface (β-regions), complete sandblasted surface (γ-region) and hybrid surfaces with various patterns are discussed. The complete sandblasted surface (γ-region) is fabricated using 50 microns of silicon carbide sand while the complete hydrophobic surface (β-region) is prepared using self-assembled monolayer (SAM) coating. Hydrophobic patterns are fabricated on complete sandblasted surfaces to study the influence of patterns' size on condensation heat transfer. Moreover, hydrophilic patterns with various sizes and gap distances are modified on complete hydrophobic surfaces in this study. The effect of the patterns' size and the gap distance between the adjacent patterns on condensation performance are discussed. The influence of the patterns' wettability and designs on droplets dynamic during condensation are analyzed. The droplets departure frequency and the droplets' departure diameter are computed for the surfaces during condensation. The renewal area frequency for the patterns were calculated and optimized with other hybrid surfaces. The optimum patterns' size and optimum gap between the patterns are found in this study. In addition, the influence of the patterns' geometry on the droplets dynamics and heat transfer performance are discussed in this study.

4.1 Condensation on complete sandblasted (γ-region) and complete hydrophobic (β-region) surfaces

A series of condensation experiments were performed on compete dropwise (β-region) surface and sandblasted surface (γ-region). The two surfaces were coated with self-assembled monolayer SAM coating. The heat transfer rates for both surfaces is shown in Figure 4.1 compared with Nusselt model for filmwise condensation. The droplets' contact angle on the sandblasted surface (γ-region) is 62 degree during the experiment but its value is 134 degree before condensation occurs. The lower contact angle during condensation causes low performance of heat transfer rate. The droplets' size on the surface is large and cause a liquid film which reduce the heat transfer rate. However, the heat transfer rate for complete dropwise (β-region) surface is higher than the heat transfer rate for complete sandblasted surface. Figure 4.2 shows images of condensation on the complete sandblasted (γ-region) surface and complete DROPWISE (β-region) surface. The large performance of condensation rate on hydrophobic surface was regards to large contact angle during the experiment and lower droplets size on the surface. The droplets departure frequency for the surfaces is determined as shown in Figure 4.3. The droplet departure frequency for complete dropwise (β-region) surface is higher than complete sandblasted (γ-region) surface because the droplets move fast and they do not form a film on the surface. The droplets departure diameter for the surfaces is calculated as shown in Figure 4.4. The droplet departure diameter for complete sandblasted surface (γ-region) is bigger than droplet departure diameter for complete dropwise (β-region) surface due to the liquid film formed on the surface. The low contact

angle on complete sandblasted surface (γ-region) forces the droplets to spread and form a film on the surface.

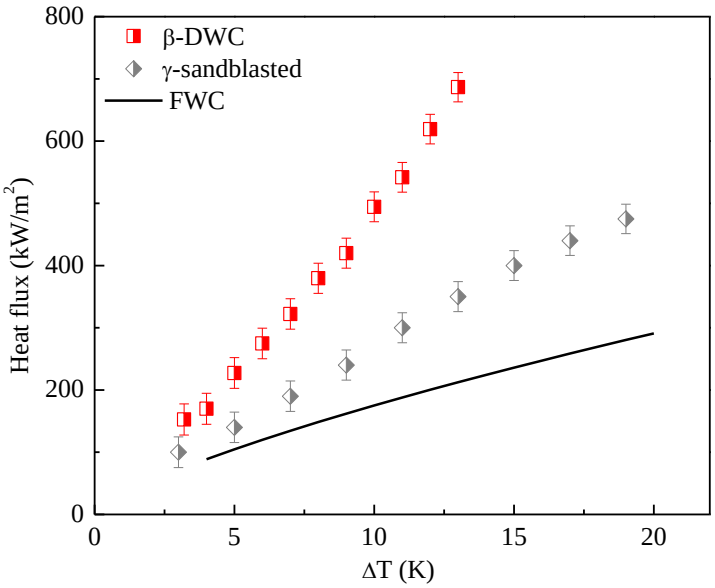

Figure 4.1: The heat transfer rates for (complete sandblasted (γ-region) surface (b) complete (β-region) surface

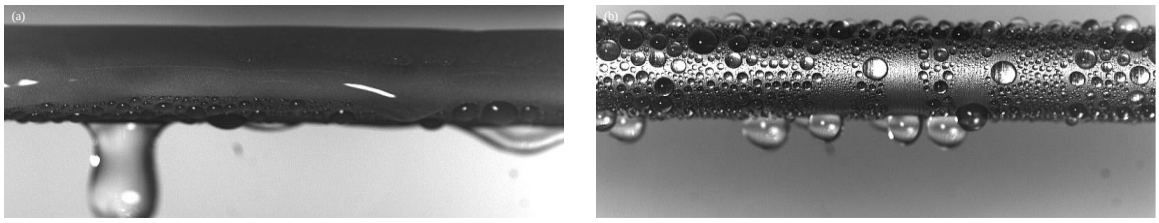

Figure 4.2: images of condensation on the (a) complete sandblasted (γ-region) surface (b) complete dropwise (β-region) surface.

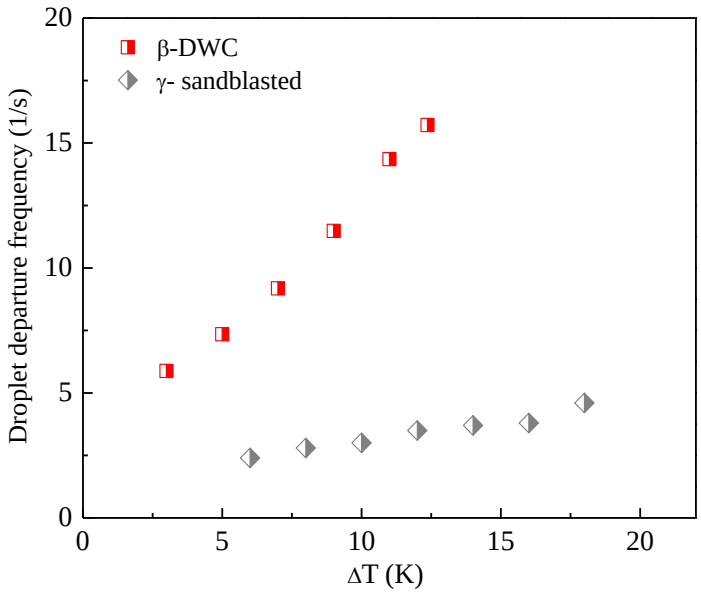

Figure 4.3: The droplets departure frequency for the sandblasted (γ-region) and complete dropwise (β-region) surfaces.

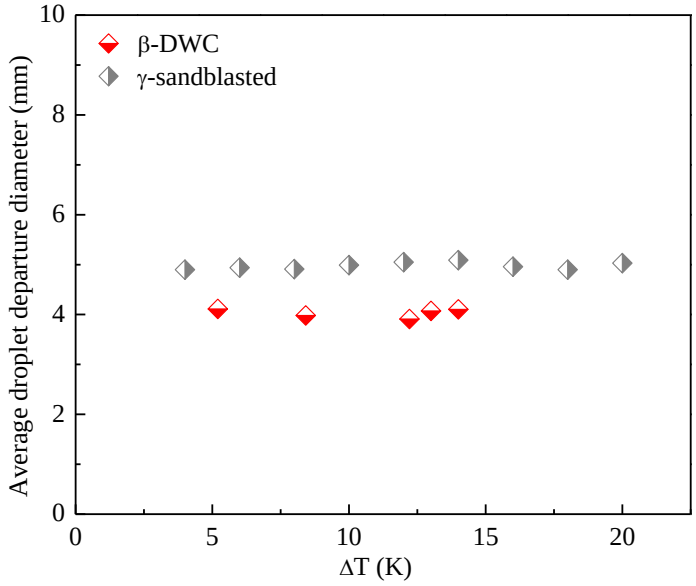

Figure 4.4: The droplets departure diameter for sandblasted (γ-region) and complete dropwise (β-region) surfaces.

4.2 Condensation heat transfer on hybrid surface (hydrophobic patterns)

Experiments of steam condensation have been performed on hybrid surfaces consisting of circular hydrophobic patterns which are compared with a complete

dropwise (β-region) surface and complete sandblasted (γ-regions) surface. The sizes of the patterns were changed while the horizontal and vertical hydrophilic gap scales between each adjacent hydrophobic circle were maintained constant as listed in Table 4.1. The schematic design for the hybrid surfaces is shown in Figure 4.5. The visualization study shows that the droplets nucleate, coalescence and migrate from the hydrophobic patterns to the hydrophilic surrounding regions during condensation because of the surface tension differences between the hydrophilic (γ-region) regions and the hydrophobic patterns (β-region) as shown in Figure 4.6. Most of the hydrophobic (β-regions) patterns were seen to be covered by water flowing from the hydrophilic (γ-region) regions during the condensation experiment as shown in Figure 4.6. All the hybrid surfaces show the same trends for the heat transfer rate. However, the maximum heat transfer rates observed for each surface were different depending on the diameter of the hydrophobic circles.

Table 4.1: The parameters and dimensions of the (hydrophobic patterns).

	β-Hydrophobic circles diameter (mm)	γ-Hydrophilic gap distance (mm)	Name (β- γ)
1	0.75	0.5	(β 0.75- γ 0.5)
2	1	0.5	(β 1.0- γ 0.5)
3	1.25	0.5	(β 1.25- γ 0.5)
4	0.5	0.5	(β 1.5- γ 0.5)

From the visualization study of condensation on hybrid surfaces, the droplets nucleate, coalescence and migrate from the patterns to the hydrophilic regions during the

condensation because of the surface tension differences between the hydrophilic regions and the patterns. The mechanism of the droplets transition from the hydrophobic circles to the hydrophilic regions is shown in Figure 4.6. Dropwise condensation was observed on the patterns as shown in Figure 4.6 where hydrophilic region bounds the patterns. All the hybrid surfaces show the same trends for the heat transfer rate. However, the maximum heat transfer rates observed for each surface were different depending on the size of the hydrophobic patterns.

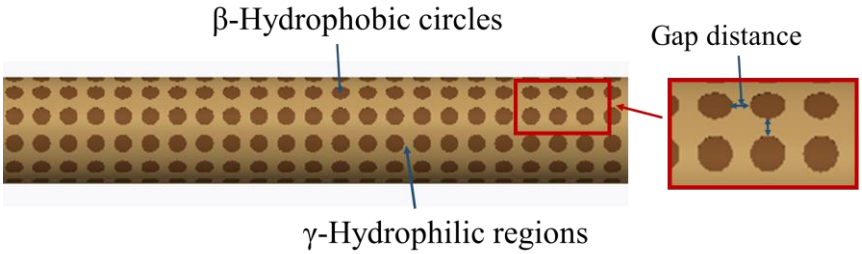

Figure 4.5: The schematic design of the hydrophobic patents on copper tubes.

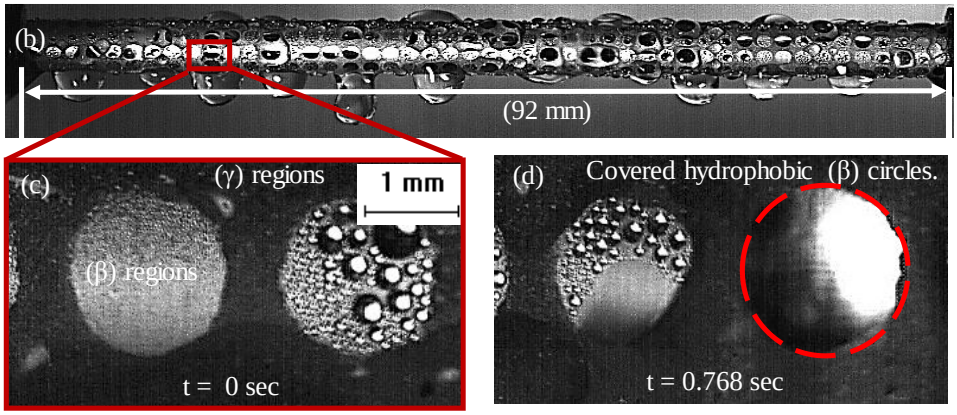

Figure 4.6:The condensation phenomena on hydrophobic patterns on copper tube (a) copper tube which has hydrophobic patterns where the length of tube is 92 mm (b) new droplets nucleate from hydrophobic circles while the hydrophilic regions surround the circles from all directions. (c) The droplets migrate from hydrophobic circles to hydrophilic regions and most of hydrophobic circles covered by the condensing water from hydrophilic regions.

The influence of the pattern's size on dropwise condensation heat transfer performance for the first series (hydrophobic patterns) is shown in Figure 4.7. Four hybrid patterned surfaces (β 0.75- γ 0.5, β 1.0- γ 0.5, β 1.25- γ 0.5, and β 1.5- γ 0.5 with a constant distance (gap) of (0.5 mm) were studied. The heat transfer results were compared with a complete dropwise (β-region) surface, complete sandblasted (γ-region) surface, and Nusselt model of filmwise condensation, shown in Figure 4.7. Initially the heat transfer rate increases with the decrease of the patterns' size. However, with further decreasing patterns size, the trend becomes the opposite. The heat transfer rates for those hybrid surfaces are lower than a complete dropwise surface. Based on the visualization study, it was found that the liquid film which is flowing from the hydrophilic surrounding regions (γ) covers most of the hydrophobic patterns and provides thermal resistance. The hydrophobic patterns become at this point inactive for dropwise condensation and not generate new droplets. Therefore, enlarging hydrophobic patterns leads to a larger covered area which is demonstrating a reduction in the heat transfer performance due to the increase in the thermal resistance. The optimum pattern size which shows the maximum heat transfer rate is for circles diameter of 1 mm and a gap of 0.5 mm as shown in Figure 4.8 for various temperature differences. The lower performance of heat transfer rate for big patterns size was due to the increased thermal resistances resulting from larger covered areas by the hydrophilic (γ-regions).

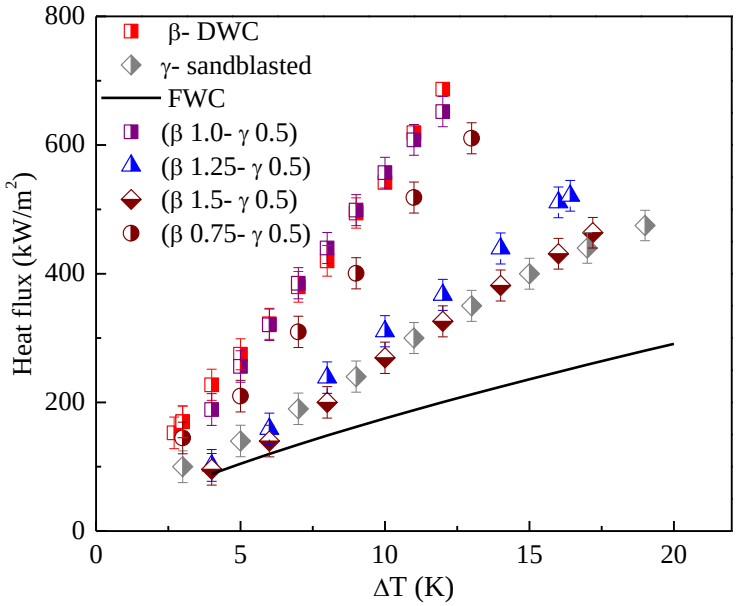

Figure 4.7: Heat flux of hydrophobic circles-hybrid surface at different diameters size versus with temperature difference (ΔT).

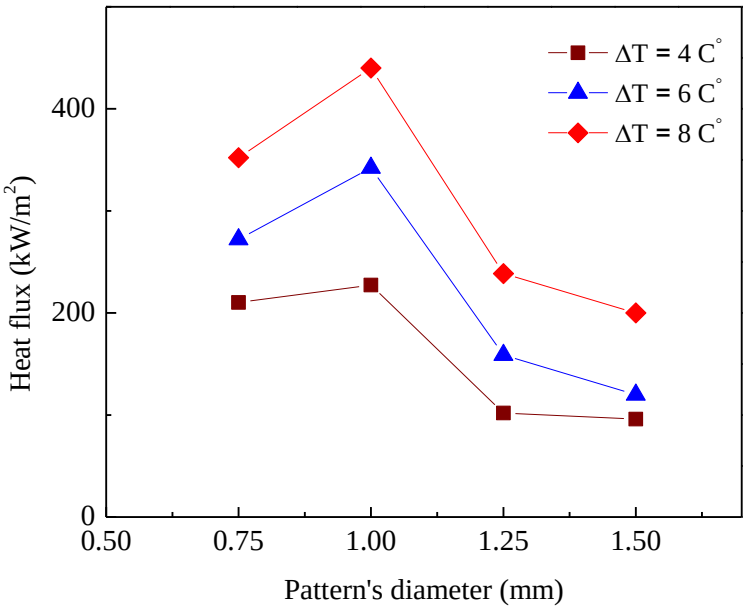

Figure 4.8: Effect of pattern's diameter on the heat transfer rate under different sub-cooling temperatures.

4.3 Condensation heat transfer on hybrid surfaces (hydrophilic patterns)

Condensation experiments on hybrid surfaces series 2 consist of hybrid surfaces (hydrophilic patterns) being investigated and compared with a complete dropwise (β-region) surface, a complete sandblasted (γ-region) surface, and Nusselt Model of filmwise condensation. The details of the patterns' diameter and gap distance of the hydrophilic circles are presented in Table 4.2. The schematic design and an actual image of a sample of this hybrid surface which has 0.5 mm gap and the size of pattern of 1.5mm is shown in Figure 4.9. All condensation experiments were conducted under same conditions. The results show that hybrid surfaces perform differently upon condensation compared to complete dropwise surface. The heat transfer rate was influenced by the size of the patterns and the gaps distance. Therefore, in this parametric study, the effects of the patterns size and the gap distance on the heat transfer rate were discussed.

4.3.1 Effect of the pattern's size

Figure 4.10 shows the heat transfer rate for complete dropwise (β-region) surface, a complete sandblasted (γ-region) surface, hybrid surfaces and Nusselt model of filmwise condensation. The study was conducted using four hybrid surfaces of different sizes (γ 1.0- β 0.5, γ 1.25- β 0.5, γ 1.5- β 0.5, and γ 2.0- β 0.5) with a constant pattern gap of (0.5 mm) to study the influence of pattern's size on condensation heat transfer rate. The results show that the heat transfer rates for all hybrid surfaces increase with increasing the size of the circles diameter and followed by a reduction with a further pattern size increase.

Table 4.2: Feature sizes of hybrid surfaces (hydrophilic patterns).

	γ-Hydrophilic circles diameter (mm)	Gap distance (mm)	Name (γ-β)	Area Ratio %
1	1	0.5	(γ 1.0- β 0.5)	35
2	1	0.75	(γ 1.0- β 0.75)	25.6
3	1	1	(γ 1.0- β 1.0)	19.6
4	1	1.5	(γ 1.0- β 1.5)	12.5
5	1.25	0.5	(γ 1.25- β 0.5)	40
6	1.25	0.75	(γ 1.25- β 0.75)	30.6
7	1.25	1	(γ 1.25- β 1.0)	24.2
8	1.25	1.5	(γ 1.25- β 1.5)	16.2
9	1.5	0.5	(γ 1.5- β 0.5)	44
10	1.5	0.75	(γ 1.5- β 0.75)	35
11	1.5	1	(γ 1.5- β 1.0)	28
12	1.5	1.5	(γ 1.5- β 1.5)	19.6
13	2	0.5	(γ 2.0- β 0.5)	50
14	1.5	2	(γ 1.5- β 2.0)	12

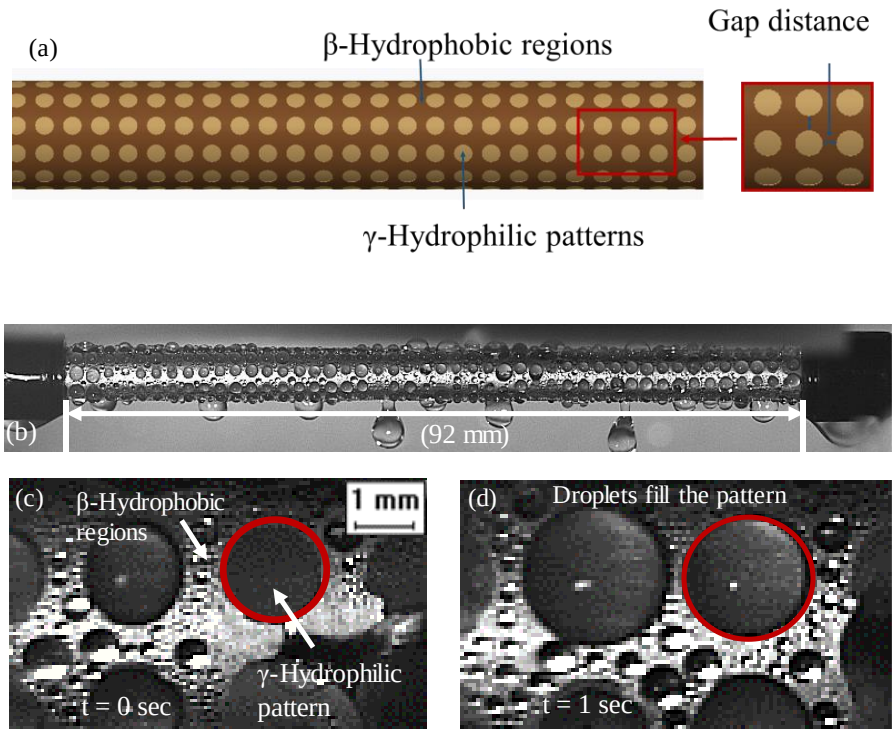

Figure 4.9: (a) The schematic design of hybrid surface with hydrophilic patterns (b) The hybrid surface that has hydrophilic patterns where their size is 1.5mm and the gap is 0.5 mm (c) The initial nucleation of droplets and migrating to the patterns (d) the pattern is filled by droplets and start to merge to neighbor pattern.

The maximum heat flux was about 12% higher than that of the complete dropwise (β-region) surface in case γ 1.5- β 0.5, while its performance is 20% lower than the complete dropwise (β-region) surface in case γ 1.0- β 0.5. The effect of hydrophilic circles on the heat flux at constant gap distance at different sub cooling temperature was discussed. The droplets migrate from the hydrophobic surrounding regions (β-region) at high momentum to the hydrophilic pattern (γ-region) until they filled the pattern. When the gap distance was relatively small (i.e. 0.5 mm), the condensed droplet on the pattern have the tendency to merge with another droplet located on the neighboring pattern. The connected/bridging droplets grow until it becomes large enough to roll off the surface as shown in Figure 4.11 when the pattern diameter is 1mm. A series of images of

condensation on hybrid surfaces when the circle's diameter is 1.0 mm show that the merging occurs between four neighboring circles. However, the number of connections in case γ 1.5- β 0.5 was fewer than that in case γ 1.0- β 0.5, as shown in Figure 4.12, when the circle's diameter was 1.5 mm. A series of images of condensation on hybrid surface when the circle's diameter is 1.5mm show the merging occurs between two neighboring circles. This increases the thermal resistance since more hydrophobic area percentage will be covered.

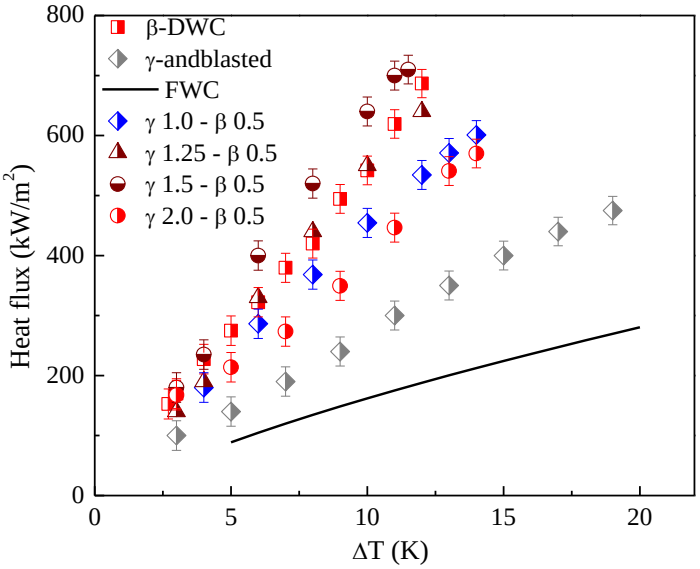

Figure 4.10: Effect of circle size on heat transfer rate (gap =0.5 mm) versus with temperature difference (ΔT).

As a result the hydrophobic regions (β-region) between the patterns became inactive during the condensation and generated no more nucleated droplets. Increasing the number of bridging between the patterns reduced the falling droplet velocity, droplet departure frequency and heat transfer rate. In addition, the droplets migrate from the patterns in case of γ 1.5- β 0.5 faster than that for case γ 1.0- β 0.5 during condensation due to less number of bridging between the patterns. Consequently, the number of migrating droplets to the patterns in case γ 1.5- β 0.5 was larger than for case γ 1.0- β 0.5

because of the bigger pattern circumference. Figure 4.13 shows the effect of pattern size on heat transfer rate at different temperature differences where the gap was constant. The maximum patterns size was identified (1.5mm) which enhances the heat transfer rate. However, the heat transfer rate was reduced when the size of the pattern is increased to 2 mm at same gap distance. The circle's diameter become equal to droplet size for complete dropwise (β-region) surface 2.2± 0.25, and the hybrid surface becomes inactive.

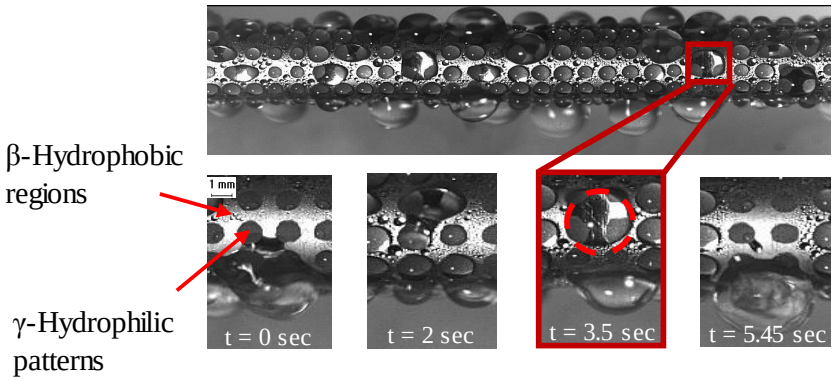

Figure 4.11 The condensation phenomenon on hybrid surface which has hydrophilic patterns, when the diameter of the pattern is 1mm, and the gap is 0.5mm, under different sub-cooling temperatures. The initial patterns connect with another pattern then extend to merge with another two patterns. The four connecting patterns and grow until they roll off from the surface.

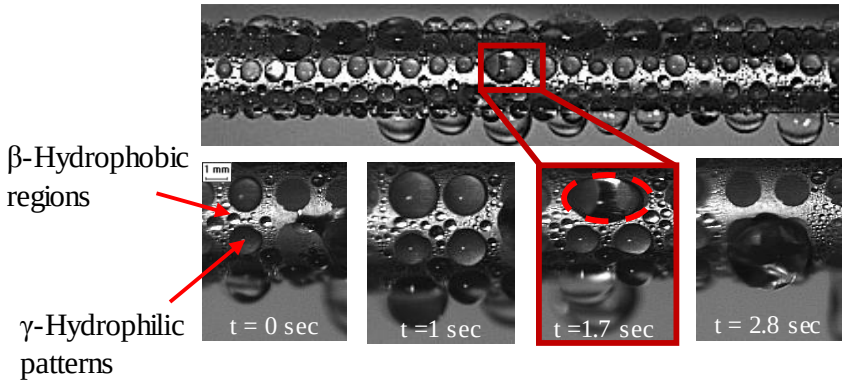

Figure 4.12: The condensation phenomenon on hybrid surface for cross section from copper tube which has hydrophilic patterns, when the diameter of the circles is 1.5mm, and the gap is 0.5mm. The initial pattern was filled by droplets and connected with another pattern. The droplets roll from the patterns and surface.

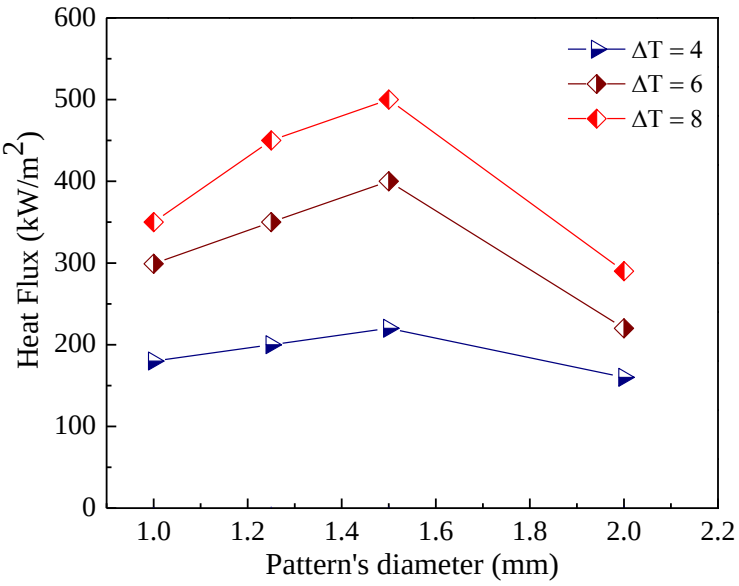

Figure 4.13: The effect of circle diameter on heat transfer rate (gap distance is 0.5 mm).

4.3.2 Effect of the gap

The influence of hydrophobic gap distance between patterns on condensation heat transfer rate was investigated. In this section, the heat transfer performance for different patterns gap distances and sizes were compared with that of a complete sandblasted (γ-region) surface, a complete dropwise (β-region) surface, and Nusselt's model of filmwise under the same experimental conditions. The heat transfer rate was increased significantly with the increase in the gap distance between patterns when the patterns' size (γ-region) is 1-mm as shown in Figure 4.14. The heat transfer rate for case γ 1.0- β 1.5was 30% higher than for case γ 1.0- β 0.5, as shown in Figure 4.14. Increasing the gaps leads to reduction in the bridging between the patterns and minimize the thermal resistance. The visualization study of droplet dynamics on hybrid surfaces having circles diameter of 1-mm and gap distance of 1.5mm is shown in Figure 4.15. The number of bridging between the patterns was reduced significantly compared to number of bridging when gap distance is 0.5 mm as shown in Figure 4.15. The hydrophobic regions between

the patterns increase which reduces the thermal resistance and enhance condensation heat transfer rate. The number of new nucleated droplets increased as the merging between the patterns decreased with increase the gap between the circles. Therefore, the droplet departure frequency increases and the droplets roll off from the patterns with high rates.

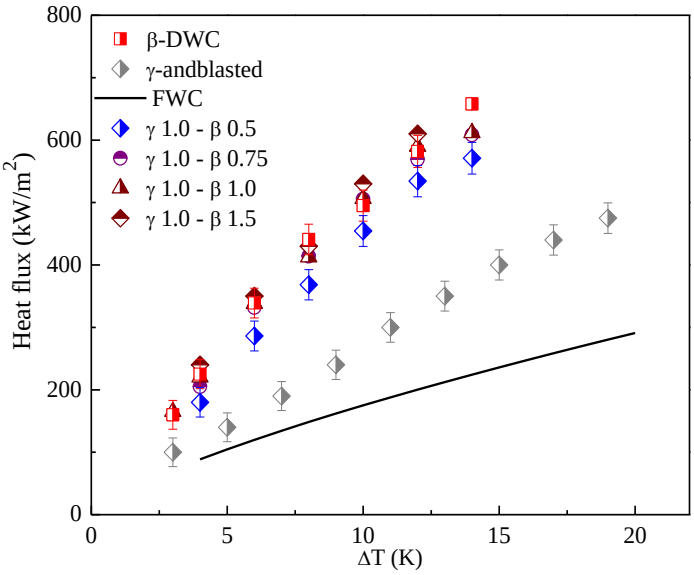

Figure 4.14: Effect of the gap on hybrid surface performance versus with temperature difference (ΔT) when the circle's diameter is 1mm.

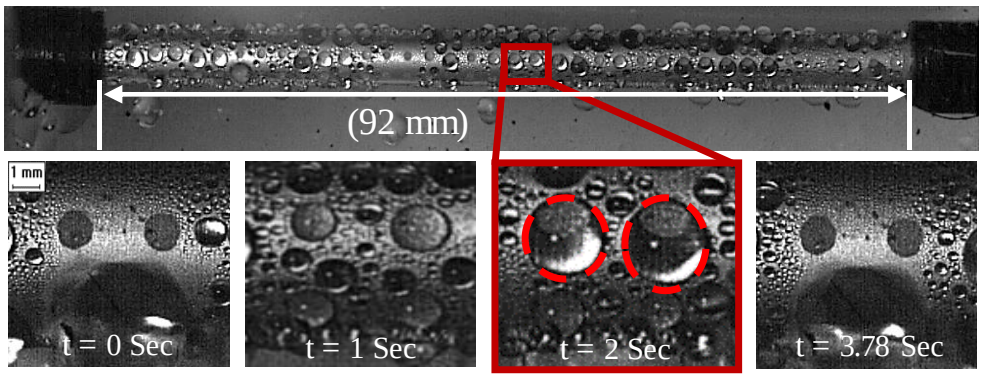

Figure 4.15: The influence of the gap on condensation performance for hybrid surface when the pattern's diameter is 1mm and the gap is 1.5mm. (a) copper tube which has 1mm hydrophilic patterns. The initial patterns are filled by migrating droplets and the droplets roll off from the patterns completely.

Figure 4.16 demonstrates the effect of the gap distance on the heat transfer rate for hybrid surfaces when the size of the pattern was 1.25mm. The figure also shows the heat transfer performance of a sample complete dropwise (β-region) surface, complete sandblasting (γ-region) surface, and Nusselt's model of filmwise condensation for comparison. The heat transfer rates for hybrid surfaces increased with increase the gap distance between patterns. The heat transfer rate was 51% higher than that of the complete dropwise (β-region) surface when the hydrophobic gap was 1.5 mm. The promotion of heat transfer rate resulted from increasing the number of droplets that nucleated and migrated to the patterns due to the decrease the number of bridging between the patterns. Moreover, the droplet departure frequency increased with increase the gap between patterns because the merging between patterns decreased and droplets fall quickly from the tube instead of sinking to the briging. The heat transfer rate increased as the number of bridging between the patterns reduced and the the new nucleated droplets increased.

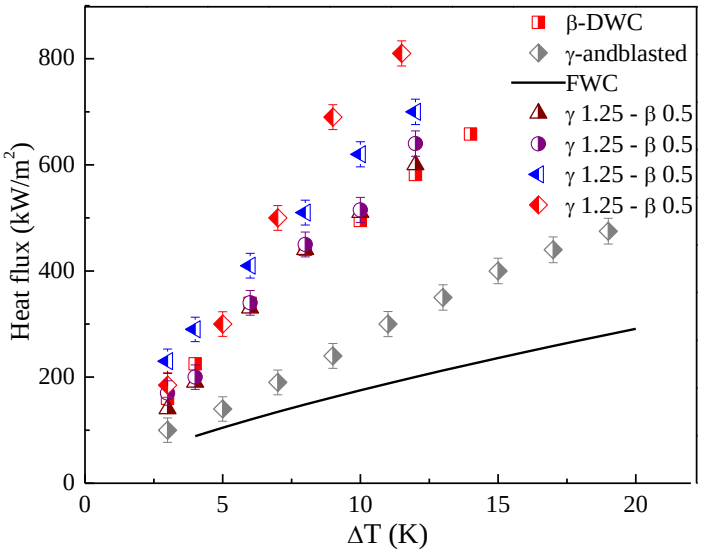

Figure 4.16: Effect of the gap on hybrid surface performance versus with temperature difference (ΔT) when the circle's diameter is 1.25mm.

The visualization study of condensation and droplet dynamics on hybrid surfaces which have 1.25 mm pattern's size and 1.5mm gap is shown in Figure 4.17. The hydrophobic areas between the patterns increases and droplets migrate without delay from the bridging phenomena. The thermal resistance reduced dramatically and the condensation heat transfer rate enhaned. Therefore, the condensate droplets roll off from the patterns faster than the droplet dynamic at 0.5mm gap distance.

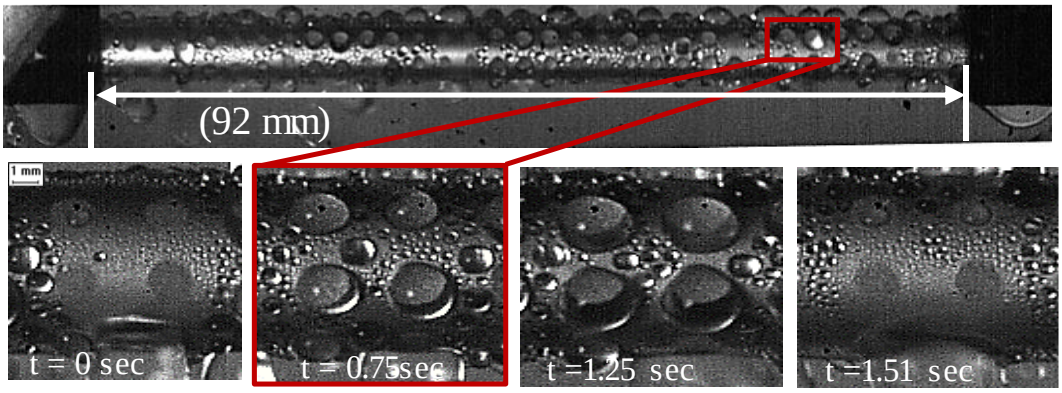

Figure 4.17: The influence of the gap on condensation performance for hybrid surface when the pattern's diameter is 1.25mm with the gap distance 1.5mm. (b) Copper tube which has 1.25 mm hydrophilic patterns. The initial patterns filled by migrating droplets until the droplets roll off from the patterns.

Figure 4.18 shows the heat transfer rate for hybrid surfaces with the same patterned size (1.5 mm) while the gap between the patterns changed. The figure also shows the heat transfer performance of a sample with complete dropwise (β-region) surface, complete sandblasted (γ-region) surface, and Nusselt's model of filmwise condensation for comparison. The hybrid patterned surfaces have different gap values (0.5, 0.75, 1.0, 1.5, and 2 mm, respectively) as listed in Table 4.2. The heat transfer rates for hybrid surfaces increased with increase the gap between patterns, but the performance decreased with further gap increases, as Figure 4.18 shows. The heat transfer rate was 79% higher than that of a complete dropwise (β-region) surface when the gap between

the patterns was 1.5 mm. The increase in the heat transfer rate resulted from the increase in droplet departure frequency because the bridging phenomena between the patterns at this gap length completely vanished. Figure 4.19 shows series of images of droplets dynamics on hybrid surface when the diameter of the circles is 1.5mm, and the gap distance is 1.5mm. The droplets move freely with high velocity across the surface and migrate to each pattern without motion resistance from the bridging. The droplets rolled off from the patterns in a faster and shorter time when the gap was 1.5mm than the droplet migrations when it was 0.5mm. The thermal resistance decreased because of the invisible bridging phenomena between the patterns during the droplet dynamic when the gap was 1.5mm. However, the heat transfer rate decreased as the gap length further increased between the patterns. The heat transfer rate decreased when the gap is 2-mm because the gap becomes equal to the size of droplets 2.25 $\pm$ 0.25-mm on the complete dropwise (β-region) surface. Therefore, the enhancement became trivial at this gap scale and the hybrid surface becomes inoperative for this patterns design.

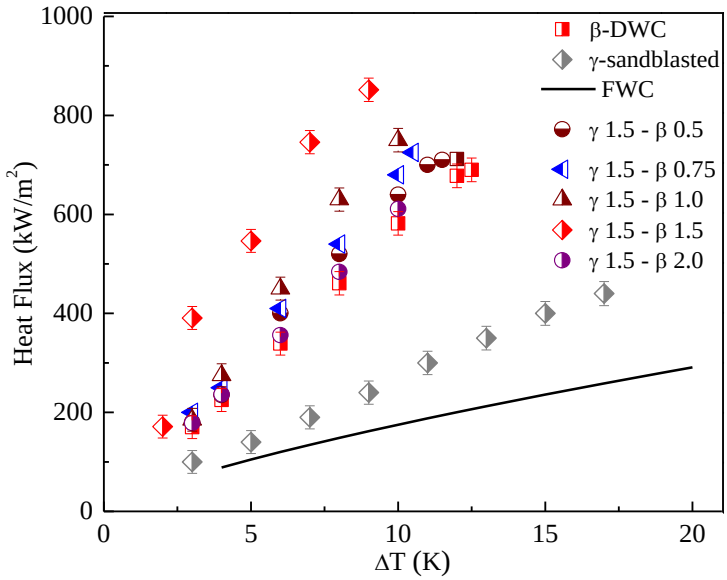

Figure 4.18: Effect of the gap on hybrid surface performance (circle diameter is1.5mm).

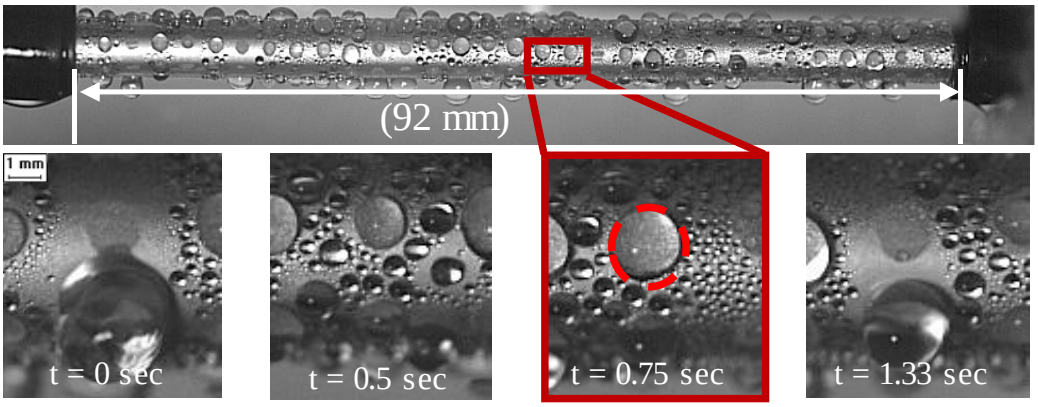

Figure 4.19: The influence of the gap on condensation performance for hybrid surface when the pattern's diameter 1.5 mm with the gap distance 1.5mm. Copper tube which has 1.5 mm hydrophilic patterns. The droplets migrate to the initial patterns they fill the patterns and then the droplets falls from the surface.

Figure 4.20 shows the optimum gap of hydrophobic distance that provide the maximum heat transfer rate. However, when the gap distance is 2 (i.e. a gap distance of 2 mm) the heat transfer was reduced because the circlular patterns become inactive when the gap distance was almost equal to the diameter of the droplets on the complete dropwise (β-region) surface.

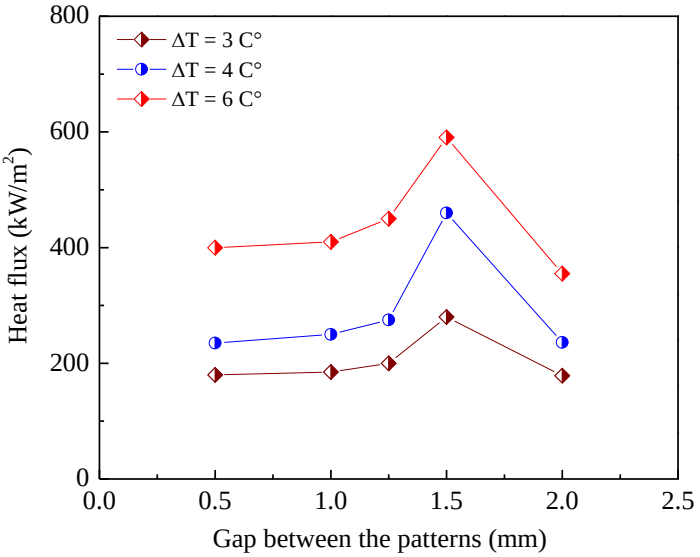

Figure 4.20: The optimum gap which affects heat transfer under different sub-cooling temperatures.

4.4 Droplet dynamic analysis of condensation phenomena on hybrid surfaces (hydrophobic patterns)

The droplet dynamics and departure frequency during condensation can be improved using two wettability regions as hybrid surfaces. Experiments have been performed on hybrid surfaces that have hydrophobic patterns while the remaining tube areas are hydrophilic regions. The designs of the hybrid surfaces (hydrophobic patterns) are listed in Table 4.1. The droplet dynamic mechanism on the hybrid surfaces (hydrophobic patterns) is shown in Figure 4.21. The series of images explain the droplet's transition from hydrophobic patterns to the hydrophilic regions. The droplets nucleate, grow, coalescence inside each hydrophobic pattern and migrate to hydrophilic regions due to the gradient wettability regions. However, most of the patterned regions are covered by water film that formed on the hydrophilic regions. The droplet departure frequency of droplets and departure diameter for the hybrid surfaces (hydrophobic patterns) is shown in Figure 4.22 compared to complete dropwise (β-region) and sandblasted (γ-region) surfaces. The gap between the patterns remains constant (0.5mm) while the sizes of the patterns changes. The droplet departure frequency for hybrid surfaces (hydrophobic patterns) slightly increases with decreasing the size of the patterns. But with further decrease of the pattern size, the departure frequency will decrease. The droplets departure frequencies for those hybrid surfaces (hydrophobic patterns) are lower than complete dropwise (β-region) surface. The hydrophobic patterns that covered by water prevent new droplets from rolling off from the surface and force the droplets to sink into the covered circles and hydrophilic regions instead of migrating from the tube.

The increase of the patterned circle's diameter increases the resistance of the droplets to roll off from the surface and decreases the droplet departure frequency.

In addition, the droplet departure diameters for hybrid surfaces that shown in Figure 4.23 are compared to the complete dropwise (β-region) and complete sandblasted (γ-region) surfaces. The droplet departure diameters for hybrid surfaces are the same with complete sandblasted surface. The big departure diameters of hybrid surfaces (hydrophobic patterns) lead to the increase of thermal resistance which decreases the droplet departure frequency and condensation heat transfer compared to the complete dropwise (β-region) which has a smaller departure diameter.

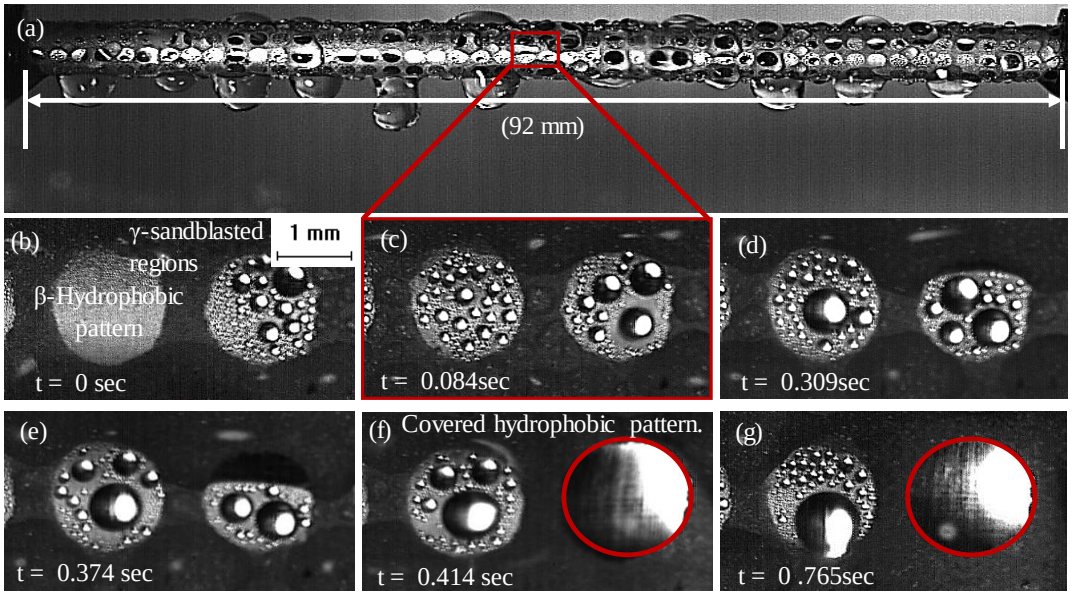

Figure 4.21: The droplet dynamic mechanism on the hybrid surface, which has hydrophobic patterned circles with remaining hydrophilic (γ-regions). (a) Copper tube which has hydrophobic patterns. (b) Initial hydrophobic pattern. (c) Droplets nucleate, coalescence, and grow inside the pattern. (d) Some droplets migrate to hydrophilic regions (e) Some patterns start to be covered. (f) Patterns covered completely. (g) droplets migration from pattern to hydrophilic regions while some patterns covered.

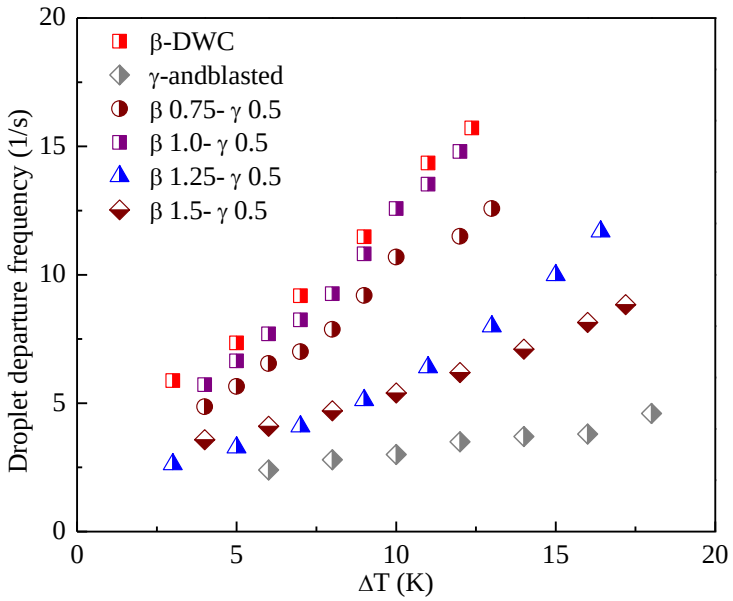

Figure 4.22: Droplet departure frequency for hydrophobic patterns-hybrid surface at different size with fixed gap 0.5 mm versus with temperature difference (ΔT).

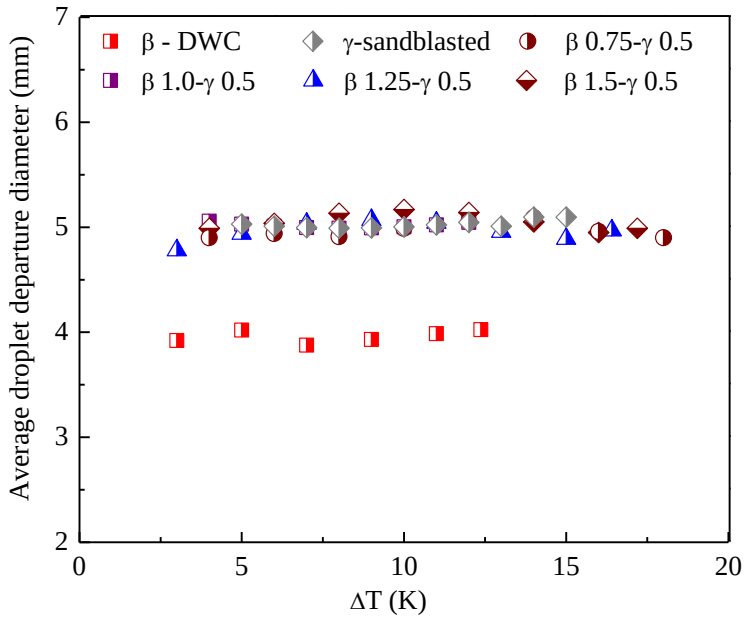

Figure 4.23: Droplet departure diameter for hydrophobic patterns-hybrid surface at different circle's diameters with fixed gap 0.5 mm versus with temperature difference (ΔT).

4.5 Droplet dynamics analysis of condensation phenomena on hybrid surfaces (hydrophilic patterns)

Experiments have been implemented on modified hybrid surfaces that have hydrophilic circular patterns. The phenomenon of condensation on hybrid surfaces (hydrophilic patterns) show that the hydrophobic regions border the hydrophilic patterns from all directions. The design and parameters of the hybrid surfaces (hydrophilic patterns) was listed in Table 4.2. The mechanism of the droplets transition from the hydrophobic regions to the hydrophilic patterns is shown in Figure 4.24. The series of images shown in Figure 4.24 explain the droplet's transition from hydrophobic regions to the patterns. The droplets nucleate, grow, coalescence and migrate to the patterns in high momentum during the condensation because of the surface energy differences between the hydrophilic patterns and the hydrophobic regions. Then, the droplets filled the hydrophilic patterns and rolled off due to the gravitational force. The hybrid surfaces (hydrophilic patterns) show different droplet dynamic and departure frequency depending on the size of the hydrophilic patterns and the gap distance between the patterns. The droplet dynamic behavior and departure frequency of droplets rely mainly on the size of the pattern's boundary and the gap between the adjacent patterns. The pattern's size and the length of the gap between the patterns were changed until the optimum pattern size and the optimum gap that yielded the maximum departure frequency were obtained.

4.5.1 Influence of patterns size

The droplet departure frequency for the hybrid surfaces is shown in Figure 4.25 compared to complete dropwise (β-region) and sandblasted (γ-region) surfaces. The gap between the patterns was remained constant (0.5mm) while the size of the patterns was

changed gradually. The droplet departure frequency for hybrid surfaces slightly enhances with an increase in the size of the patterns, but it decreases with further size increase. The optimum size of the pattern's area that obtains the peak departure frequency was found in this study. The maximum departure frequency is about 10 % higher than the complete dropwise (β-region) surface for case (γ 1.5-β 0.5) while it is 25% lower than the complete dropwise (β-region) surface for case (γ 1.0-β 0.5).

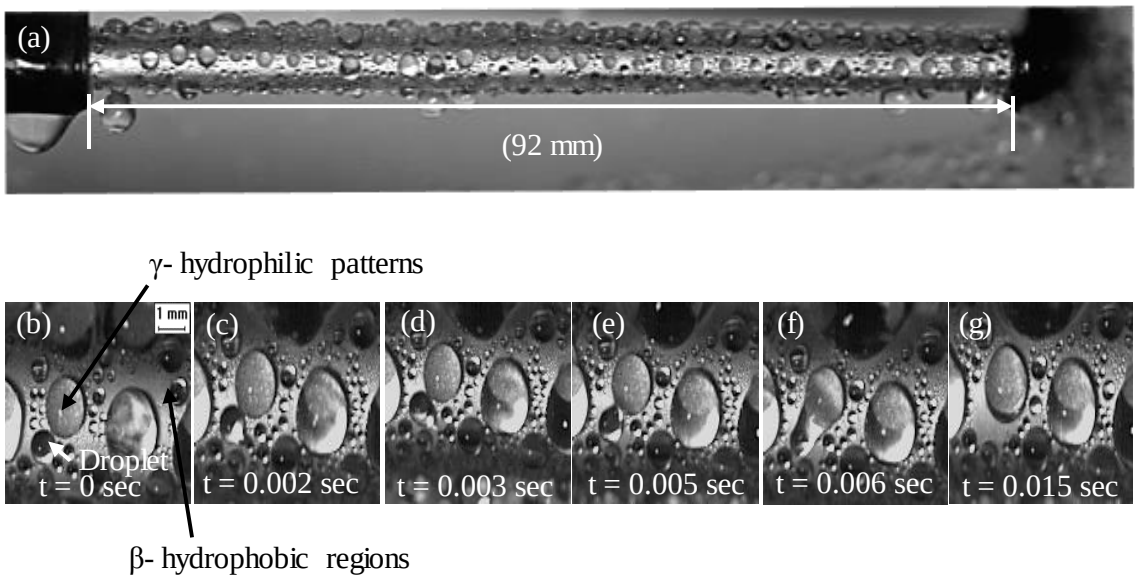

Figure 4.24: The mechanism of droplet transition for the hydrophobic regions to the hydrophilic regions. (a) Copper tube that has hydrophilic circular patterns (b) Droplet on hydrophobic region. (c) Droplet coalescences with adjacent droplets. (d) Growing. (e) Droplet moves toward hydrophilic pattern. (f) Droplet transition. (g) Droplet migration.

Figure 4.26 shows the condensation phenomena and droplets dynamics on the hybrid surface when the pattern's diameter is (1mm), and the gap between the patterns is (0.5mm). The condensate droplets move to the boundary of the patterns from all directions until they fill the patterns completely. The droplets migrating into the patterns adhere on each pattern and lead the pattern to merge with another neighboring pattern. Most of the two merging patterns merge with two adjacent merging patterns as a bridge

as shown in Figure 4.26. The hydrophobic gaps between the patterns are covered during the merging of the patterns. Then, the gaps become inactive during condensation because of the continuous merging between the patterns.

The surface area that is covered by the merging of the patterns during the bridging is 8.353 mm^2 including the hydrophobic regions. Therefore, the total active hydrophobic regions become smaller with an increase in the number of bridging, and the number of renewal condensed droplets is diminished. The number of migrating droplets to the patterns are sinking in the bridging areas instead of flowing down from the tube and allowing for more new droplets to nucleate. In addition, the bridging phenomena increases resistance that prevents droplets from rolling off of the surface because of the existence of large bridign areas which postphone movement of droplets. Therefore, the droplet departure frequency decreases due to increase the merging between the patterns and the increase in the resistance of falling droplets from the surface which reduces the number of new nucleated droplets on the surface.

Figure 4.27 shows series of images of the condensation phenomena and droplets dynamic on the hybrid surface when the pattern's diameter is (1.5mm), and the gap between the patterns is also (0.5mm). The number of bridging between the patterns for case (γ 1.5-β 0.5) is less compared to case (γ 1.0-β 0.5), as shown in Figure 4.27. The bridging take place only between two adjacent patterns for this case. The active hydrophobic regions become higher and significant. The number of renewal droplets and the droplet dynamics increase due to decrease the merging between the patterns. The surface area that covered the patterns during the bridging is 5.44 mm^2 including the hydrophobic regions.

Moreover, the water departs from the patterns in less time compared to other cases because of the lacking number of bridging as shown in Figure 4.27. In addition, the circle's boundary in case (γ 1.5-β 0.5) is bigger than the other cases, and then the number of droplets that nucleate and merge to these circles is higher. Therefore, the droplet departure frequency increases because of the reduction of the droplets' falling resistance due to decrease the number of bridging and increase the number of fresh droplets to the pattern's boundary. However, the departure frequency decreases with further increase of a pattern's boundary size as in case (γ 2.0-β 0.5). The droplets departure frequency is lower than complete dropwise surface when the pattern's diameter is 2mm because the coverage area by bridging is bigger compared to case (γ 1.5-β 0.5). Also, the pattern's diameter is almost the same as the droplet's diameter for complete dropwise surface (2-2.25) mm when the hybrid surface does not work efficiently at this size scale.

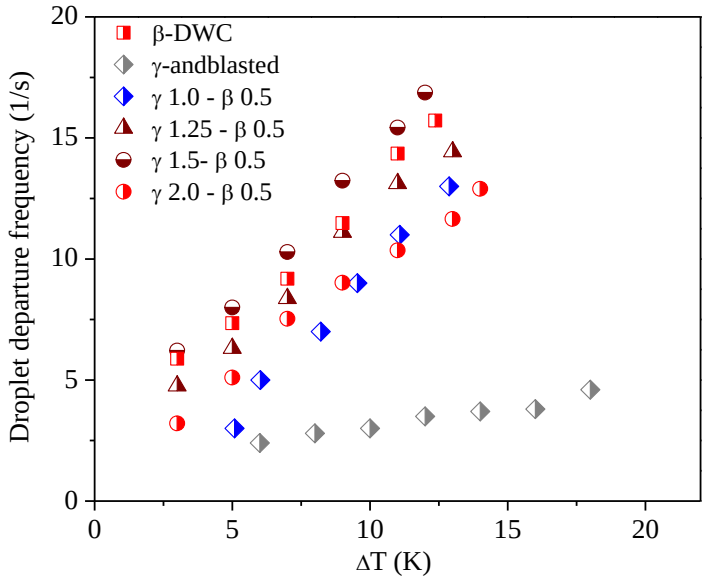

Figure 4.25: Droplet departure frequency for different pattern's diameter with fixed gap 0.5 mm versus with temperature difference (ΔT).

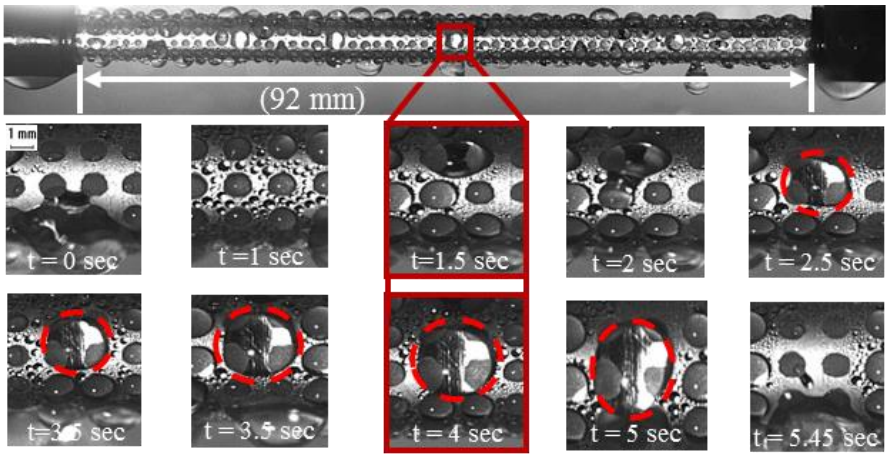

Figure 4.26: The influence of patterns size on droplet dynamic and departure frequency for the hybrid surface where the diameter of the hydrophilic patterns is 1mm and 1.5mm while the gap scale is 0.5mm. Copper tube has 1mm diameter of hydrophilic patterns. The series of images show the fresh patterns and how droplets nucleate and migrate to the patterns. The two patterns merge and connect with each other and then the two patterns merge to another pattern to cover four patterns as a bridging. The bridging area grows and the droplets continue sinking to the bridging. The water droplets roll off from the patterns and tube.

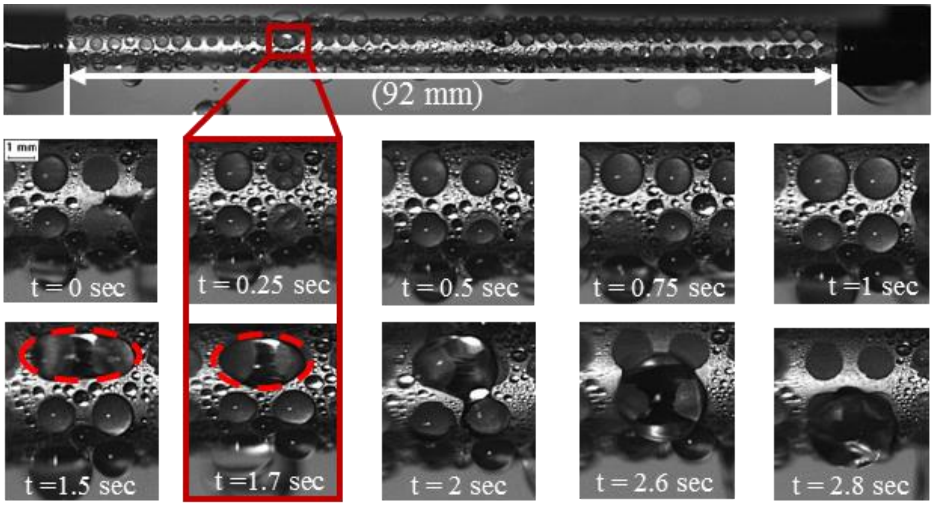

Figure 4.27: The influence of patterns size on droplet dynamic and departure frequency for the hybrid surface where the diameter of the hydrophilic patterns is 1mm and 1.5mm while the gap scale is 0.5mm. Copper tube has 1.5 mm diameter of hydrophilic patterns. The series of images shows the fresh pattern and how droplets nucleate and migrate to the patterns. The droplets continue migrating and then the droplets move toward the pattern. The pattern filled by droplets and merges and connect with another pattern. The bridging area roll off from the patterns and tube.

The renewal area frequency of the patterns on hybrid surfaces is different. Figure 4.28 shows the renewal area frequency for hybrid surfaces has various sizes and same gap between them. The RAF for case (γ 1.5-β 0.5) is higher than other cases since the patterns are filled quickly by droplets due to a lower number of bridging. The renewal area frequency for other surfaces is the low because of the high number of bridging that delay the water departure from the patterns. The droplet departure diameter is shown in Figure 4.29 for the hybrid surfaces compared to the complete dropwise (β-region) and complete sandblasted (γ-region) surfaces. The droplet departure diameter for hybrid surfaces is the same departure diameter with complete dropwise (β-region) surface. The optimum size of the pattern that affects the droplets departure frequency and droplet dynamic existed in this study.

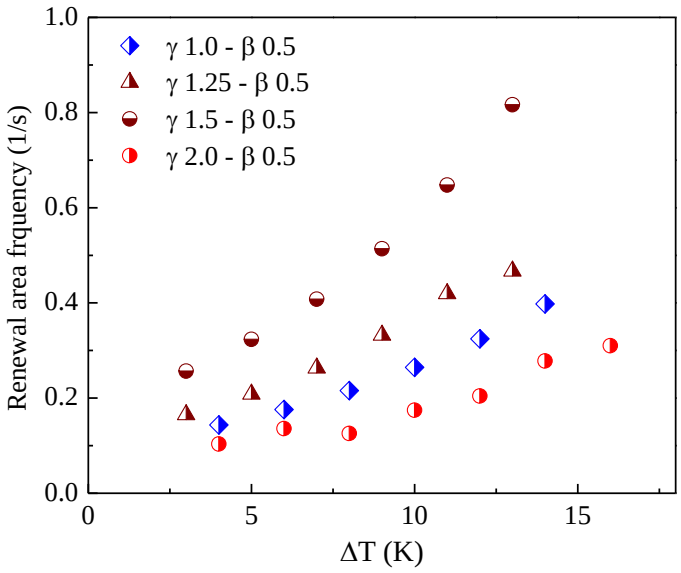

Figure 4.28: Renewal area frequency for various patterns' diameter and same gap distance is 0.5mm.

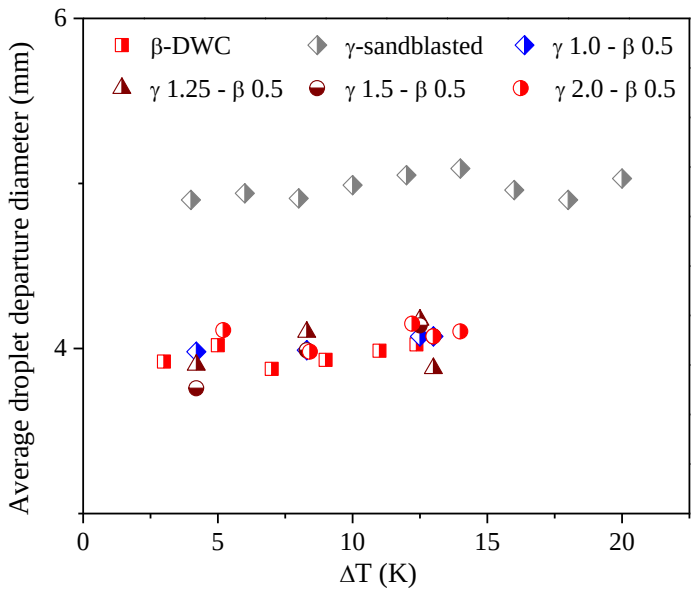

Figure 4.29: Droplet departure diameter for different pattern's diameter and gap distance is 0.5mm.

4.5.2 Influence of patterns' gap

The effect of the gap between the patterns on droplet departure frequency and droplet dynamic during condensation on hybrid surfaces (hydrophilic patterns) is discussed. Figure 4.30 shows the effect of the pattern's size on droplet departure frequency for hybrid surfaces when the diameter of the circle patterns is constant (1mm) and various gap distances. The tested surfaces design and parameters were listed in Table 4.2. The renewal area frequency for the patterns and the droplets departure diameter from tube are studied. The droplet departure frequency increases with the increase in the gap between the patterns due to the reduction in the number of merging between the patterns. As mentioned in Figure 4.26, the hydrophilic patterns merge with each other as a bridge during the droplets migrations when the gap is 0.5mm between the patterns. The bridging phenomena will extend to cover more than two patterns. Then the gap between the patterns is covered because of bridging phenomena which cause a resistance against the

droplet falling from the surface. The velocity of droplets' departure from each pattern decreases due to the bridging between the patterns which resist droplet's movements. However, the number of bridging between the patterns was diminished and the droplet dynamics improved when the gap increased. Figure 4.31 shows the droplet dynamic and droplet departure from the same patterns when the gap is 1.5mm between each of the two patterns. The number of merging between the patterns reduced dramatically at this gap scale. The gap between the patterns becomes more efficient and creative for more new droplets moving toward patterns. The total active hydrophobic regions become bigger with the increase of gap and the amount of renewal droplets increased. In addition, the resistance of droplets falling from the patterns and surface decreases because of the decrease of the number of bridging between the patterns. The droplet departure frequency increases with the number of new nucleated droplets increases and the resistance of droplets falling decreases.

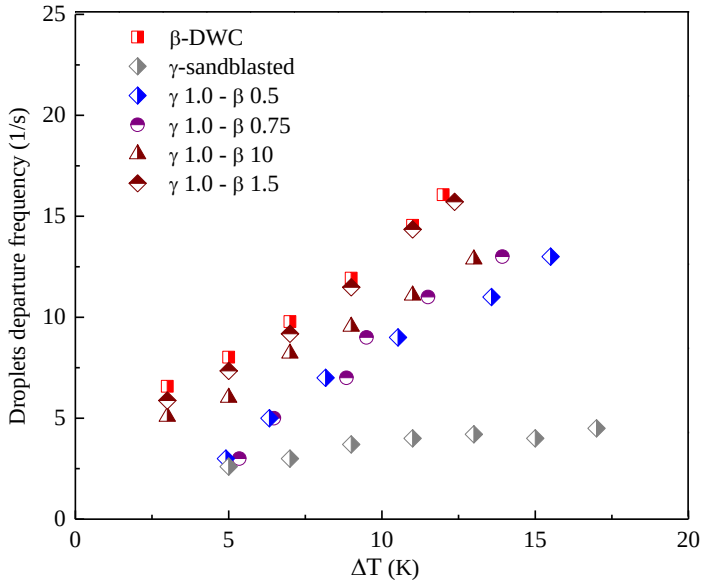

Figure 4.30: Effect of the gap distance on droplet departure frequency at the same patterns size (d = 1mm).

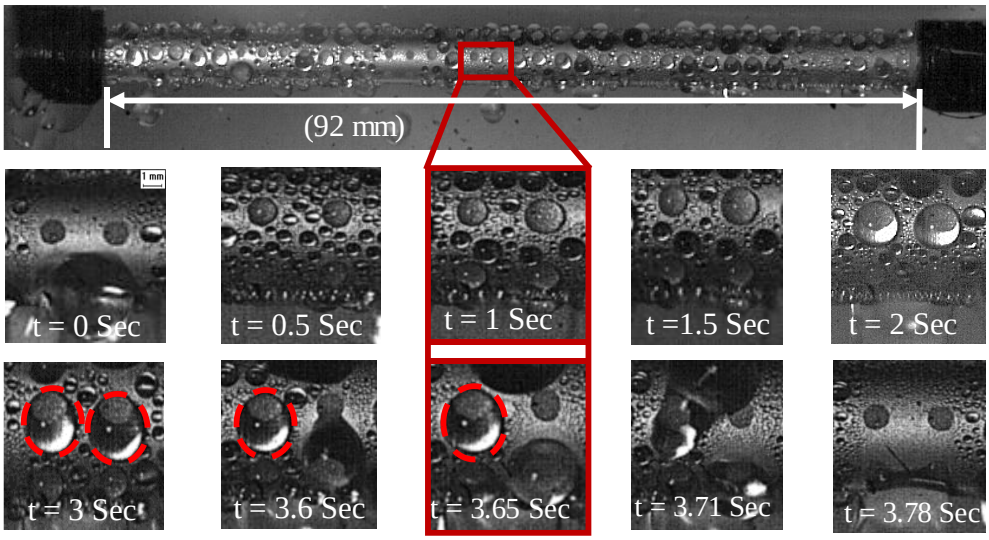

Figure 4.31: The influence of gap between patterns on droplet departure frequency and droplet dynamic for hybrid surfaces. The copper tube has circular patterns where the diameter of the patterns is 1mm, and the gap is 1.5mm. The series of images show condensation and droplets migration from the patterns. Most of the patterns do not connect with each other, and then the thermal resistance is reduced.

The renewal area frequency, which demonstrates the number of droplets roll off from the patterns per second, was shown in Figure 4.32 with different gap distances and constant pattern's sizes. The renewal area frequency increases with increase of the gap between the patterns, because of the diminishing the bridging phenomena between the patterns and reducing the resistance of droplets movement from the patterns. Then, the hydrophobic areas between the patterns become active and more new droplets start nucleating and migrating to the patterns. However, the droplet departure diameter which is shown in Figure 4.33 for hybrid surfaces (hydrophilic patterns) at different gap scale is almost the same as complete dropwise (β-region) surface.

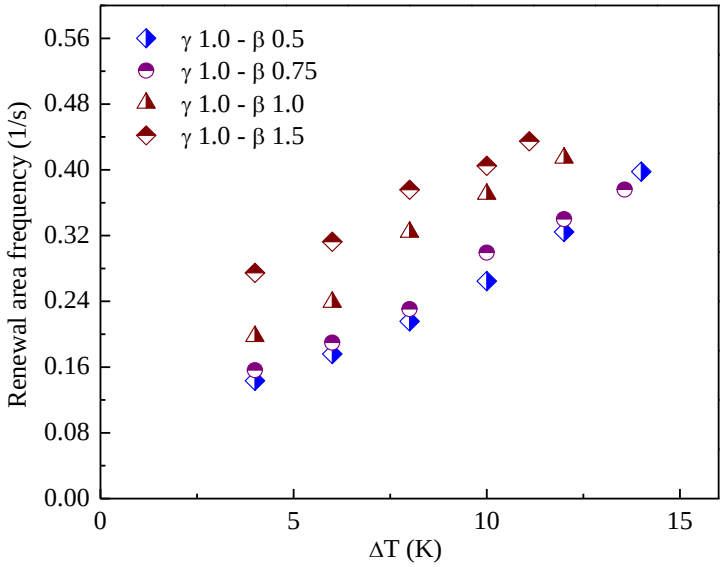

Figure 4.32: Renewal area frequencies for hybrid surfaces at different gaps with fixed pattern diameter 1 mm versus with temperature difference (ΔT).

Figure 4.34 explains the effect of the gap distance on droplet departure frequency for hybrid surfaces (hydrophilic patterns), which have the patterns size (1.25mm). The features design of patterns was listed in Table 4.2. The renewal area frequencies for the patterns and droplets departure diameter are introduced. The droplet departure frequency increases gradually with increase of the gap between the patterns.

The condensate droplets between the patterns migrate to patterns with high momentum from all directions because of the surface tension force differences. When the gap length is 0.5mm the patterns merge with other patterns during droplet's migrations. The connection of two merging patterns extends as a bridge to cover another two merging patterns. The bridging area grows until they reach a certain size and then roll off from the surface. The hydrophobic gaps between the patterns are covered during the merging of the patterns and transform to isolated areas for fresh nucleated droplets. Therefore, the

droplet departure frequency decreases at this gap and size scales because of the decrease of the total hydrophobic areas due to the bridging phenomena.

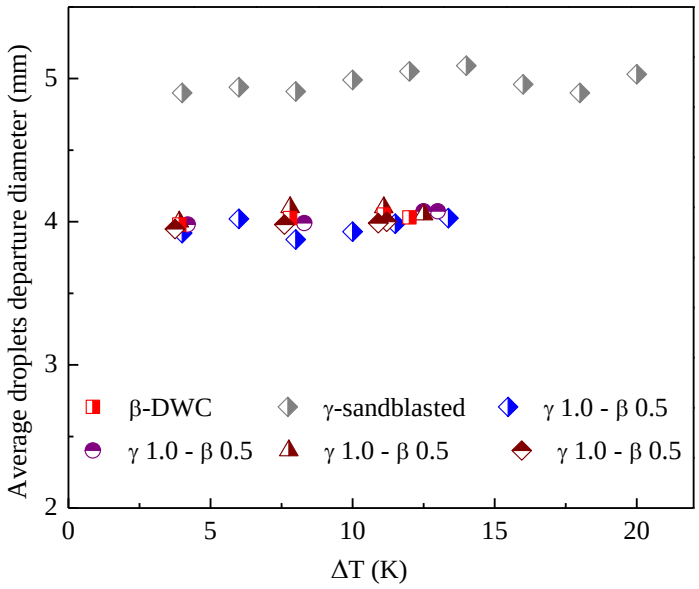

Figure 4.33: Droplet departure diameter for hybrid surfaces at various gaps with fixed pattern diameter 1 mm versus with temperature difference (ΔT).

The visualization study on condensation and droplet dynamic on hybrid surface which has the patterns size (1.25mm) with 1.5mm gap distance. The number of merging and bridging phenomena between the patterns are highly reduced at the gap scale (1.5mm) as shown in Figure 4.35. The hydrophobic areas increase with increase of the gap between the patterns and the number of new nucleated droplets increases as well. The time scale for droplets departure from the patterns decreases due to the decrease in the number of bridging between the patterns. The droplet departure frequency for this gap scale (1.5mm) is bigger compared to gap scale (0.5mm) since the gap is not covered as a bridge during droplets migrating. The renewal area frequency for the patterns on the surfaces is higher when the gap length is 1.5 mm compared to other gap scales as shown in Figure 4.36. Reducing the merging between the patterns increases the renewal area

frequency and thereby increases droplet departure frequency. However, the droplets departure diameter for those hybrid surfaces does not change for the entire hybrid surfaces as shown in Figure 4.37. The droplet departure diameter for hybrid surfaces is same as complete dropwise surface.

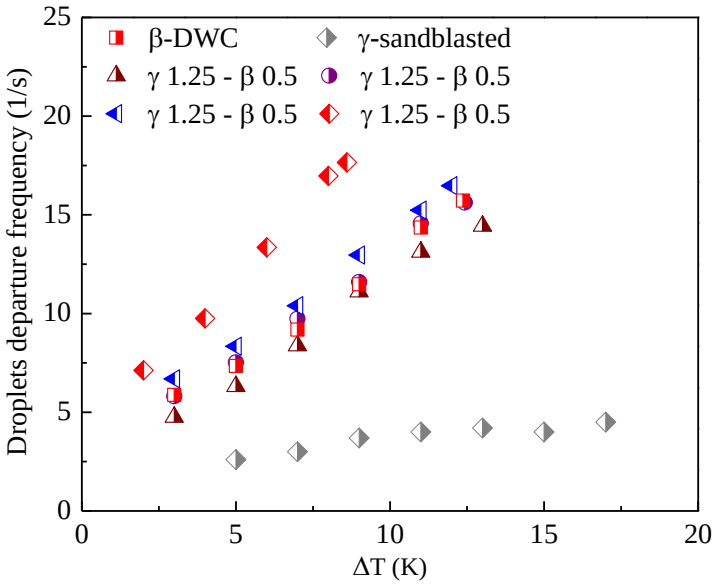

Figure 4.34: Droplet departure frequency for hybrid surfaces at different gaps with fixed pattern diameter 1.25mm versus with temperature difference (ΔT).

Figure 4.38 shows the departure frequency for the hybrid surfaces when the pattern's size is 1.5mm and the gap distances are changed. The figure shows the droplets departure frequency for completed sandblasted (γ-region) and completed dropwise (β-region) surfaces for comparison. The features and designs of the patterns were listed in Table 4.2. The droplet departure frequency is improved with increasing the gap between the patterns. The visualization study of droplet dynamic is shown in Figure 4.39 when the gap scale is 1.5 mm.

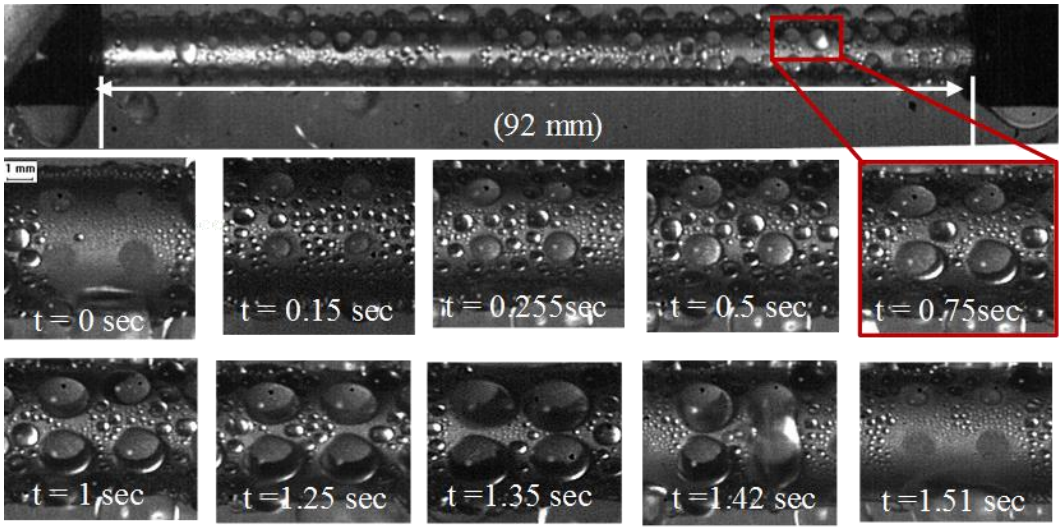

Figure 4.35: The influence of gap between circles on dropwise condensation heat transfer for the hybrid surface. The copper tube has patterns with diameter of the circle1.25mm, and the gap 1.5mm. The pattern does not connect with each other, and then the thermal resistance is reduced. The series of images show Fresh pattern and how the droplets migrate to the patterns. The patterns are filled by droplets and the pattern is filled by droplets. Then, the water droplets start to slide from the pattern and the droplets roll off from the patterns and tube.

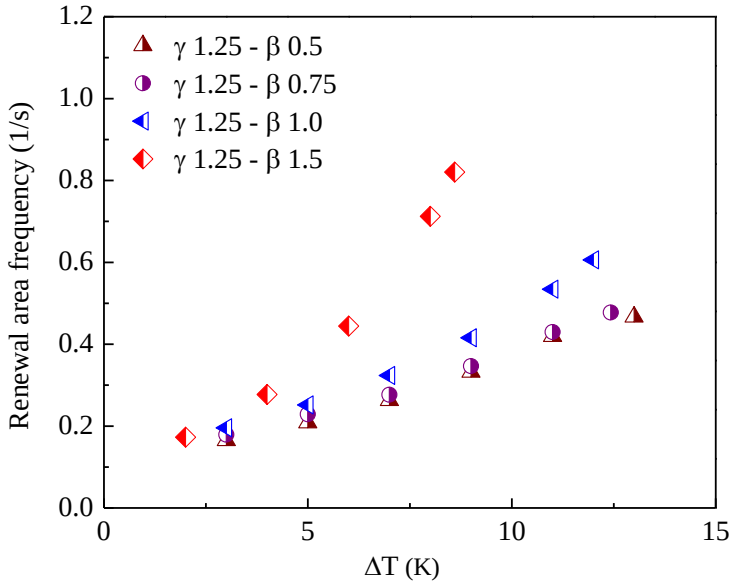

Figure 4.36: Renewal area frequency at different gap with fixed pattern diameter 1.25mm versus with temperature difference (ΔT).

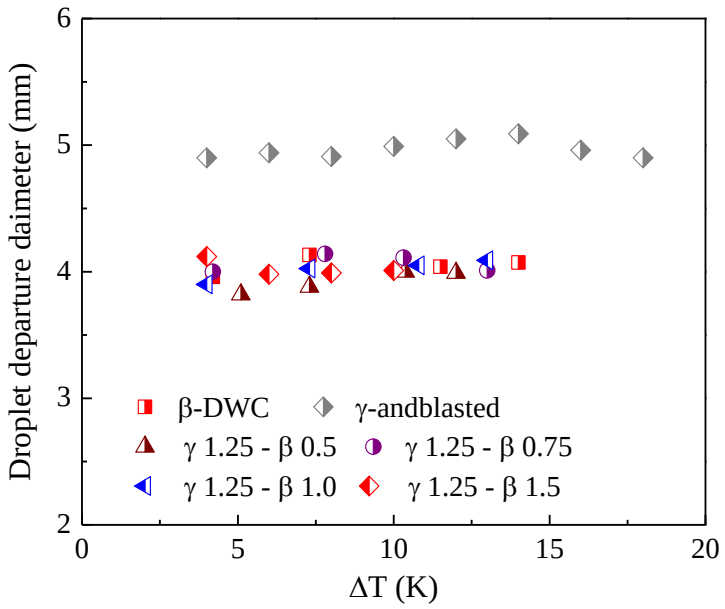

Figure 4.37 Droplet departure diameter for hybrid surfaces at various gaps with fixed pattern diameter 1.25mm versus with temperature difference (ΔT).

As noticed in Figure 4.27, the droplets move from the gaps to patterns with high velocity because of the wettability gradient on the surface when the gap length is 0.5mm. Some of the patterns merge with another pattern as a bridge until they roll off from the surface. The hydrophobic areas between the pattern is covered during the merging for a long time at the gap 0.5mm. Therefore, the droplet departure frequency is the low at the gap scale 0.5 mm because of the reducing the hydrophobic areas and decreasing the number of fresh droplets induced by hydrophobic regions. However, the number of merging and the bridging phenomena between the patterns vanishes completely when the gap length is 1.5 mm, and the droplets can move freely through the patterns as shown in Figure 4.39. The amount of area which covers the hydrophobic regions during merging for (γ 1.5-β 0.5) surface is 5.12 mm^2 while it is 3.43 mm^2 for (γ 1.5-β 1.5) surface including the hydrophilic region's area. The departure frequency for case (γ 1.5-β 1.5) is higher than case (γ 1.5-β 0.5) because the covered hydrophobic area between the patterns

does not exist at the gap scale1.5mm. Moreover, the number of new nucleated droplets increase with this gap distance and droplets can move free and fast across the patterns and surface. The droplet departure frequency and the heat transfer performance for this hybrid surface enhanced because of reducing the thermal resistance which are resulted from the bridging phenomena. The droplet departure frequency for case (γ 1.5-β 1.5) is 1.37 times the departure frequency for the complete dropwise (β-region) surface. However, the departure frequency decreases with further increase in the gap scale as shown in Figure 4.38. The departure frequency reduces when the gap scale is 2mm as in case (γ 1.5-β 2.0) since the gap scale is the same of droplet's diameter for complete dropwise surface. Then, the hybrid surface minimizes droplets dynamics to the patterns and its enhancement becomes inactive. The optimum gap than enhance departure frequency and droplet dynamic are existing in this study.

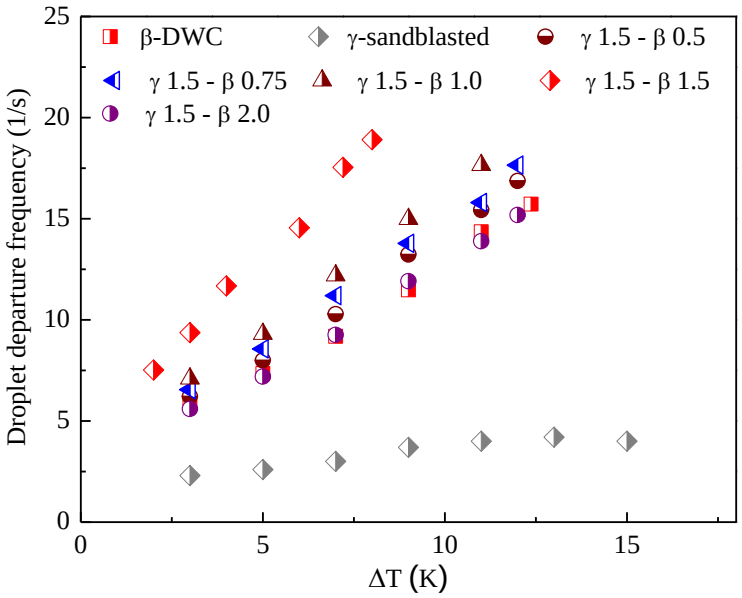

Figure 4.38: Droplet departure frequency at different gaps with fixed pattern diameter 1. 5 mm versus with temperature difference (ΔT).

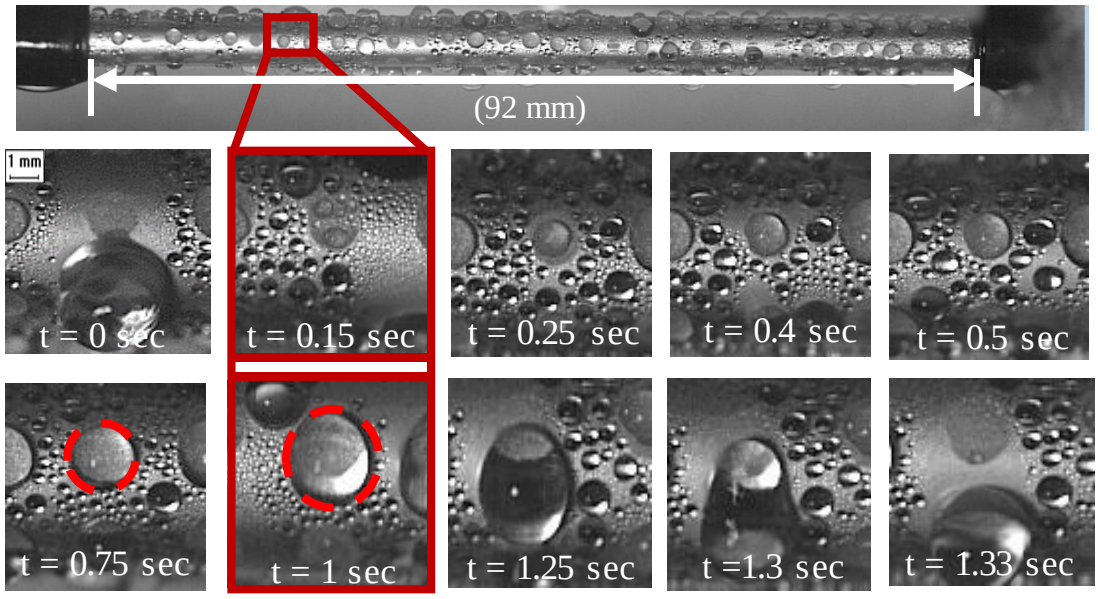

Figure 4.39: The influence of gap between circles on dropwise condensation heat transfer for the hybrid surface. The copper tube has patterns where the diameter of the circle is 1.5mm, and the gap is 0.5mm. The diameter of the circle is 1.5mm, and the gap is 1.5mm. The circle does not connect with each other, and then the thermal resistance is reduced. The series of images shows the droplets movement toward the circles at high momentum.

Figure 4.40 shows the renewal area frequency for the hybrid surface at different gap scales when the pattern's diameter is (1.5mm). The renewal frequency increases with increasing the gap between the patterns due to dyeing out the bridging between the patterns and reduction of the resistances for migration of droplets from the patterns and surface. However, the droplets departure diameter for those hybrid surfaces is not changing and still has the same diameter with the complete dropwise (β-region) surface as shown in Figure 4.41. The optimum gap scale that gives the peak departure frequency is found in the study.

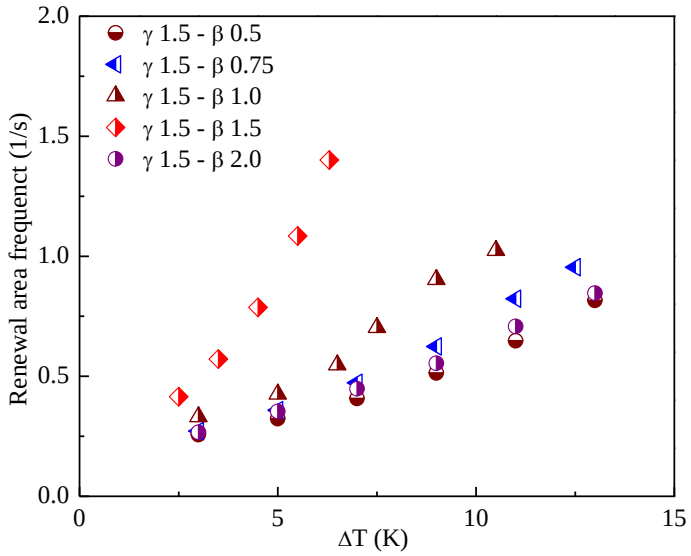

Figure 4.40: Renewal area frequency at different gaps with fixed pattern diameter 1.5mm versus with temperature difference (ΔT).

4.6 Condensation heat transfer and droplets dynamics on different patterned geometry of hybrid surfaces

4.6.1 Condensation on different geometry of hybrid surfaces.

The corresponding importance of the pattern geometry and gap between the patterns during condensation on hybrid surfaces are studied. Experiments regarding condensation on various surfaces which are complete dropwise (β-region) surface, complete sandblasted (γ-region) surface, and hybrid surfaces were performed. The hybrid surfaces have various patterns geometry and different identical gap between each adjacent pattern. The experimental conditions were the same for all tested surfaces. The performance of condensation for all hybrid surfaces is different from that for the complete sandblasted (γ-region) and complete dropwise (β-region) surfaces. The heat transfer rate was influenced by the geometry of the patterns and the gaps between the patterns.

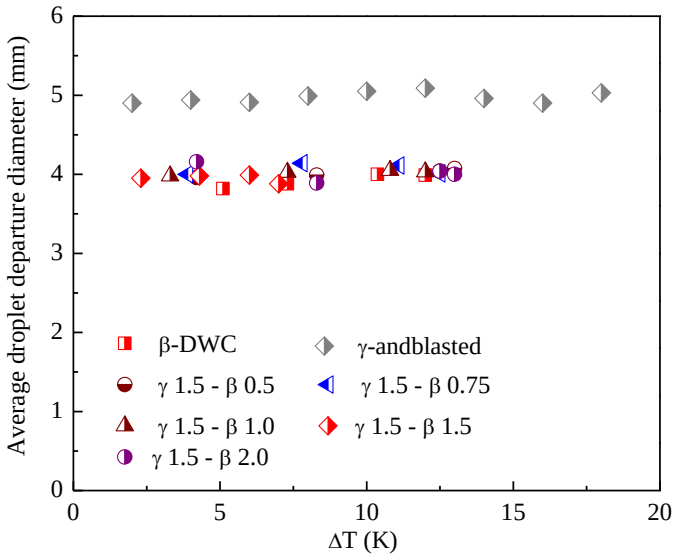

Figure 4.41: Droplet departure diameter at various gaps with fixed pattern diameter 1.5mm versus with temperature difference (ΔT).

During condensation on hybrid surfaces, the geometry of the pattern has a significant impact on the droplets geometry, droplets dynamic, condensation phenomena and the performance of heat transfer rates. Also, the gap between adjacent patterns plays an important factor to enhance condensation on hybrid surfaces. Therefore, the parametric study is needed to discuss the effect of the geometry of the patterns and the gaps among them on the condensation heat transfer rate and droplet departure frequency. Three patterns have been developed on different copper tubes which are a circle, ellipse, and diamond. First, the effect of the geometry has been studied while the pattern's size and the gap between the patterns remained the same. Second, the influence of the gap between the patterns is discussed while the size of the patterns is maintained constant for each pattern geometry. During, condensation on each hybrid surface, the droplets nucleate, grow, coalescence on hydrophobic regions and then migrate to the hydrophilic patterns which has high wettability characteristics. Figure 4.42 shows images on

condensation on various hybrid surfaces. The geometry of the droplets during the experiment is influenced by the shape of the patterns. The droplet's geometry on circular and diamond hybrid surfaces are almost the same while the droplets have a different shape on elliptic hybrid surface. All the hybrid surface has the same heat transfer trend where the heat transfer rate of the various hybrid surfaces is compared to the complete dropwise (β-region) surface and complete sandblasted (γ-region) surface.

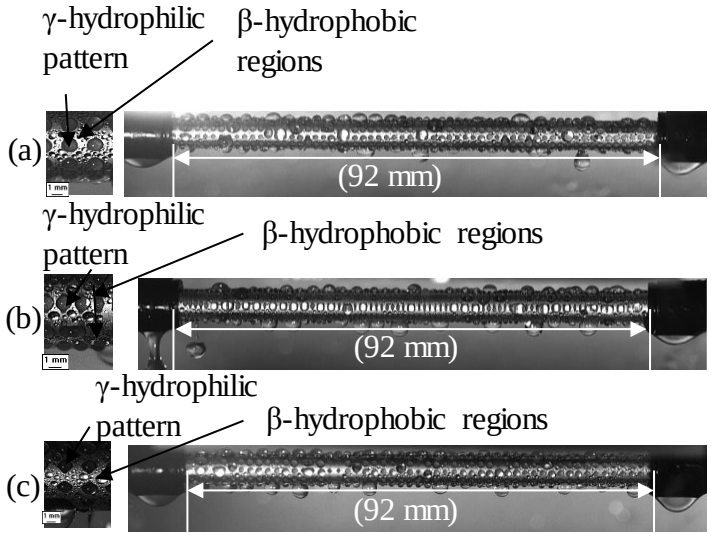

Figure 4.42: The condensation phenomena and droplet transition on hybrid surfaces (a) Circular hybrid surface (b) Elliptic hybrid surface (c) Diamond hybrid surface.

4.6.2 Effect of patterns geometry

Figure 4.43 shows the schematic designs of the patterns which designed on horizontal copper tubes. The patterns have the same size, and the gap distance, but the geometry of the patterns is changed. The hybrid surfaces parameters and design are listed in Table 4.3 where the size for each patterns are equal to circle pattern size which has 1mm diameter. The area ratios occupied by the patterns on tubes are listed in Table 4.3.

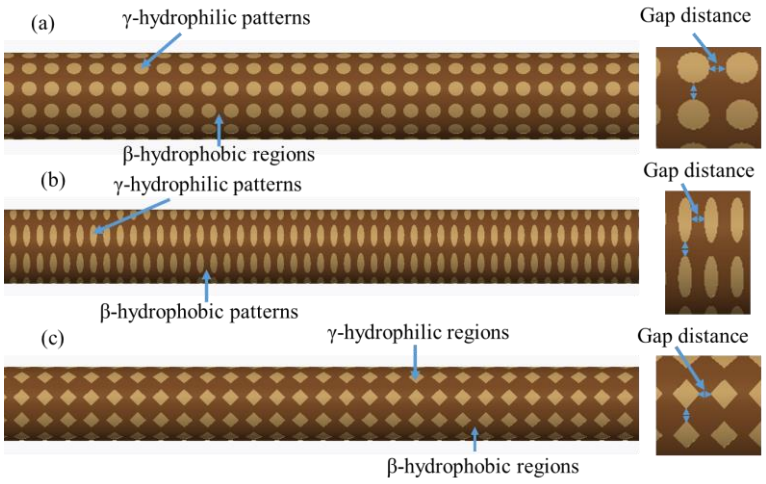

Figure 4.43: The design of the patterns on copper tubes (a) Circular hybrid surface (b) Elliptic hybrid surface (c) Diamond hybrid surface.

Table 4.3: The Parameters and design dimensions of patterns.

Name	Gap distance(mm)	Area ratio %
Circular	0.5	35
Elliptic	0.5	36
Diamond	0.5	25

Figure 4.44 shows the heat transfer rates for complete dropwise (β-region) surface, complete sandblasted (γ-region) surface, hybrid surfaces have different geometry and Nusselt model. In this figure, the influence of pattern geometry on the dropwise condensation heat transfer is discussed. The heat transfer rate for the diamond hybrid surface is higher than complete dropwise (β-region) surface, complete sandblasted (γ-region) surface and both elliptic, circular hybrid surfaces. The heat transfer rate for the diamond hybrid surface is 10% greater than complete dropwise (β-region) surface while the heat transfer is 20% and 15% lower than complete dropwise (β-region) surface for

both circular and elliptic hybrid surfaces respectively. The schematic diagram for the phenomena of condensation on hybrid surfaces is shown in Figure 4.45 where the patterns are surrounded by hydrophobic regions from all directions. From visualization study, the patterns merge with another adjacent pattern during the condensation as a bridge on the three hybrid surfaces. Figure 4.46 shows multiple images of condensation on the three hybrid surfaces. Due to the bridging between the patterns, the hydrophobic areas between the patterns are covered by droplets. The bridging extends to occupy more than two adjacent patterns for ellipse and circle patterns on tubes. The bridging prevents new droplets from rolling off from the patterns and the new droplets sunk into the bridging areas between the patterns instead.

The covered hydrophobic areas become inactive and provide a thermal resistance for condensation. However, the number of bridging between the patterns for the diamond hybrid surface is less than both circular and elliptic hybrid surfaces. Figure 4.47 shows images that explain the number of merging between the patterns on three hybrid surfaces. As shown in Figure 4.47, the diamond hybrid surface has the lowest number of bridging. The droplet's size on the elliptic and circular hybrid surfaces is bigger compared to droplet' size on the diamond hybrid surface. The covered hydrophobic area between the patterns for the ellipse and circles geometries is larger compared to the diamond hybrid surface. In diamond hybrid surface, the area sizes of hydrophilic patterns at the point of contact with hydrophobic regions is less compared with circles and ellipses patterns.

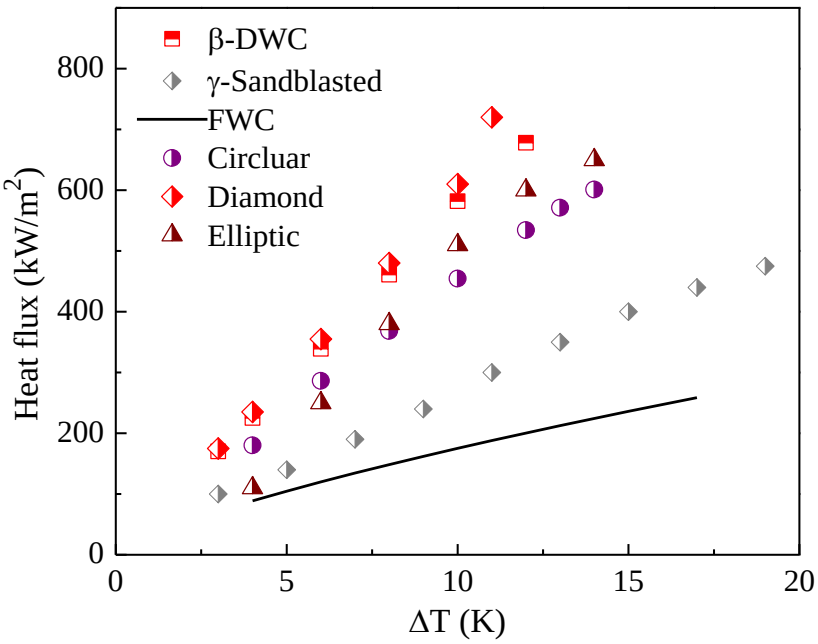

Figure 4.44: The heat transfer rate for hybrid surfaces which have different pattern's geometry.

Then, the tendency of the patterns to be merged becomes slower at the merging points compared to circle and ellipse patterns. The small and sharp edges in diamond patterns reduce the number of merging and bridging between the patterns at the same gap as in circles and ellipse patterns.

Moreover, the hydrophobic area ratios decrease with increasing the number of bridging between the patterns because the bridging freezes the droplet dynamic on the covered hydrophobic regions. The area ratio for hydrophilic regions increases which increase the thermal resistances and then reduces the heat transfer rate. The time which the droplets sweep from patterns in the diamond hybrid surface is less than circular and elliptic hybrid surfaces. In addition, the diamond patterns have larger boundary than circle patterns although the patterns have same size. Then, the number of droplets that migrate around the diamond pattern's boundary of is higher than migrating droplets

around circles pattern's boundary. Increasing the number of migrating droplets to the patterns creates new areas for new droplets to nucleate and migrate to the hydrophobic regions. However, the ellipse patterns have bigger perimeter than diamond hybrid surface, but the heat transfer rate is lower compared to the diamond hybrid surface. The size of the ellipse patterns is bigger than droplet's diameter for complete dropwise (β-region) surface. The heat transfer rate declines if the pattern size is bigger than droplet diameter on the complete dropwise surface because the thermal resistance becomes higher. Moreovere, the area ratio for ellipse and circle patterns on tube is larger than area ratio for diamond patterns on hybrid surface as described in the Table 4.3. The higher hydrophilic area percentage decrease the heat transfer rate since the thermal resistance increases.

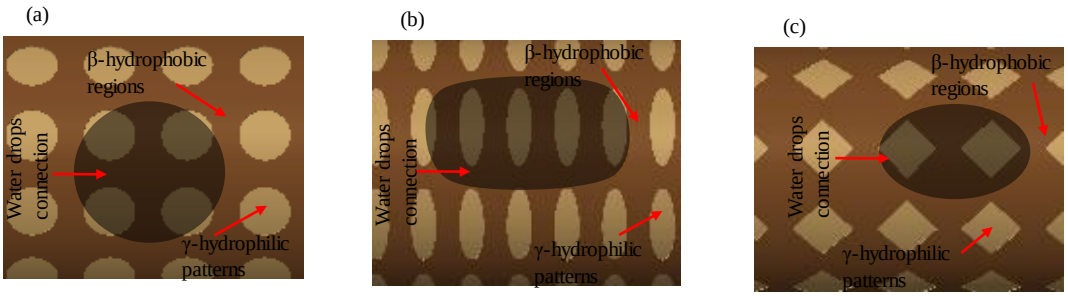

Figure 4.45: The schematic diagram of condensation phenomena on different hybrid surfaces that have same size and the gap is 0.5mm between each two neighbor patterns (a) Circular hybrid surface (b) Elliptic hybrid surface (c) Diamond hybrid surface.

Figure 4.48 shows the influence of patterns geometry on condensation heat transfer when subcooling temperature difference ΔT = 8 ℃ compared with Nusselt model, complete dropwise (β-region), sandblasted (γ-region) and hybrid surfaces. In addition, the droplets departure frequency for the hybrid surfaces is shown in Figure 4.49 compared to complete dropwise (β-region) and complete sandblasted (γ-region) surfaces.

The patterns geometry influences the droplet departure frequency. The departure frequency for the diamond hybrid surface is larger the both circular and elliptic hybrid surfaces because of the lower number of bridging among the patterns. The bridging between the pattern delay the droplet movement on the surface and resist the falling droplets from the surface. Some droplets sink in the bridging among the patterns. Therefore, increasing the number of the bridging enhances the number of sinking droplet and then reduces the droplet departure frequency.

The renewal area frequency of the patterns for the hybrid surfaces during condensation is shown in Figure 4.50. The renewal area frequency for diamond patterns is higher than both circles and ellipse patterns since the number of bridging is less. The time which droplets departs from diamond patterns is less than the time that droplets depart from circle and ellipse patterns. The droplet departure frequency and the heat transfer rate increase with increasing the renewal frequency of the patterns because the number of migrating droplets increases and the thermal resistance decreases.

4.6.3 Effect of the gap between the patterns

Figure 4.51 shows the improved schematic design of the patterns on hydrophobic copper tubes. The parameters of patterns and designs are listed in Table 4.4. The gap between the adjacent patterns is changed for each geometry while the pattern's size remains constant. Figure 4.52 and Figure 4.53 shows the influence of the gap between the patterns on the heat transfer performance for hybrid surfaces. The pattern size remained constant, while the geometry and the gap distances are (0.75mm and 1 mm) respectively.

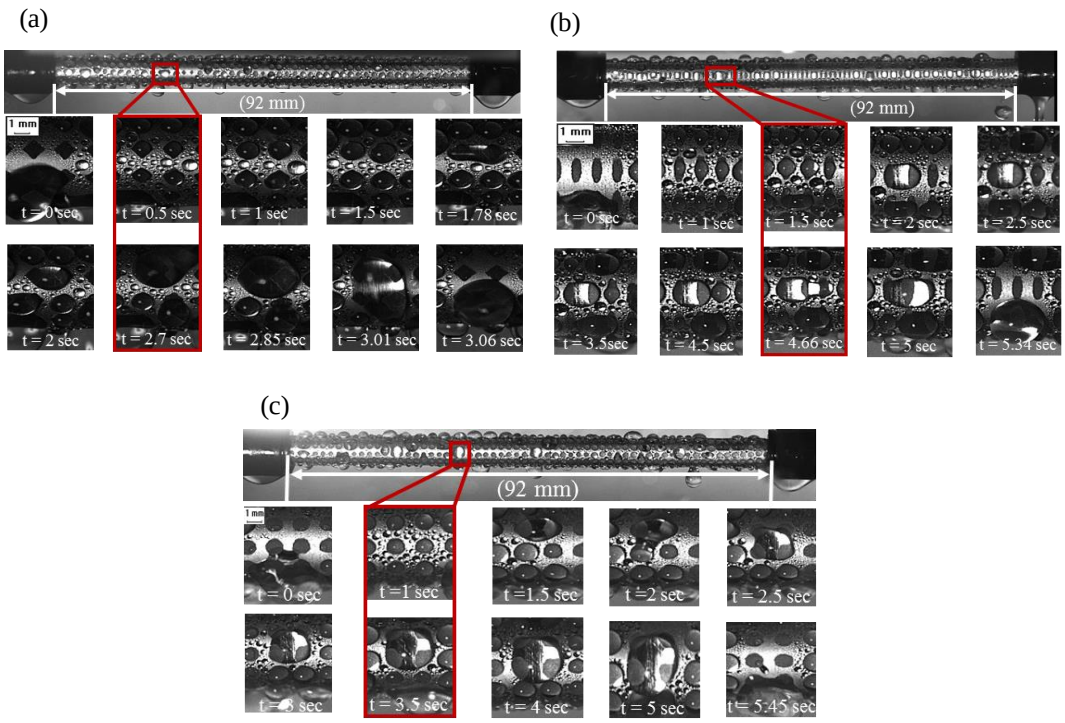

Figure 4.46: Condensation phenomenon on various hybrid surface geometries (a) Diamond hybrid patterns on copper tube. The gap between the patterns is 0.5mm and the pattern's size equal to sizes of ellipse and circles patterns. The images show condensation and droplets migration on diamond hybrid surface and the patterns merge with another pattern during condensation (b) Elliptic hybrid surface where the gap between the patterns is 0.5mm and the pattern's size equal to sizes of diamond and circle hybrid patterns. The images from show condensation and droplets migration on diamond hybrid surface. The patterns merge with another pattern during condensation and then the merging patterns merge with other connecting patterns as a bridge. (c) Circular hybrid surface where the gap between the patterns is 0.5mm and the pattern's size equal to sizes of diamond and elliptic hybrid surfaces. The images from show condensation and droplets migration on diamond hybrid surface. The two patterns merge with two another pattern during condensation patterns where the droplets spend time to migrate from the patterns.

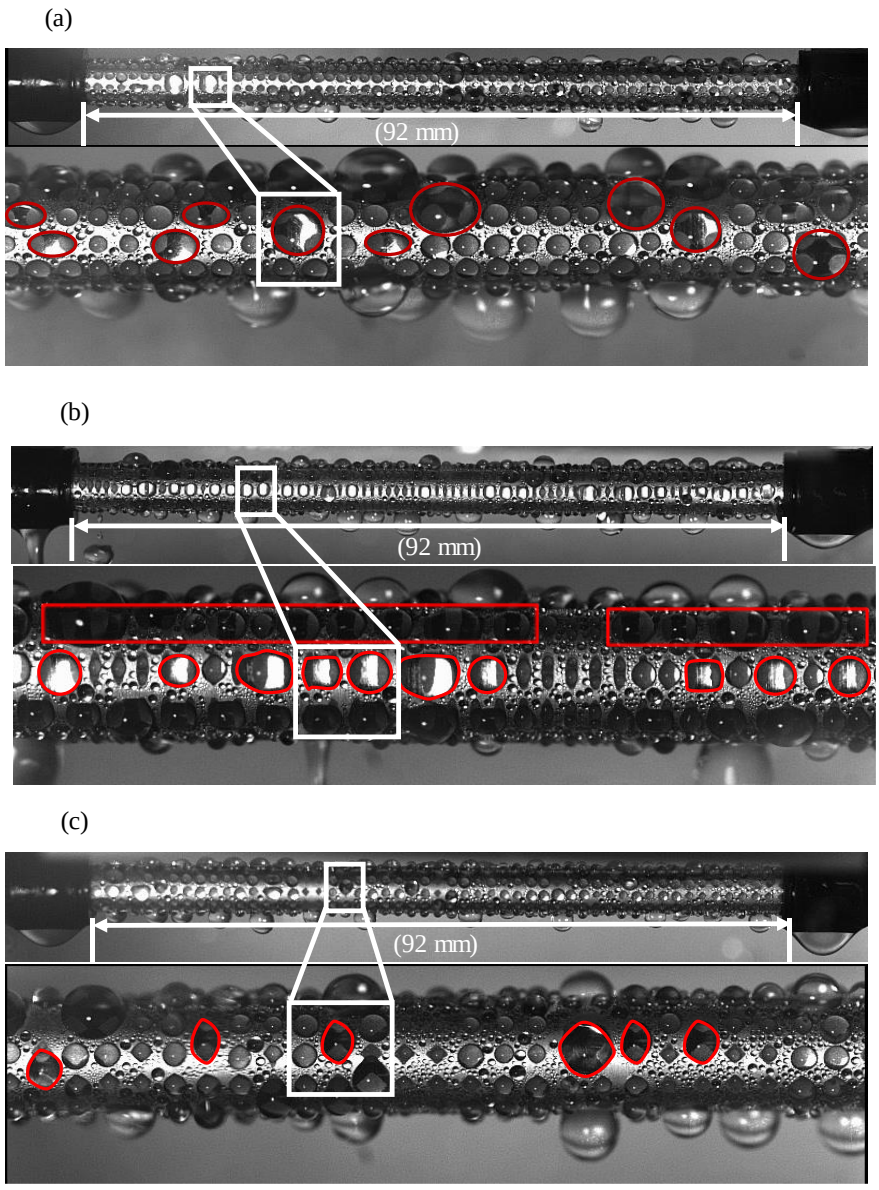

Figure 4.47: The connection phenomena between adjacent patterns for various hybrid surfaces when the patterns have same size while the gap is 0.5mm between the patterns. (a) Bridging phenomena between the patterns on circular hybrid surface where the image shows the condensation on circular hybrid surface when the pattern's diameter is 1 mm and the gap is 0.5mm. The number of bridging between the patterns is explained (b) Bridging phenomena between the patterns on elliptic hybrid surface where the image shows the condensation on ellipse hybrid surface when the pattern's size equals to circles pattern's size and the gap is 0.5mm. The number of bridging between the patterns is studied (c) Bridging phenomena between the patterns on diamond hybrid surface when the pattern's size equals to circles pattern's size and the gap is 0.5mm. The number of bridging was explained between the patterns.

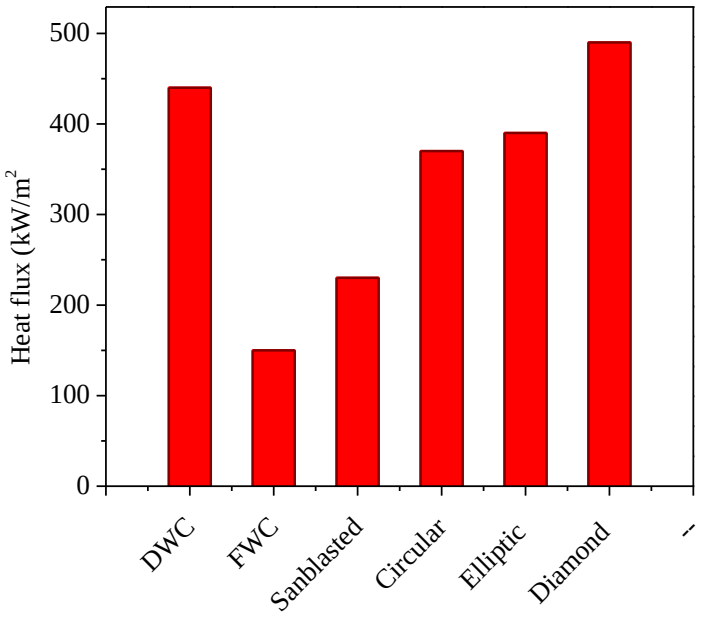

Figure 4.48: The effect of pattern's geometry on heat transfer rates for hybrid surface compared with dropwise, sandblasted and Nusselt model when ΔT = 8 ℃ and the gap distance is 0.5 mm.

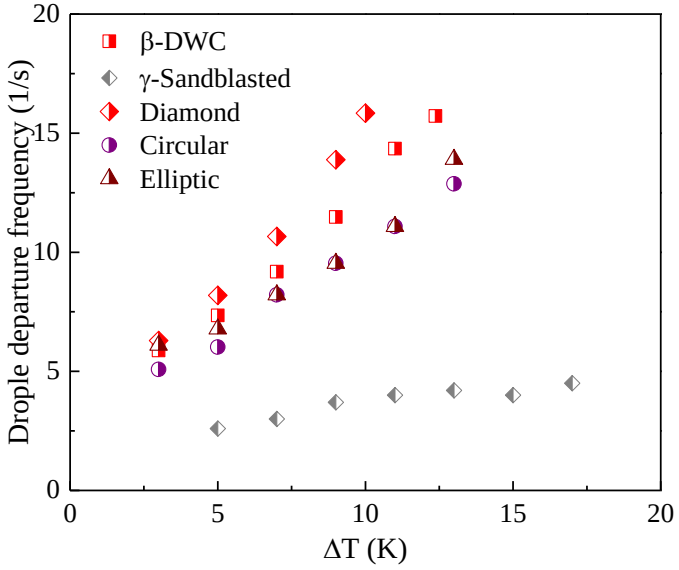

Figure 4.49: Droplet departure frequency for different hybrid surface geometry.

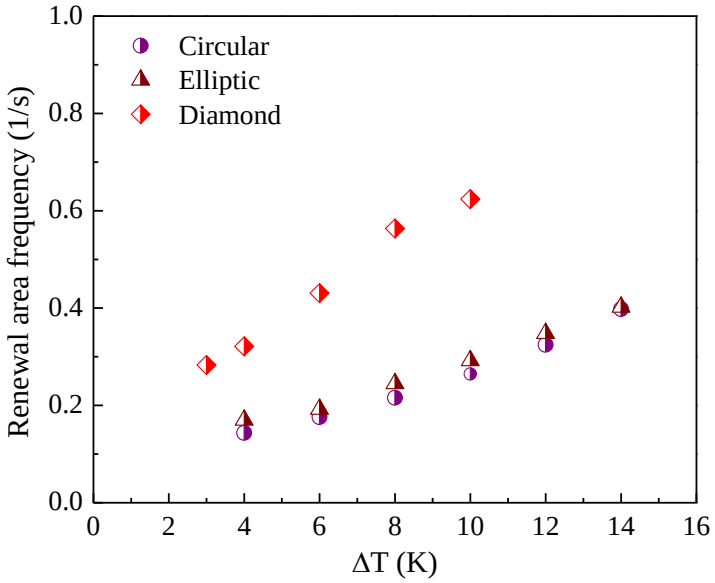

Figure 4.50: Renewal area departure frequency for various hybrid surface geometry.

The two figures show the heat transfer performance of a sample with a complete sandblasted (γ-region) surface, complete dropwise (β-region) surface, hybrid surfaces and Nusselt model of filmwise condensation for comparison. The experimental conditions for all the tube surfaces were the same. The heat transfer rates for the hybrid surfaces depend on the pattern's geometry and the gap distance between patterns. The gap between the patterns has a significant influence on the heat transfer results and droplet departure frequency as well. From visualization study, when the gap between two patterns increases the bridging between the patterns decreases. Then, the hydrophobic areas between the patterns return to be active, and lots of new droplets nucleate and migrate to the patterns. The number of bridging decreases when the gap is 0.75mm and 1mm for all hybrid surfaces compared to the number of bridging with 0.5 mm gap distance.

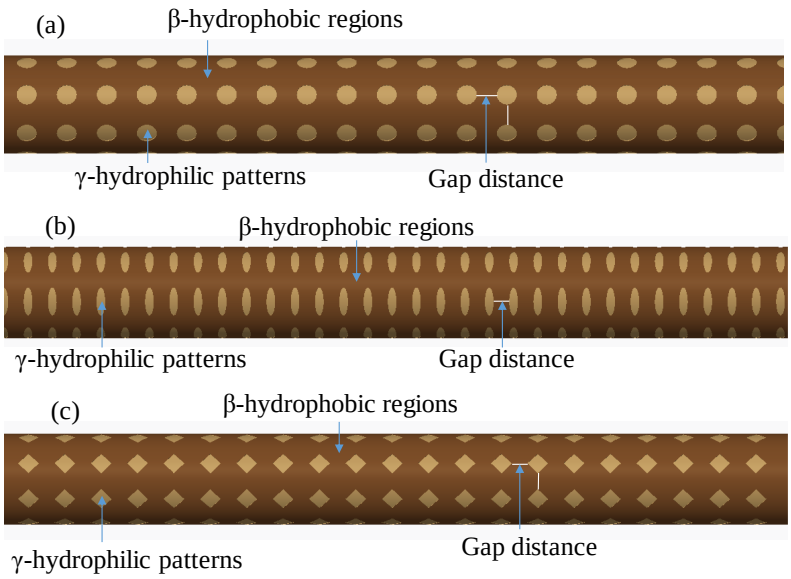

Figure 4.51: The design of the patterns on copper tubes when the gap scale is 1mm (a) Circular hybrid surface (b) Elliptic hybrid surface (c) Diamond hybrid surface.

Figure 4.54 shows the condensation phenomena and the number of bridging for the three hybrid surfaces when the gap between the patterns is 1mm. The number of bridging is completely invisible for diamond hybrid surface when the gap is 1mm while the bridging still exists for elliptic and circular hybrid surfaces at the same gap scale.

The enhancement of heat transfer rates with increasing the gap between the patterns was due to the decrease the thermal resistance results from fewer bridging phenomena. The number of new nucleated droplets increases and the migration of droplets to the patterns is enhanced. Moreover, the total hydrophobic area percentage increases with increasing the gap between the patterns although the bridging still appearing on the surfaces.

Table 4.4: The parameters for the improved hybrid surfaces.

Hybrid surface sample	Gap distance (mm)	Area ratio %
Circular	0.5	35
	0.75	25.6
	1	19.6
Elliptic	0.5	36
	0.75	24.4
	1	18.7
Diamond	0.5	25
	0.75	20
	1	15

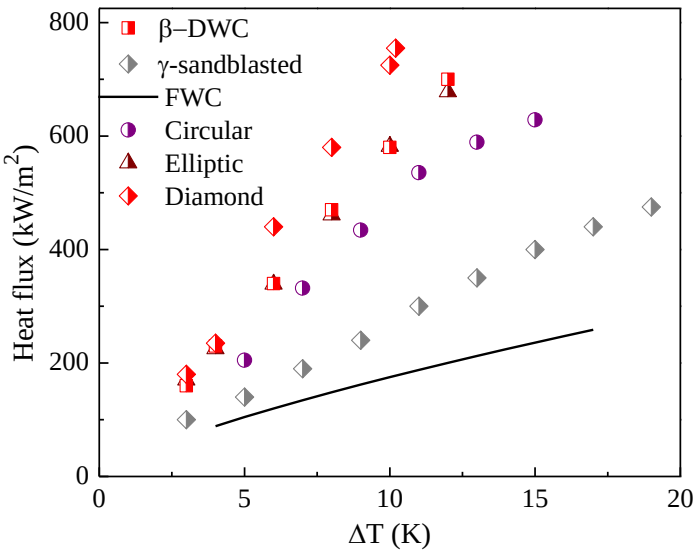

Figure 4.52: The heat transfer rate for different geometry hybrid surfaces when the gap between two geometries is 0.75 mm.

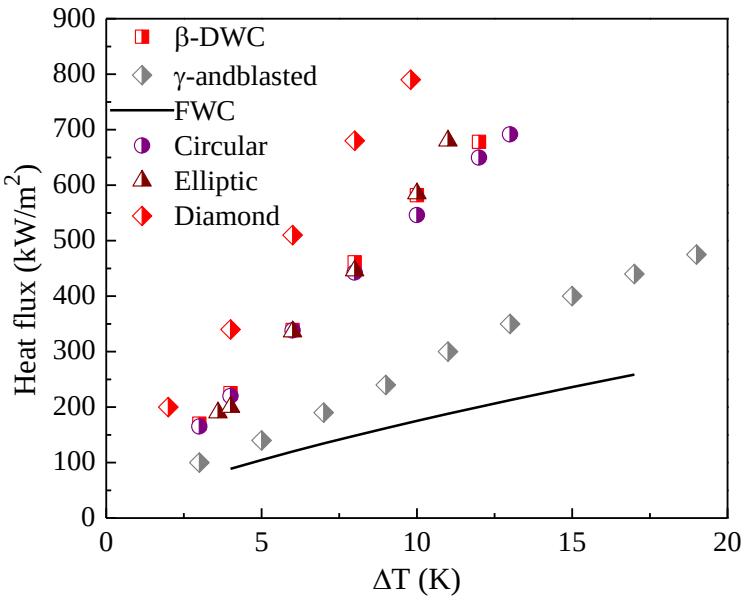

Figure 4.53: The heat transfer rate for different geometry hybrid surfaces when the gap between two geometries is 1 mm.

The effect of gap distances between the patterns on condensation heat transfer is explained in Figure 4.55 compared with Nusselt model, complete dropwise (β-region), complete sandblasted (γ-region), and hybrid surfaces when ΔT = 8℃. The highest performance for all hybrid patterned surfaces obtained at 1mm gap distance while the lowest performance obtained at 0.5 mm gap distance. Figure 4.56 and Figure 4.57 show the droplet departure frequency for hybrid surfaces at (0.75 mm and 1 mm) gap distance respectively. The droplet departure frequency for hybrid surfaces compared to complete dropwise (β-region) and complete (γ-region) sandblasted surfaces. The droplet departure frequency improves with increase the gap between two patterns because of the reducing in the bridging between the patterns. The droplets move freely in high momentum to the patterns without resistance from the bridging in case of the diamond hybrid surface when the gap is 1mm. However, some droplets were sinking to the bridging in case of the circular and elliptic hybrid surfaces when the same gap distance is 1 mm.

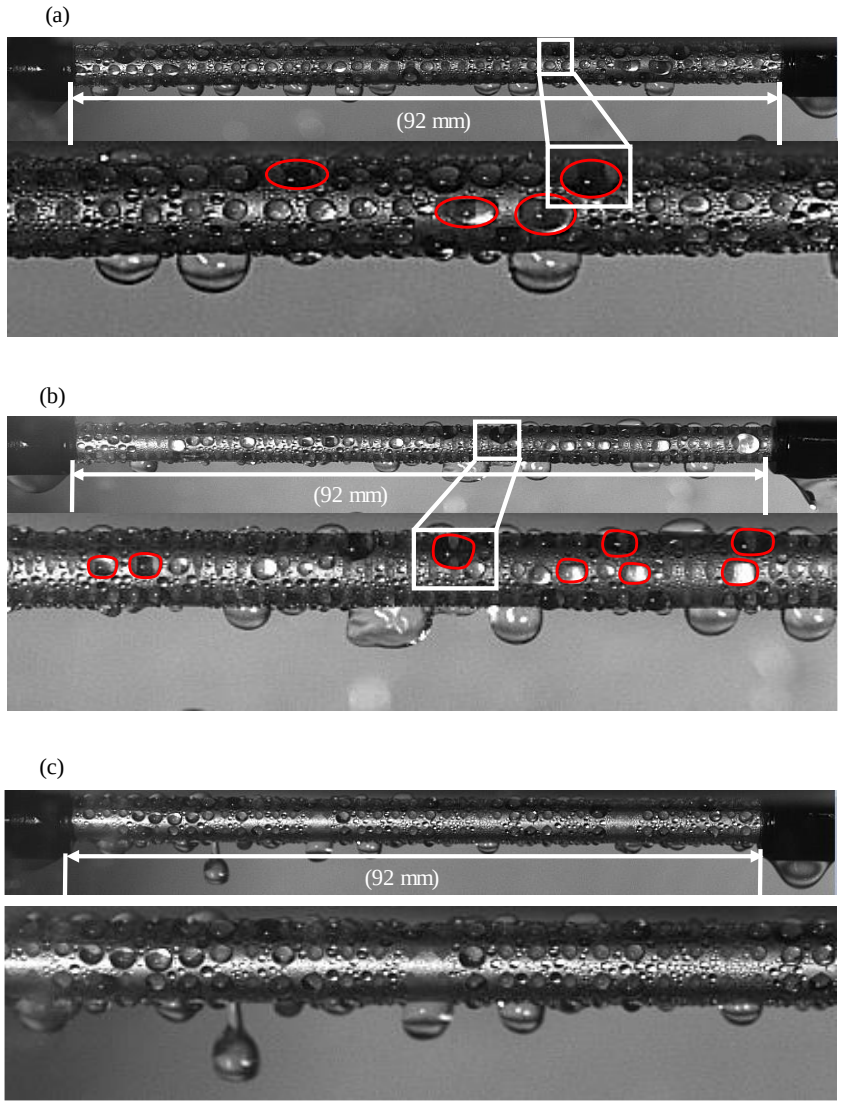

Figure 4.54: The bridging phenomena between adjacent patterns for various hybrid surfaces when the patterns have same size while the gap distance is 1 mm between the patterns. (a) Bridging phenomena between the patterns on circular hybrid surface when the pattern's diameter is 1 mm and the gap is 1 mm. (b) The bridging phenomena between the patterns on elliptic hybrid surface when the pattern's size equals to circles pattern's size and the gap are 1 mm. (c) Invisible bridging phenomena between the patterns on diamond hybrid surface when the pattern's size equals to circles pattern's size and the gap is 1 mm.

Figure 4.58 and Figure 4.59 show the renewal area frequency for hybrid surfaces have different pattern's geometry and gap distances. The renewal area frequency increases with increasing the gap distance between the adjacent patterns. The diamond

patterns on hybrid surface have the highest renewal frequency at different gap distance since the number of bridging is less compared to circular and elliptic hybrid surfaces.

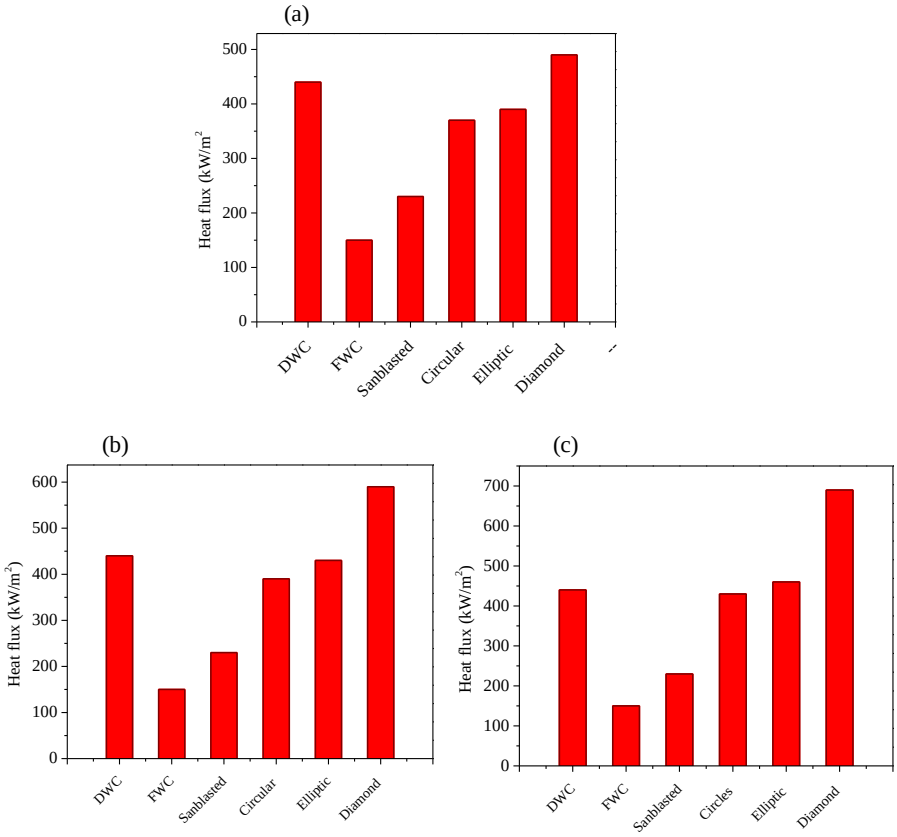

Figure 4.55: The effect of gap distances on heat transfer rates for hybrid surface compared with dropwise, sandblasted and Nusselt model when ΔT = 8 ℃ (a) Gap distance is 0.5 mm (b) Gap distance is 0.75 mm (c) Gap distance is 1 mm.

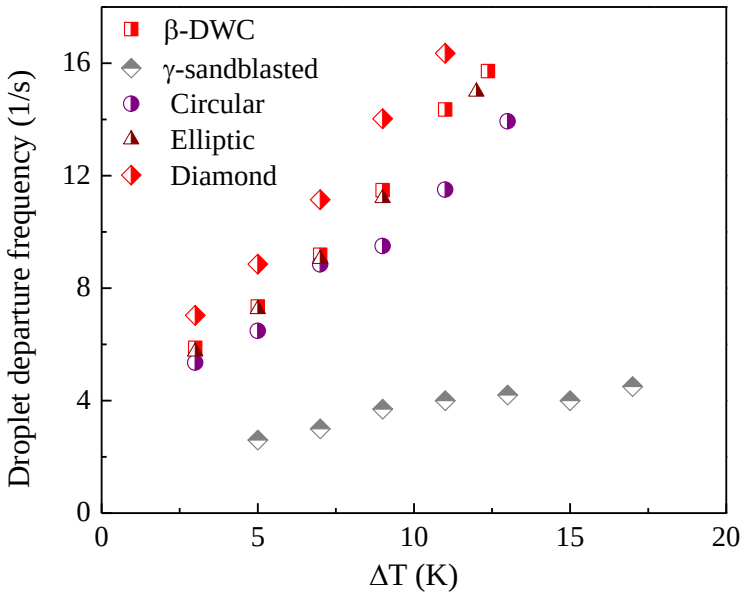

Figure 4.56: Droplet departure frequency for different geometry hybrid surfaces when the gap between two geometries is 0.75 mm.

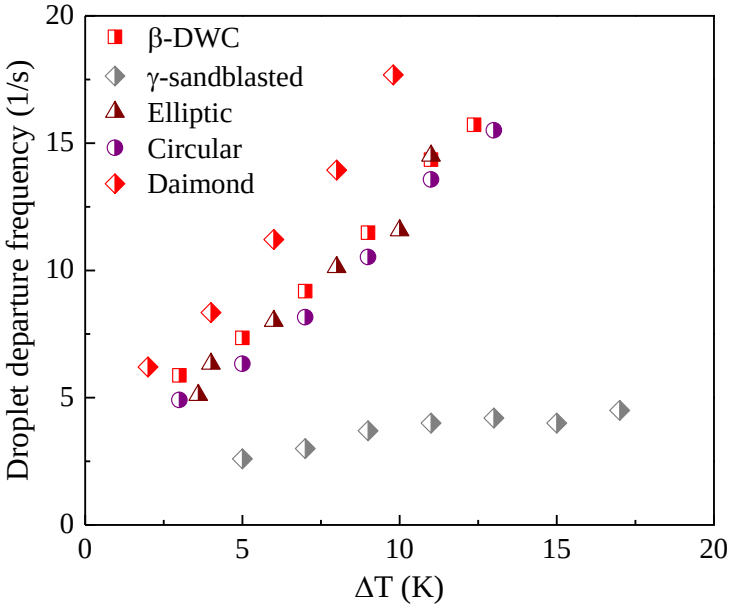

Figure 4.57: Droplet departure frequency for different geometry hybrid surfaces when the gap between two geometries is 1 mm.

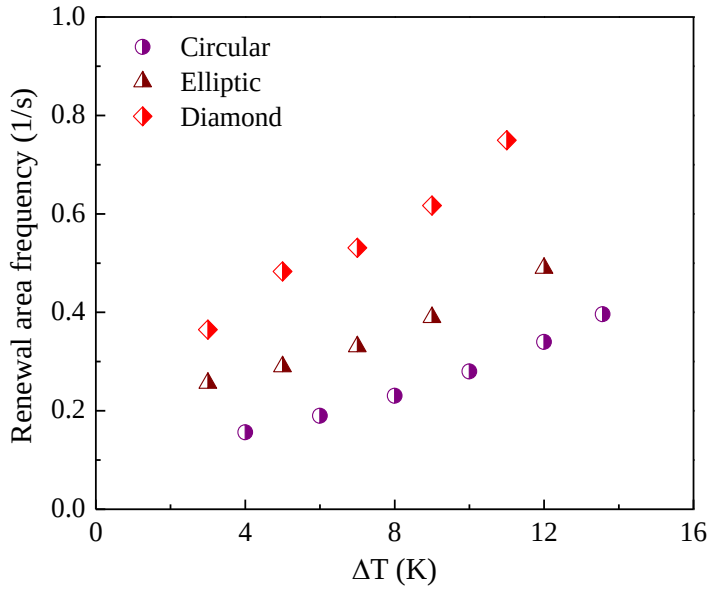

Figure 4.58: Renewal area frequency for different geometry hybrid surfaces when the gap between two geometries is 0.75 mm.

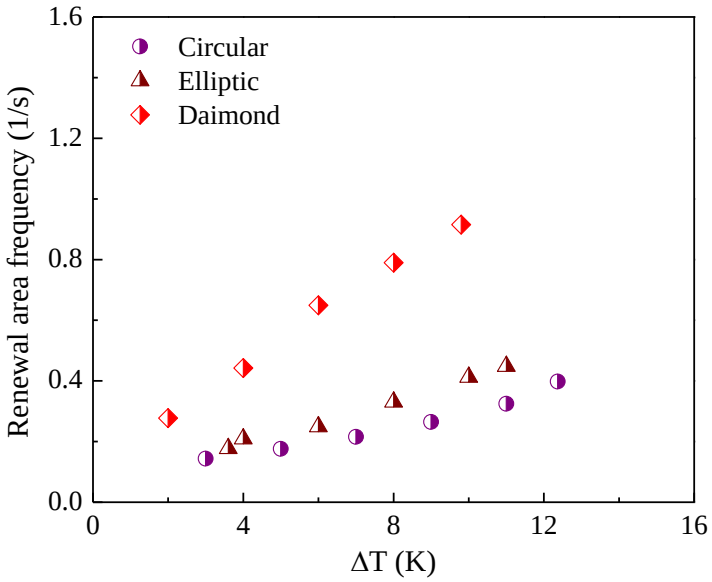

Figure 4.59: Renewal area frequency for different geometry hybrid surfaces when the gap between two geometries is 1 mm.

CHAPTER 5

CONCLUSIONS AND FUTURE WORK

5.1 Conclusions

The interest of condensation enhancement using hybrid surface designs has been inspired by its wide application and by numerous research studies. A parametric study of condensation was achieved on various types of surfaces, i.e., complete sandblasted, complete dropwise and hybrid surfaces. A bare copper tube was completely sandblasted using 50 microns silicon carbide to obtain complete sandblasted surface. On the other hand, the hydrophobic surface was obtain using self-assembled monolayer (SAM) coating. The hybrid surfaces were partially coated with SAM and the other regions were sandblasted. The experiments of all surfaces were performed at atmospheric pressure, and the steam was at saturated conditions.

The heat transfer performance for complete sandblasted surface is slightly higher than Nusselt model for complete filmwise condensation. The surface characterizations for complete sandblasted surface before condensation was different for contact angle of 62 degree during condensation versus contact angle of 134 degree before condensation occurs. However, the heat transfer rate for complete dropwise surface coated with SAM was higher than complete sandblasted surface and Nusselt model for complete filmiwise condensation. The contact angle was approximately 97 degree during condensation and the phenomenon was completely dropwise. The droplet departure frequency of complete

dropwise surface was higher than complete sandblasted surface because the droplets migrate faster with smaller sizes. The droplet departure diameter for complete dropwise surface is lower than complete sandblasted surface.

Numerous research has focused on the enhancement of dropwise condensation using hybrid surfaces. In this study, it has been studied and discussed different hybrid surface designs that all share the same boundary conditions. The heat transfer rates for hybrid surface (hydrophobic patterns) increase with the decrease in the size of the hydrophobic patterns but it decreases with further patterns size decrease. However, the heat transfer rates for hybrid surfaces (hydrophobic patterns) are less the complete dropwise for all sizes. Therefore, the hybrid surfaces (hydrophobic patterns) were not good for condensation enhancements. The optimum hydrophobic patterns' size was found in this study.

The condensation heat transfer rates on hybrid surfaces (hydrophilic patterns) increase with the increase of the modified hydrophilic patterns' size but the heat transfer rates decrease with further increase of the hydrophilic size. The optimum patterns' size which maximizes the heat transfer rate was determined. Moreover, the heat transfer rate increases with the increase the gap between the patterns until the bridging among patterns vanish. However, the heat transfer rates decrease if hydrophobic gap distances increase further. An optimum pattern's gap distance is existing for promoting heat transfer.

In addition, the effect of patterns' size and gaps on droplet departure frequency and droplets mobility during dropwise condensation at atmospheric pressure were clarified. The droplet departure frequency increases with increasing the hydrophilic

pattern's diameter. However, the departure frequency decreases with a further increase for hydrophilic pattern's size. The departure frequency increases gradually with increase the hydrophobic gap until the bridging among patterns totally vanish. Then, the departure frequency decreases with increasing the hydrophobic gaps. The optimum size and the maximum gap that leads the departure frequency reaches the peak values exist in this study. However, in case of hydrophobic patterns, the droplet departure frequency increases with decrease the patterns' size but it decreases with further size decrease and the optimum patterns' size was found.

Furthermore, the renewal area frequency for the patterns was calculated under different patterns' sizes and gap scales. The renewal area frequency improved with increasing the gap between the patterns because the patterns do not merge at large gap scales. Then, the renewal frequency decreases with further increase in the gap because the patterns became inactive since its size equals approximately the droplet size on complete dropwise surface. The droplet departure diameters for hybrid surfaces (hydrophilic patterns) are almost the same with complete dropwise surface. However, the droplet departure diameters for hybrid surfaces (hydrophobic patterns) were less than droplet departure diameter for complete dropwise surface.

In addition it was found that, the geometry of patterns on hybrid surfaces has a significant influence on the heat transfer rate and droplet departure frequency during condensation. The heat transfer rate for the diamond hybrid surface was 40% higher than complete dropwise surface. However, the heat transfer rate for both circular and elliptic hybrid surfaces is lower than the diamond hybrid surface at the same pattern's size and gap distances. The droplet departure frequency is higher for diamond hybrid surfaces

compared the both elliptic and circular hybrid surfaces. The heat transfer rate increases gradually with increase the hydrophobic gap for all hybrid surfaces. The heat transfer rate for the diamond surface was the optimum compared with other hybrid surfaces.

5.2 Future work

The current studies about evaluation of condensation on various hybrid surfaces have achieved and visual observation of condensation phenomena, droplet dynamics and obtaining the heat transfer enhancements. In condensation, therefore, a theoretical modeling is needed to get the heat transfer rates and droplet dynamics during condensation on hybrid surfaces. The effect of the patterns' shape should be modeled at different patterns' size and gap distances. The effect of bridging between the patterns on droplet dynamics would be modeled during condensation on hybrid surfaces.

Currently, little research findings exist on the modeling of condensation on hybrid surfaces. Therefore, there are several open questions and further studies are needed to develop to understand condensation on hybrid surfaces which have different patterns' geometry. In addition, recommendation for further studies is to optimize the condensation performance of low surface tension steam such as refrigerant instead of pure steam. In addition, the same study can be achieved on different tube parameters and inclinations at different steam conditions.

REFERENCES

[1] E.J. Lefevre, J.W. Rose, An Experimental Study of Heat Transfer by Dropwise Condensation, International Journal of Heat and Mass Transfer, 8 (1965) 1117-1133

[2] H. TANAKA, T. TSURUTA, A Microscopic Study of Dropwise Condensation, international Journal of Heat and Mass Transfer, 27 (1984) 327-335.

[3] P. J. Marto, D. J. Looney, J. W. Rose, A.S. Wanniarachchi, Evaluation of organic coatings for the promotion of dropwise condensation of steam, International Journal of Heat and Mass Transfer, 29 (1986) 1109-1117.

[4] X. Ma, J.W. Rose, D. Xu, J. Lin, B. Wang, Advances in dropwsie condensation heat transfer: Chinese research, Chemical Engineering 78 (2000) 87-93.

[5] M.H. Rausch, A. Leipertz, A.P. Fröba, On the Mechanism of Dropwise Condensation of Steam on Ion Implanted Metallic Surfaces, Journal of Heat Transfer, 132(9) (2010) 094503.

[6] M.R.N. Reddy, M. Yohan, K.H. Reddy, Heat Transfer Co-Efficient Through Dropwsie Condensation and Filmwsie Condensation Apparatus, international Journal of Science and Research Publications, 2(12) (2012).

[7] Y. Yuan, T.R. Lee, Contact Angle and Wetting Properties, 51 (2013) 3-34.

[8] X. Ma, S. Wang, Z. Lan, B. Peng, H.B. Ma, P. Cheng, Wetting Mode Evolution of Steam Dropwise Condensationon Superhydrophobic Surface inthe Presence of Noncondensable Gas, Journal of Heat Transfer, 134 (2012) 1-9.

[9] E. Bormashenko, Why does the Cassie–Baxter equation apply?, Colloids and Surfaces A: Physicochemical and Engineering Aspects, 324(1-3) (2008) 47-50.

[10] W. Choi, A. Tuteja, J.M. Mabry, R.E. Cohen, G.H. McKinley, A modified Cassie-Baxter relationship to explain contact angle hysteresis and anisotropy on non-wetting textured surfaces, J Colloid Interface Sci, 339(1) (2009) 208-216.

[11] M. Nahavandi, A. Mehrabani-Zeinabad, Effect of Contact Angle on Steam Dropwise Condensation: A Simulation Approach, ISRN Chemical Engineering, 2012 (2012) 1-7.

[12] AAron Ston, A. Razani, Enhanced Steam Condensation as a Result of Heat Transfer Additives, International Journal of Environmentally Conscious Design and Manufacturing, 10 (2001) 1-7.

[13] H. Purhonen, M. Puustinen, J. Laine, A. Räsänen, R. Kyrki-Rajamäki, J. Vihavainen, Steam Blowdown Experiments with the Condensation Pool Test Rig, International Conference Nuclear Energy for New Europe, (2005) 1-10.

[14] M. Isard, A. Blake, Condensation Conitional Density Propgation for Visual Tracking, Internation Journal of Computer Vision, (1998) 1-36.

[15] Y. Bhuiyan, Y. Shen, V. Giurgiutiu, Ultrasonic inspection of multiple-rivet-hole lap joint cracks using global analysis with local finite element approach, in, 2016, pp. 98051Z-98051Z-98015.

[16] Y.M. Bhuiyan, Y. Shen, V. Giurgiutiu, Guided Wave Based Crack Detection in the Rivet Hole Using Global Analytical with Local FEM Approach, Materials, 9(7) (2016).

[17] J.B. Boreyko, C.H. Chen, Self-propelled dropwise condensate on superhydrophobic surfaces, Physical Review Letter, 103(18) (2009) 184501.

[18] K. Rykaczewski, J.H.J. Scott, S. Rajauria, J. Chinn, A.M. Chinn, W. Jones, Three dimensional aspects of droplet coalescence during dropwise condensation on superhydrophobic surfaces, Soft Matter, 7(19) (2011) 8749.

[19] R. Wen, Z. Lan, B. Peng, W. Xu, X. Ma, Droplet dynamics and heat transfer for dropwise condensation at lower and ultra-lower pressure, Applied Thermal Engineering, 88 (2015) 265-273.

[20] R. Wen, Z. Lan, B. Peng, W. Xu, X. Ma, Y. Cheng, Droplet Departure Characteristics and Dropwise Condensation Heat Transfer at Low Steam Pressure, Journal of Heat Transfer, 138(7) (2016) 071501.

[21] C. Dorrer, Condensation and Wetting Transitions on Microstructured Ultrahydrophobic Surfaces, Langmuir : the ACS journal of surfaces and colloids, 23 (2007) 3820-3824.

[22] K.A. Wier, T.J. McCarthy, Condensation on Ultrahydrophobic Surfaces and Its Effect on, Langmuir : the ACS journal of surfaces and colloids, 22 (2006) 2433-2436.

[23] J. Feng, Y. Pang, Z. Qin, R. Ma, S. Yao, Why condensate drops can spontaneously move away on some superhydrophobic surfaces but not on others, Applied Material Interfaces, 4(12) (2012) 6618-6625.

[24] J. Feng, Z. Qin, S. Yao, Factors affecting the spontaneous motion of condensate drops on superhydrophobic copper surfaces, Langmuir : the ACS journal of surfaces and colloids, 28(14) (2012) 6067-6075.

[25] Y. Ito, M. Heydari, A. Hashimoto, T. Konno, A. Hirasawa, S. Hori, K. Kurita, A. Nakajima§, The Movement of a Water Droplet on a Gradient Surface Prepared by

Photodegradation, Langmuir : the ACS journal of surfaces and colloids, 23 (2007) 1845-1850.

[26] M. Izumi, S. Kumagai, R. Shimada, N. Yamakawa, Heat transfer enhancement of dropwise condensation on a vertical surface with round shaped grooves, Experimental Thermal and Fluid Science, 28(2-3) (2004) 243-248.

[27] H.W. Hu, G.H. Tang, D. Niu, Experimental investigation of condensation heat transfer on hybrid wettability finned tube with large amount of noncondensable gas, International Journal of Heat and Mass Transfer, 85 (2015) 513-523.

[28] C.W.M. Van Der Geld, F.L.A. Ganzevles, C.T.P.F. Simons, F. Weitz, Geometry Adaptations to Improve the Performance of Compact, Polymer Condensers, Chemical Engineering Research and Design, 79(4) (2001) 357-362.

[29] B. Kundu, Approximate analytical method for prediction of performance and optimum dimensions of pin fins subject to condensation of quiescent vapor, International Journal of Refrigeration, 32(7) (2009) 1657-1671.

[30] B. Kundu, G.K. Ghosh, An approximate analytical prediction about thermal performance and optimum design of pin fins subject to condensation of saturated steam flowing under forced convection, International Journal of Refrigeration, 32(5) (2009) 809-825.

[31] J.W. Rose, An Analysis of Film Condensation on a Horizontal Wire-Wrapped Tube, Chemical Engineering Research and Design, 80(3) (2002) 290-294.

[32] T. Murase, A. Briggs, H.S. Wang, J.W. Rose, Condensation on a Horizontal Wire-Wrapped Tube, Journal of Heat Transfer, 127(11) (2005) 1207.

[33] H.M. Ali, M.Z. Qasim, M. Ali, Free convection condensation heat transfer of steam on horizontal square wire wrapped tubes, International Journal of Heat and Mass Transfer, 98 (2016) 350-358.

[34] Y. Utaka, S. Wang, Characteristic curves and the promotion effect of ethanol addition on steam condensation heat transfer, International Journal of Heat and Mass Transfer, 47(21) (2004) 4507-4516.

[35] S.-H. Hu, J.-J. Yan, J.-S. Wang, Y. Li, J.-P. Liu, Effect of temperature gradient on Marangoni condensation heat transfer for ethanol–water mixtures, International Journal of Multiphase Flow, 33(9) (2007) 935-947.

[36] T. Murase, H.S. Wang, J.W. Rose, Marangoni condensation of steam–ethanol mixtures on a horizontal tube, International Journal of Heat and Mass Transfer, 50(19-20) (2007) 3774-3779.

[37] J. Wang, J. Yan, S. Hu, J. Liu, Marangoni condensation heat transfer of water–ethanol mixtures on a vertical surface with temperature gradients, International Journal of Heat and Mass Transfer, 52(9-10) (2009) 2324-2334.

[38] X. Ma, Z. Lan, W. Xu, M. Wang, S. Wang, Effect of surface free energy difference on steam-ethanol mixture condensation heat transfer, International Journal of Heat and Mass Transfer, 55(4) (2012) 531-537.

[39] Z. Dongchang, Z. LIN, J. Lin, A New Method for Achieving Dropwsie Condensation (II) New Surface Materials for Dropwise Condensation Journal of Chemical Industry and Engineering, 3 (1988) 263-271.

[40] Q. Zhao, B.M. Burnside, Dropwise Condensation of Steam on Ion Implanted Condenser Surfaces Heat Recover Systems, 14 (1994) 525-534.

[41] M.H. Rausch, A.P. Fröba, A. Leipertz, Dropwise condensation heat transfer on ion implanted aluminum surfaces, International Journal of Heat and Mass Transfer, 51(5-6) (2008) 1061-1070.

[42] M.H. Rausch, A. Leipertz, A.P. Fröba, Dropwise condensation of steam on ion implanted titanium surfaces, International Journal of Heat and Mass Transfer, 53(1-3) (2010) 423-430.

[43] A. Bani Kananeh, M.H. Rausch, A.P. Fröba, A. Leipertz, Experimental study of dropwise condensation on plasma-ion implanted stainless steel tubes, International Journal of Heat and Mass Transfer, 49(25-26) (2006) 5018-5026.

[44] Q. Yang, A. Gu, Dropwise Condensation on SAM and Electroless Composite Coating Surfaces, Journal of Chemical Engineering of Japan, 39(8) (2006) 826-830.

[45] G.B. Gore, N.V. Sali, A.B. Ghodake, of Dropwise Condensation Heat Transfer Enhancement on Silver Coated Copper Surface using n-Heptane as Surfactant Additive, International Advanced Research Journal in Science, Engineering and Technology, 3 291-294.

[46] S. Vemuri, K.J. Kim, An experimental and theoretical study on the concept of dropwise condensation, International Journal of Heat and Mass Transfer, 49(3-4) (2006) 649-657.

[47] S. Vemuri, K.J. Kim, B.D. Wood, S. Govindaraju, T.W. Bell, Long term testing for dropwise condensation using self-assembled monolayer coatings of n-octadecyl mercaptan, Applied Thermal Engineering, 26(4) (2006) 421-429.

[48] B.J. Zhang, C. Kuok, K.J. Kim, T. Hwang, H. Yoon, Dropwise steam condensation on various hydrophobic surfaces: Polyphenylene sulfide (PPS), polytetrafluoroethylene

(PTFE), and self-assembled micro/nano silver (SAMS), International Journal of Heat and Mass Transfer, 89 (2015) 353-358.

[49] K. M.D, P. P.L, P. A.T, Study of Dropwise Condensation on Teflon Coated Surface, International Advanced Research Journal in Science, Engineering and Technology, 2(8) (2015) 26-29.

[50] N. Wang, D. Zhou, H. Fang, Y. Shi, F. Sun, X. Huang, Dropwsie Condensation on Nickel-based Coating Tube, International Conference on Power Engineering, (2007) 666-669.

[51] S. Lee, K. Cheng, V. Palmre, M.D.M.H. Bhuiya, K.J. Kim, B.J. Zhang, H. Yoon, Heat transfer measurement during dropwise condensation using micro/nano-scale porous surface, International Journal of Heat and Mass Transfer, 65 (2013) 619-626.

[52] A.K. Das, H.P. Kilty, G.B. Andeen, A. Kumar, The Use of an Organic Self-Assembled Monolayer Coating to Promote Dropwise Condensation of Steam on Horizontal, journal of Heat Transfer, 122 (2000) 278-286.

[53] G.A. Oneill, J.W. Westwater, Dropwise condensation of steam on electroplated on silver, International Journal of Heat and Mass Transfer, 27 (1984) 1539-1549.

[54] S.S. Finnicum, J.W. Westwater, Dropwise vs filmwise condensation of steam on chromuim, International Journal of Heat and Mass Transfer, 32 (1989) 1541-1549.

[55] G. Koch, D.C. Zhang, A. Leiperrtz, M. Grischke, K. Trojan, H. Dimigen, Study on plasma enhanced CVD coated material to promote dropwsie condensation of steam, journal of Heat and Mass Transfer, 41 (1998) 1899-1906.

[56] Q. Baojin, Z. Li, X. Hong, S. Yan, Experimental study on condensation heat transfer of steam on vertical titanium plates with different surface energies, Experimental Thermal and Fluid Science, 35(1) (2011) 211-218.

[57] K. Rykaczewski, A.T. Paxson, M. Staymates, M.L. Walker, X. Sun, S. Anand, S. Srinivasan, G.H. McKinley, J. Chinn, J.H. Scott, K.K. Varanasi, Dropwise condensation of low surface tension fluids on omniphobic surfaces, Scientific reports, 4 (2014) 4158.

[58] I.O. Ucar, H.Y. Erbil, Dropwise condensation rate of water breath figures on polymer surfaces having similar surface free energies, Applied Surface Science, 259 (2012) 515-523.

[59] M.H.M. Grooten, C.W.M. van der Geld, Surface property effects on dropwise condensation heat transfer from flowing air-steam mixtures to promote drainage, International Journal of Thermal Sciences, 54 (2012) 220-229.

[60] M. Roudgar, J. De Coninck, Condensation heat transfer coefficient versus wettability, Applied Surface Science, 338 (2015) 15-21.

[61] L. Zhong, M. Xuehu, W. Sifang, W. Mingzhe, L. Xiaonan, Effects of surface free energy and nanostructures on dropwise condensation, Chemical Engineering Journal, 156(3) (2010) 546-552.

[62] N. Moumen, R.S. Subramanian, J.B. Mclaughlin, Experiments on the Motion of Drops on a Horizontal Solid Surface Due to a Wettability Gradient Langmuir : the ACS journal of surfaces and colloids, 22 (2006) 2682-2690.

[63] S. Daniel, M.K. Chaudhury, Rectified Motion of Liquid Drops on Gradient Surfaces Induced by Vibration Langmuir : the ACS journal of surfaces and colloids, 18 (2002) 3404-3407.

[64] R.W. Bonner, Dropwise-Condensation-on-Surfaces-with-Graded-Hydrophobicity, in: Proceedings of the ASME 2009 Heat Transfer Summer Conference 2009, pp. 1-5.

[65] F.M. Mancio Reis, P. Lavieille, M. Miscevic, Toward enhancement of water vapour condensation using wettability gradient surface, Experimental Thermal and Fluid Science, 67 (2015) 70-74.

[66] D.-J. Huang, T.-S. Leu, Fabrication of high wettability gradient on copper substrate, Applied Surface Science, 280 (2013) 25-32.

[67] T. Brest, K.F. Eid, A.D. Sommers, Using Surface Tension Gradients to Reduce Condensate Retention and Improve Heat Exchanger Performance in Air Conditioning Systems, International Refrigeration and Air Conditioning Conference (2012) 1-10.

[68] B. Peng, X. Ma, Z. Lan, W. Xu, R. Wen, Experimental investigation on steam condensation heat transfer enhancement with vertically patterned hydrophobic–hydrophilic hybrid surfaces, International Journal of Heat and Mass Transfer, 83 (2015) 27-38.

[69] B. Peng, X. Ma, Z. Lan, W. Xu, R. Wen, Analysis of condensation heat transfer enhancement with dropwise-filmwise hybrid surface: Droplet sizes effect, International Journal of Heat and Mass Transfer, 77 (2014) 785-794.

[70] A. Ghosh, S. Beaini, B.J. Zhang, R. Ganguly, C.M. Megaridis, Enhancing Dropwise Condensation through Bioinspired Wettability Patterning, Langmuir : the ACS journal of surfaces and colloids, 30(43) (2014) 13103-13115.

[71] P.S. Mahapatra, A. Ghosh, R. Ganguly, C.M. Megaridis, Key design and operating parameters for enhancing dropwise condensation through wettability patterning, International Journal of Heat and Mass Transfer, 92 (2016) 877-883.

[72] T.-S. Leu, H.-W. Lin, T.-H. Wu, Enhancement of phase change heat transfer by using surface energy pattering techniques, Proceedings of the 1st IEEE International Conference on Nano/Micro Engineered and Molecular Systems, (2006).

[73] A. Chatterjee, M.M. Derby, Y. Peles, M.K. Jensen, Condensation heat transfer on patterned surfaces, International Journal of Heat and Mass Transfer, 66 (2013) 889-897.

[74] A. Chatterjee, M.M. Derby, Y. Peles, M.K. Jensen, Enhancement of condensation heat transfer with patterned surfaces, International Journal of Heat and Mass Transfer, 71 (2014) 675-681.

[75] Y.-A. Lee, L.-S. Kuo, T.-W. Su, C.-C. Hsu, P.-H. Chen, Orientation effects of nanoparticle-modified surfaces with interlaced wettability on condensation heat transfer, Applied Thermal Engineering, 98 (2016) 1054-1060.

[76] J.W. Rose, Heat-transfer coefficients, Wilson plots and accuracy of thermal measurements, Experimental Thermal and Fluid Science, 28(2-3) (2004) 77-86.

[77] I. Frank, D. DeWitt., Fundamentals of Heat and Mass Transfer, New York, J. Wiley, (2002).

[78] M. Alwazzan, K. Egab, B. Peng, J. Khan, C. Li, Condensation on hybrid-patterned copper tubes (I): Characterization of condensation heat transfer, International Journal of Heat and Mass Transfer, 112 (2017) 991-1004.

[79] McClintock, S.J. Kline, F. A., Describing Uncertainties in Single-Sample Experiments, Mechanical Engineering, 75 (1953) 3-8.